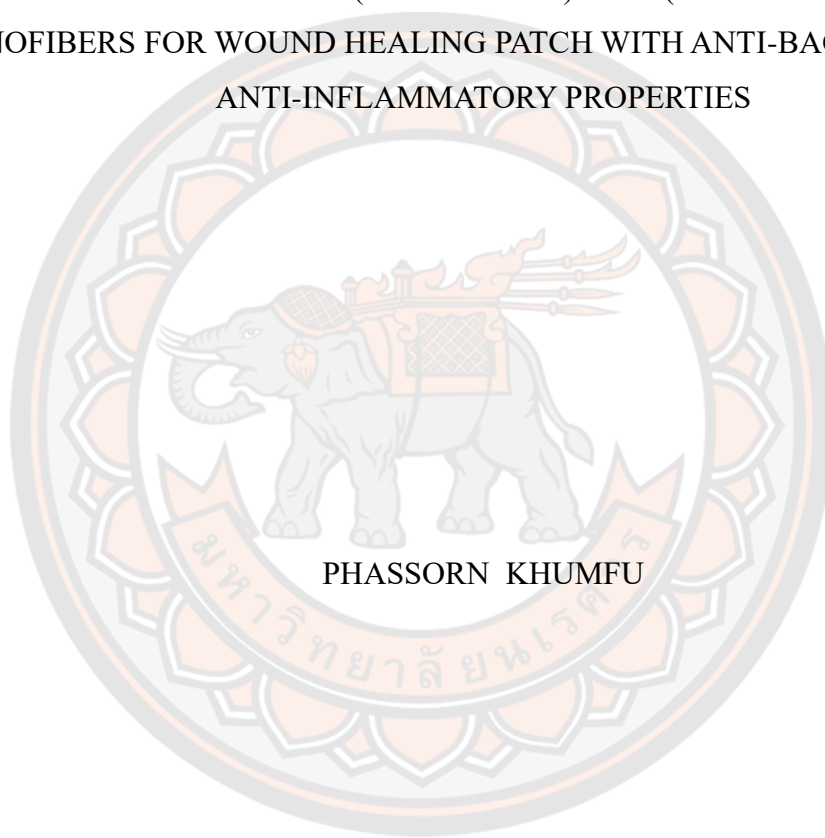




DEVELOPMENT OF POLY(LACTIC ACID)/POLY(ETHYLENE GLYCOL)
NANOFIBERS FOR WOUND HEALING PATCH WITH ANTI-BACTERIAL AND
ANTI-INFLAMMATORY PROPERTIES



A Thesis Submitted to the Graduate School of Naresuan University
in Partial Fulfillment of the Requirements
for the Master of Science in Industrial Chemistry

2023

Copyright by Naresuan University

DEVELOPMENT OF POLY(LACTIC ACID)/POLY(ETHYLENE GLYCOL)
NANOFIBERS FOR WOUND HEALING PATCH WITH ANTI-BACTERIAL AND
ANTI-INFLAMMATORY PROPERTIES



A Thesis Submitted to the Graduate School of Naresuan University
in Partial Fulfillment of the Requirements
for the Master of Science in Industrial Chemistry
2023

Copyright by Naresuan University

Thesis entitled "Development of Poly(lactic acid)/Poly(ethylene glycol) Nanofibers for Wound Healing Patch with Anti-bacterial and Anti-inflammatory Properties"

By Phassorn Khumfu

has been approved by the Graduate School as partial fulfillment of the requirements for the Master of Science in Industrial Chemistry of Naresuan University

Oral Defense Committee

..... Chair
(Associate Professor Dr. Sukunya Ross)

..... Advisor
(Assistant Professor Dr. Yupin Phuphuak)

..... Co Advisor
(Dr. Autchara Pangon)

..... Internal Examiner
(Assistant Professor Dr. Supatra Pratumshat)

..... External Examiner
(Dr. Chutima Vanichvattanadecha)

Approved

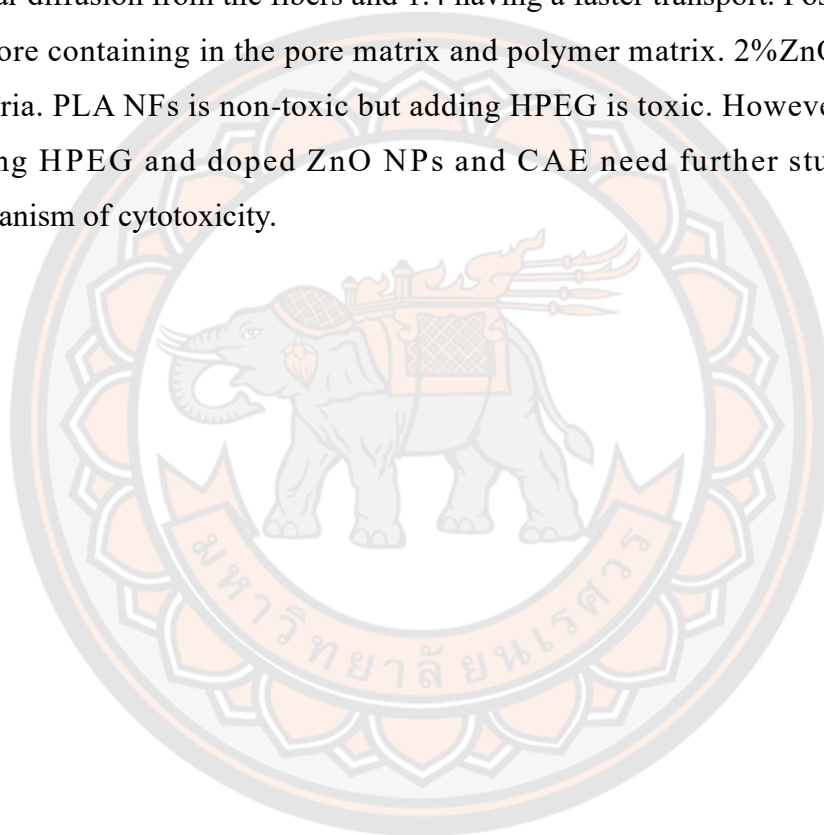
.....
(Associate Professor Krongkarn Chootip, Ph.D.)
Dean of the Graduate School

| | |
|-----------------------|--|
| Title | DEVELOPMENT OF POLY(LACTIC ACID)/POLY(ETHYLENE GLYCOL) NANOFIBERS FOR WOUND HEALING PATCH WITH ANTI-BACTERIAL AND ANTI-INFLAMMATORY PROPERTIES |
| Author | Phassorn Khumfu |
| Advisor | Assistant Professor Dr. Yupin Phuphuak |
| Co-Advisor | Dr. Autchara Pangon |
| Academic Paper | M.S. Thesis in Industrial Chemistry, Naresuan University, 2023 |
| Keywords | Wound healing, Nanofibers, Poly(lactic acid), Poly(ethylene glycol), Anti-bacterial |

ABSTRACT

This work proposes the fabrication of blended poly(lactic acid) (PLA) electrospun nanofibers which were separated into 3 parts. The first part is investigation of blending PLA nanofibers (NFs) with low molecular weight poly(ethylene glycol) (LPEG)(Mw=4000) and chitosan (CS) loaded with *Centella Asiatica* extracts (CAE) using the mixture solvents formic acid/chloroform/acetone and adding ethanol, PLA/PEG/CS/CAE can be electrospun into smooth nanofibers but there is still a problem with immiscibility of PLA, PEG, and CS. Although the addition of CS and PEG improves mechanical properties, all samples show hydrophobicity evidenced by water-contact angle (WCA) and Fourier Transform Infrared (FTIR) results. Therefore, we need to develop a new solvent system and change the type of anti-bacterial by using ZnO nanoparticles (NPs) instead of CS to the blended polymer and try to study the effect of LPEG and HPEG for optimum wettability. The second part is development of the blended PLA electrospun nanofibers with LPEG and High Mw PEG (Mw=900,000) (HPEG) by various ratios of PLA and LPEG or HPEG as 90:10, 70:30, and 50:50 respectively dissolved in chloroform and acetonitrile by the ratio of 60:40 that are successfully fabricated via electrospinning. The result of adding LPEG made the fibers smaller, but HPEG is

large because of the difference of molecular weight which also affects the viscosity. The hydrophilicity appears in the ratios of 70:30 HPEG and increased swelling and moderated rate of degradation. Therefore, we selected 70:30 to develop in the 3rd part by adding ZnO NPs and CAE to improve anti-bacterial and cytotoxicity. The final part is the fabrication of 70PLA/30HPEG electrospun fiber loaded 2% ZnO and 0.7-2.8% CAE. When ZnO NPs and CAE were added, there was a decrease in fiber degradation. CAE release patterns related to degradation with 0.7 and 2.8 having similar diffusion from the fibers and 1.4 having a faster transport. Possibly, CAE may be more containing in the pore matrix and polymer matrix. 2%ZnO NPs inhibited bacteria. PLA NFs is non-toxic but adding HPEG is toxic. However, the effects of adding HPEG and doped ZnO NPs and CAE need further studies about the mechanism of cytotoxicity.



ACKNOWLEDGEMENTS

Thank you to the Thailand Graduate Institute of Science and Technology (TGIST) for supporting and funding for education and research thesis, Naresuan University, and the National Nanotechnology Center (NANOTEC, National Science and Technology Development Agency) for facilities of the laboratory in the thesis.

Thank you Asst. Prof. Dr. Yupin Phuphuak (Advisor) and Dr. Autchara Pangon (Co-Advisor) for supporting everything.

Thank you, Assoc. Prof. Dr. Sukunya Ross and Asst. Prof. Dr. Supatra Pratumshat from the Department of Chemistry, Faculty of Science, Naresuan University for suggestions about research methodology and other information.

Thank you, Dr. Chutima Vanichvattanadecha for being the Thesis Committee Member in the thesis defense.

Thank you, Assoc. Prof. Dr. Winita Punyodom from supporting the PLA (Bioplastic Production Laboratory, Chiang Mai University)

Phassorn Khumfu

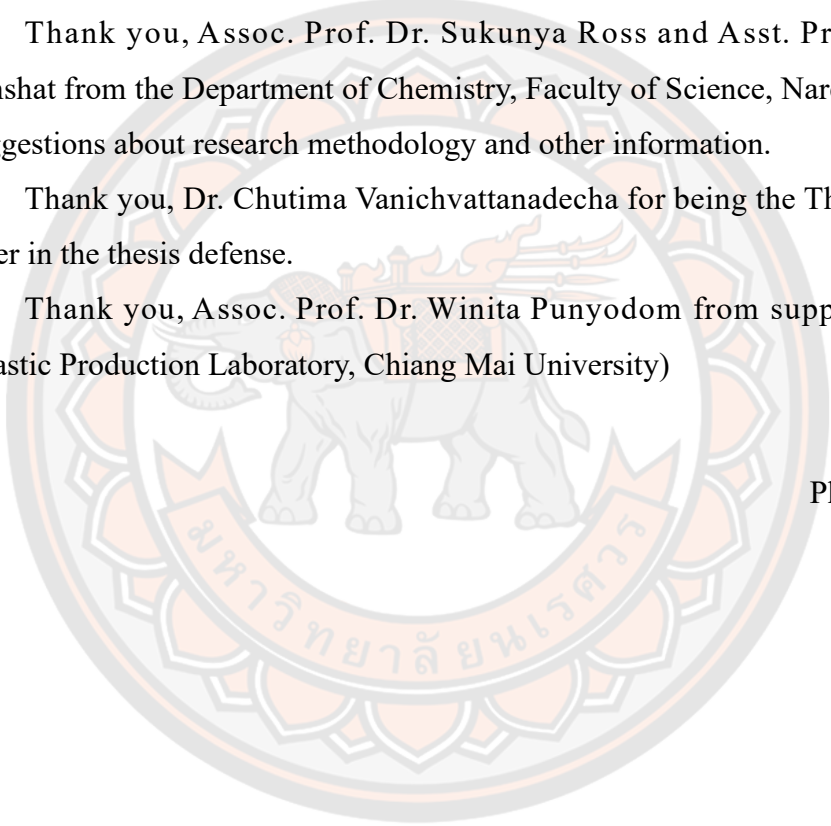


TABLE OF CONTENTS

| | Page |
|--|-------------|
| ABSTRACT..... | C |
| ACKNOWLEDGEMENTS..... | E |
| TABLE OF CONTENTS..... | F |
| LIST OF TABLE..... | J |
| LIST OF FIGURE..... | K |
| CHEPTEr 1..... | 1 |
| INTRODUCTION..... | 1 |
| 1.1 Introduction..... | 1 |
| 1.2 Objectives..... | 2 |
| 1.3 Scope of studies..... | 3 |
| 1.4 Related Works and Studies..... | 3 |
| 1.5 Definitions..... | 5 |
| 1.6 Hypothesis of Research..... | 5 |
| CHAPTER 2..... | 6 |
| LITERATURE REVIEWS..... | 6 |
| 2.1 Wound healing..... | 6 |
| 2.2 Biomaterials for wound healing..... | 9 |
| 2.2.1 Polylactic acid (PLA)..... | 9 |
| 2.2.2 Poly(ethylene glycol) (LPEG)..... | 10 |
| 2.2.3 Chitin-Chitosan (CS)..... | 11 |
| 2.3 Metal and Metal oxide nanoparticles for anti-bacterial..... | 12 |
| 2.4 Gotu kola (<i>Centella Asiatica (Linnaeus) Urban</i>) for wound healing..... | 15 |
| 2.5 Fabrication techniques of nanofibers..... | 18 |
| 2.6 Nanofiber preparation by electrospinning process [35]..... | 20 |
| 2.7 Drug delivery application of electrospun nanofibers..... | 25 |

| | |
|--|----|
| CHAPTER 3 | 27 |
| EXPERIMENTAL | 27 |
| 3.1 Chemicals and Materials..... | 27 |
| 3.2 Experimental..... | 28 |
| 3.2.1 Fabrication of blended polylactic acid (PLA) electrospun nanofibers with LPEG or HPEG, or Chitosan (CS) loaded <i>Centella Asiatica</i> extracts (CAE) via electrospinning | 28 |
| 3.2.1.1 Preparation of PLA/LPEG/CS/CAE solution..... | 28 |
| 3.2.1.2 Preparation of blended PLA electrospun nanofiber membrane..... | 29 |
| 3.2.1.3 Preparation of blend PLA with LPEG or HPEG, ZnO and CAE composite electrospun nanofibers | 30 |
| 3.2.2 Characterization of physical and chemical properties of blended PLA electrospun nanofiber loaded <i>Centella Asiatica</i> extract (CAE) via electrospinning | 33 |
| 3.2.2.1 Morphology and size of the electrospun nanofibers by Scanning Electron Microscopy (SEM) | 33 |
| 3.2.2.2 Analysis of functional group by Fourier Transform Infrared (FTIR).... | 33 |
| 3.2.2.3 Thermal properties analysis by Differential Scanning Calorimetry (DSC)..... | 33 |
| 3.2.2.4 Mechanical properties by Tensile testing | 34 |
| 3.2.2.5 Hydrophilicity analysis by water contact angles (WCA)..... | 34 |
| 3.2.3 Release Profile | 34 |
| 3.2.4 Degradation assay | 35 |
| 3.2.5 Analysis of the antibacterial activity of blended PLA electrospun nanofiber membranes..... | 36 |
| 3.2.6 Analysis of cytotoxicity using cell viability by MTT assay | 36 |
| CHAPTER 4 | 37 |
| RESULTS AND DISCUSSION..... | 37 |
| 4.1 Results of blended PLA with LPEG and CS and <i>Centella Asiatica</i> extracts (CAE) | 37 |
| 4.1.1 Solubility of polymer solutions of blended PLA with LPEG and CS | 37 |

| | |
|--|----|
| 4.1.2 Morphology of blended PLA electrospun nanofibers with LPEG and CS by Scanning Electron Microscope (SEM) | 40 |
| 4.1.3 Water-Contact Angle analysis of the blended PLA electrospun nanofiber with LPEG and Chitosan loaded CAE | 44 |
| 4.1.4 Chemical analysis for Functional group by Fourier transform infrared (FTIR) | 45 |
| 4.1.5 Thermal Properties blended PLA electrospun nanofibers with LPEG and CS loaded CAE by Differential Scanning Calorimetry (DSC) | 50 |
| 4.1.6 Mechanical properties of blended PLA electrospun nanofibers with LPEG and CS loaded CAE..... | 52 |
| 4.1.7 Conclusion of the preparation of blended PLA with LPEG and Chitosan (CS) and Centella Asiatica extracts (CAE) | 55 |
| 4.2 Result of development of Blended PLA with LPEG and HPEG | 56 |
| 4.2.1 Morphologies of blended PLA electrospun nanofibers with LPEG and HPEG by Scanning Electron Microscope (SEM) using 5 kX | 56 |
| 4.2.2 Water-contact angle analysis of Blended PLA electrospun nanofiber with LPEG or HPEG | 60 |
| 4.2.3 Chemical analysis for functional group on blended PLA/LPEG and PLA/HPEG electrospun nanofibers by Fourier transform infrared (FTIR) | 62 |
| 4.2.4 Swelling and Gel-fraction of PLA, PLA/LPEG | 64 |
| 4.2.5 Degradation of PLA, PLA/HPEG around 5 weeks | 66 |
| 4.2.6 Thermal properties of blended PLA/LPEG and PLA/HPEG electrospun nanofibers by Differential Scanning Calorimetry (DSC) | 68 |
| 4.2.7 Mechanical properties of blended PLA/LPEG and PLA/HPEG electrospun nanofibers by Tensile (ASTM D5034) | 71 |
| 4.2.8 Conclusion of the preparation of blended PLA with LPEG or HPEG various ratios | 73 |
| 4.3 Results of the effect of doped ZnO into the blended PLA from the best condition of 2 and loading <i>Centella Asiatica</i> extracts (CAE)..... | 74 |
| 4.3.1 Morphologies of 70PLA/10LPEG loaded 2%ZnO and various CAE by Scanning Electron Microscope (SEM) using 5 kX | 74 |
| 4.3.2 Functional group analysis of the blended PLA/LPEG and PLA/HPEG electrospun nanofibers by Fourier transform infrared spectroscopy (FTIR)..... | 77 |

| | |
|---|-----|
| 4.3.3 Swelling and gel-fraction of 70PLA/30HPEG and 70PLA/30HPEG/2ZnO loaded 0.7-2.8% CAE..... | 78 |
| 4.3.4 Thermal properties of blended 70PLA/30HPEG electrospun nanofibers loaded ZnO and CAE by Differential Scanning Calorimetry (DSC) | 79 |
| 4.3.5 Mechanical properties of blended PLA/LPEG and PLA/HPEG electrospun nanofibers by Tensile (ASTM D5034) | 81 |
| 4.3.6 Anti-bacterial activity of 70PLA/30HPEG/2ZnO | 83 |
| 4.3.7 Degradation of 70PLA/30HPEG loaded ZnO and CAE around 5 weeks | 85 |
| 4.3.8 Drug-control release profile of 70PLA/30HPEG/2ZnO loaded CAE | 87 |
| 4.3.9 Cytotoxicity | 89 |
| CHAPTER 5 | 91 |
| CONCLUSION..... | 91 |
| 5.1 Conclusion | 91 |
| 5.2 Recommendations..... | 93 |
| REFERENCES | 94 |
| BIOGRAPHY | 102 |

LIST OF TABLE

| | Page |
|--|-------------|
| Table 1. Various processing techniques of nanofiber fabrication | 19 |
| Table 2. Electrospinning parameters and their effects on fiber morphology [36] | 22 |
| Table 3. Preparation of blended PLA solutions | 31 |
| Table 4. Solubility and stability of blended PLA with LPEG and CS solution | 38 |
| Table 5. Solubility and stability of blended PLA with LPEG and CS solution (continued) | 39 |
| Table 6. Average diameter size of blended PLA/PEG/CS/CAE electrospun fibers..... | 41 |
| Table 7. T_g , T_{cc} , T_m , Enthalpy, and X_c of blended PLA with LPEG, CS loaded CAE. | 52 |
| Table 8. Tensile strength, elongation at break, and young's modulus of PLA, PLA/LPEG, PLA/CS, and PLA/LPEG/CS nanofiber..... | 52 |
| Table 9. Water-contact angles of blended PLA with LPEG or HPEG | 61 |
| Table 10. T_g , T_{cc} , T_m , enthalpy, and %crystallinity of blended PLA/LPEG or PLA/HPEG NFs..... | 70 |
| Table 11. Tensile strength, elongation at break, and young's modulus of blended PLA/LPEG and PLA/HPEG electrospun nanofibers..... | 71 |
| Table 12. Average diameter size of 70PLA/30PLA, 70PLA/30PLA/2ZnO and 70PLA/30PLA/2ZnO/CAE..... | 75 |
| Table 13. Thermal properties of the blended 70PLA/30HPEG NFs loaded ZnO and CAE..... | 81 |
| Table 14. Tensile strength, elongation at Break, and young's modulus of blended 70PLA/30HPEG NFs loaded ZnO and CAE | 81 |
| Table 15. Relative reduction percentage of 70PLA/30HPEG/2ZnO | 84 |
| Table 16. Fitting parameters of drug release of blended 70PLA/30HPEG NFs loaded 2%ZnO and 0.7-2.8%CAE by Korsmeyer-Peppas model | 89 |

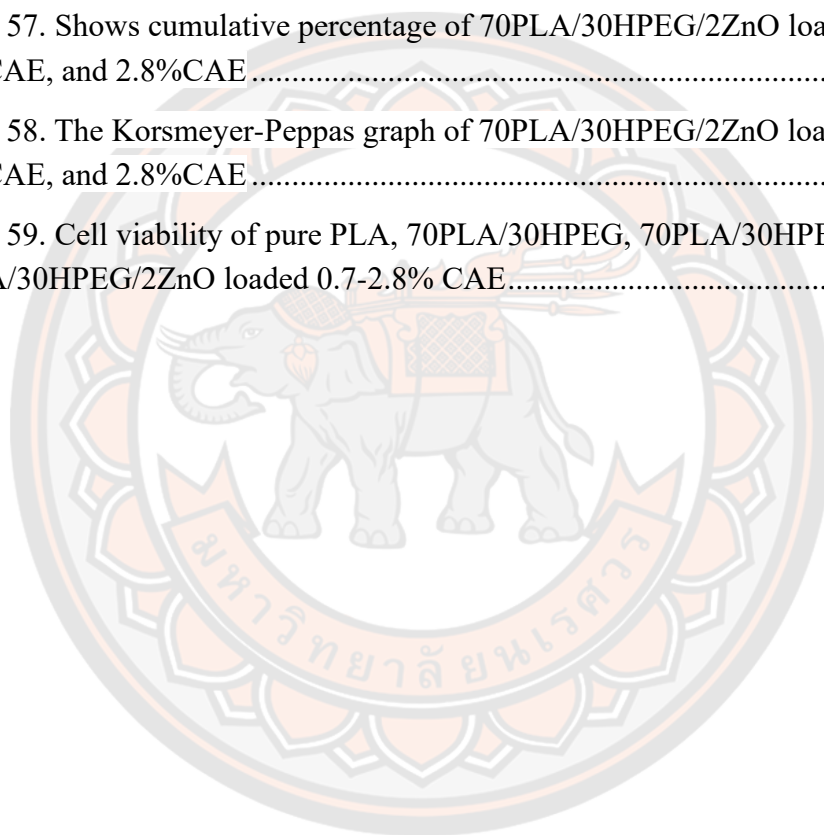
LIST OF FIGURE

| | Page |
|--|-------------|
| Figure 1. Overall concept of blended PLA electrospun nanofibers loaded CAE via electrospinning for wound healing..... | 4 |
| Figure 2. Wound healing response of the skin [9] | 7 |
| Figure 3. Chemical structure of PLA..... | 9 |
| Figure 4. Chemical structure of poly(ethylene glycol) or polyethylene oxide | 10 |
| Figure 5. N-acetyl-D-glucosamine and D-glucosamine linking by $\beta(1\rightarrow4)$ glycosidic bonds of chitin and chitosan [8]..... | 11 |
| Figure 6. ZnO crystal structure [21] | 12 |
| Figure 7. Various mechanisms of anti-microbial activity of the metal and metal oxide nanoparticles [27]..... | 13 |
| Figure 8. Gotu kola or Asiatic pennywort..... | 15 |
| Figure 9. Chemical structure of essential substances in Centella Asiatica, madecassic acid (A), asiatic acid (B), asiaticoside (C), madecassoside (D), asiaticoside B (E) | 15 |
| Figure 10. Simple electrospinning process step by step | 21 |
| Figure 11. Various adopted methods for inclusion of drug into nanofibers [35] | 26 |
| Figure 12. Scheme of preparation of blended PLA nanofibers with LPEG4000 and CS loaded on CAE processing..... | 29 |
| Figure 13. Setting up of electrospinning system..... | 30 |
| Figure 14. Schematic drawing of blended PLA/LPEG or PLA/HPEG electrospun nanofibers processing..... | 31 |
| Figure 15. Schematic drawing of blended 70PLA/HPEG electrospun nanofibers loaded 2%ZnO and 0.7-2.8% CAE processing..... | 32 |
| Figure 16. SEM illustration of blended PLA nanofibers with LPEG and CS-loaded CAE (5 kX)..... | 40 |
| Figure 17. Diameter size distribution of PLA, PLA/LPEG, PLA/CS, and PLA/LPEG/CS..... | 42 |
| Figure 18. Diameter size distribution of PLA/LPEG/CS loaded 0.05, 0.1 and 0.4% wt of CAE | 43 |

| | |
|--|----|
| Figure 19. Contact angle images of blended PLA nanofibers with LPEG and CS-loaded CAE..... | 44 |
| Figure 20. FTIR spectra of the PLA, PLA/LPEG electrospun fibers | 45 |
| Figure 21. FTIR spectra of the CS, PLA, PLA/LPEG, PLA/CS, and PLA/LPEG/CS electrospun fibers | 47 |
| Figure 22. FTIR spectra of the CS, PLA, PLA/LPEG, PLA/CS, and PLA/LPEG/CS electrospun fibers | 48 |
| Figure 23. FTIR spectra at wavenumbers in the range of 1,900-1,400 cm^{-1} of the CS, PLA, PLA/LPEG, PLA/CS, and PLA/LPEG/CS and PLA/LPEG/CS/CAE electrospun fibers | 49 |
| Figure 24. DSC thermogram of electrospun fibers: PLA, PLA/LPEG, PLA/CS, PLA/LPEG/CS, PLA/LPEG/CS/0.05CAE, PLA/LPEG/CS/0.1CAE, and PLA/LPEG/CS/0.4CAE..... | 50 |
| Figure 25. Comparison of tensile strength of PLA, PLA/LPEG, PLA/CS, PLA/LPEG/CS electrospun nanofibers..... | 53 |
| Figure 26. Comparison of elongation at break of PLA, PLA/LPEG, PLA/CS, PLA/LPEG/CS electrospun nanofibers..... | 53 |
| Figure 27. Comparison of modulus of PLA, PLA/LPEG, PLA/CS, PLA/LPEG/CS electrospun nanofibers | 54 |
| Figure 28. SEM illustrations of blended PLA electrospun nanofibers with LPEG and HPEG (5 kX)..... | 56 |
| Figure 29. Comparison of average diameter sizes of PLA, PLA/LPEG, PLA/HPEG electrospun nanofibers | 57 |
| Figure 30. Diameter size distribution of PLA and PLA/LPEG (Ratios of 90:10, 70:30 and 50:50) | 58 |
| Figure 31. Diameter size distribution of PLA and PLA/HPEG (Ratios of 90:10, 70:30 and 50:50) | 59 |
| Figure 32. Contact angle images of blended PLA nanofibers with LPEG or HPEG... | 60 |
| Figure 33. Comparison of water-contact angle of PLA, PLA/LPEG, PLA/HPEG | 61 |
| Figure 34. FTIR spectra of the pure PLA, PLA/LPEG electrospun nanofibers various ratios of 90:10, 70:30 and 50:50 | 62 |
| Figure 35. FTIR spectra of the pure PLA, PLA/HPEG electrospun nanofibers various ratios of 90:10, 70:30 and 50:50 | 63 |

| | |
|--|----|
| Figure 36. Swelling and gel fraction of adding LPEG in PLA electrospun..... | 64 |
| Figure 37. Swelling and gel fraction of adding HPEG in PLA electrospun nanofibers | 65 |
| Figure 38. SEM illustrations of degradation of PLA and PLA/HPEG for 36 days | 66 |
| Figure 39. Degradation graph of PLA and PLA/HPEG various ratios | 67 |
| Figure 40. The first heat of DSC thermograms of blended PLA electrospun fibers: PLA, PLA/LPEG, and PLA/HPEG | 68 |
| Figure 41. The second heat of DSC thermograms of blended PLA electrospun fibers: PLA, PLA/LPEG, and PLA/HPEG | 69 |
| Figure 42. Comparison of tensile strength at break of PLA, PLA/LPEG, PLA/HPEG electrospun nanofibers | 71 |
| Figure 43. Comparison of elongation at break of PLA, PLA/LPEG, PLA/HPEG electrospun nanofibers | 72 |
| Figure 44. Comparison of modulus at break of PLA, PLA/LPEG, PLA/HPEG electrospun nanofibers | 72 |
| Figure 45. SEM illustrations of 70PLA/10LPEG loaded 2%ZnO and various CAE (5 kX) | 74 |
| Figure 46. Diameter size distribution of 70PLA/30HPEG/2ZnO and 70PLA/30HPEG/2ZnO loaded CAE (0.7, 1.4 and 2.8 %wt) | 75 |
| Figure 47. EDS illustrations of 70PLA/10LPEG loaded 2%ZnO and 70PLA/30HPEG/2ZnO/0.7CAE (5 kX) | 76 |
| Figure 48. FTIR spectra of the 70PLA/30HPEG electrospun nanofibers loaded 2%ZnO and various contents of CAE..... | 77 |
| Figure 49. Swelling and gel fraction of adding ZnO and CAE in 70PLA/30HPEG electrospun nanofibers | 78 |
| Figure 50. The first heat of DSC thermograms of blended PLA electrospun fibers: PLA, 70PLA/30HPEG, 70PLA/30HPEG/2ZnO, and 70PLA/30HPEG/2ZnO loaded various contents of CAE | 79 |
| Figure 51. The second heat of DSC thermograms of blended PLA electrospun fibers: PLA, PLA/LPEG, and PLA/HPEG | 80 |
| Figure 52. Comparison of tensile strength of 70PLA/30HPEG/2ZnO and 70PLA/30HPEG/2ZnO loaded various CAE..... | 82 |

| | |
|---|----|
| Figure 53. Comparison of elongation at break of PLA 70PLA/30HPEG/2ZnO and 70PLA/30HPEG/2ZnO loaded various CAE..... | 82 |
| Figure 54. Comparison of modulus of PLA 70PLA/30HPEG/2ZnO and 70PLA/30HPEG/2ZnO loaded various CAE..... | 83 |
| Figure 55. SEM illustrations of degradation of 70PLA/30HPEG and 70PLA/30HPEG loaded 2%ZnO NPs and various contents of CAE for 36 days | 85 |
| Figure 56. %Weight loss of 70PLA/30HPEG/2ZnO loaded 0.7-2.8% CAE for 36 days | 86 |
| Figure 57. Shows cumulative percentage of 70PLA/30HPEG/2ZnO loaded 0.7%CAE, 1.4%CAE, and 2.8%CAE | 87 |
| Figure 58. The Korsmeyer-Peppas graph of 70PLA/30HPEG/2ZnO loaded 0.7%CAE, 1.4%CAE, and 2.8%CAE | 88 |
| Figure 59. Cell viability of pure PLA, 70PLA/30HPEG, 70PLA/30HPEG/2ZnO and 70PLA/30HPEG/2ZnO loaded 0.7-2.8% CAE..... | 90 |



CHAPTER 1

INTRODUCTION

1.1 Introduction

Normally, chronic wound healing is an incredibly complicated process and becomes a challenging problem for medical treatment, especially wounds from diabetes that are difficult to treat by themselves. When wound healing does not progress normally, it is a significant task to both the patient and the medical system. Thus, many researchers make a lot of efforts to develop healing methodologies and advanced medical technologies give more options for wound healing integrated with special medicine dressings. It is necessary to develop new medical materials, especially from natural products, such as drugs, surgery, and wound dressing which will be safe for the patients. Wound dressing is an interesting and important medical material for faster and higher efficient healing and is one of the selected ways for the treatment of diabetic patients or wounds of other diseases.

Currently, a variety of special wound dressing materials are being commercialized, for example, Acticoat: is a wound dressing coated with nano-sized silver metallic particles [1], and Aquacel A is a hydrogel sheet inserted with silver that can absorb lymph from the wound suitable for non-drying wounds and having an infection [2]. Bandages have different forms and characteristics enabling the use and delivery of drugs or active ingredients such as hydrogel, film, or fiber. Nanofiber materials have good physical properties because it has a high surface area and porosity. This makes the drug delivery and passes oxygen efficiently. It may aid in the cell regeneration process to produce new cells for wound healing more effectively, therefore, nanofibers with wound-healing and antimicrobial properties can improve the efficiency of treating patients better. There are several methods of forming fibers. The electrospinning technique is a common, low-cost, and tunable method for generating ultra-fine fibers with some unique properties. It can generate fibers in nano-size and continuous length using electric potential. Previous reports have indicated that nanofibers cause cell adhesion, which aids in cell growth [3]. It can also freeze the enzyme or other biomolecules on the surface of the fiber sheet. In addition, the high porosity of the fiber sheet results in good fluid or gas transmission which controls the evaporation rate of water around the wound that is suitable for use as a

dressings for accidental burns, scalds, or mild torn wounds, etc. Bio-based polymeric materials are much concerned for functional skin substitutes, and wound healing patches. A wide range of natural biopolymers (e.g., cellulose, chitosan, gelatin, hyaluronic acid, and collagen) have been used for the electrospinning of nanofibers to simulate the native tissue matrix and healing of wounds. Polylactides (PLAs), polyhydroxyalkanoates (PHAs), and Poly(ethylene glycol)s (LPEGs) are synthetic bio-based polymers that are commonly applied for electrospinning of wound dressings. Several natural extracts with medicinal properties have been reported for anti-inflammatory and antibacterial properties [3,4,5], among which a prominent extract is *Centella Asiatica* extract (CAE) [5] containing Asiatic acid, Madecassic acid, and Asiaticoside as active compounds that aid in wound healing and the reduction of bacteria. Antibacterial nanofibers are usually fabricated by containing drugs or antibacterial agents in polymers. Some researchers have reported that incorporated Zinc oxide nanoparticles (ZnO NPs) into polymeric nanofibers as multifunctional, antibacterial, and self-cleaning agents revealing a desired performance as a biosafety material with fascinating antibacterial properties for the hospital gowns. and ZnO NPs have attracted great interest worldwide. It is one of the most appropriate sources for wound healing applications by enhancing re-epithelialization while reducing inflammation and bacterial growth [6].

This thesis aims to fabricate biopolymer-based nanofibrous structures through the electrospinning method using PLA, LPEG, CS, and ZnO nanoparticles-loaded *Centella Asiatica* extracts to have solubility properties, reduce inflammation, and be antimicrobial. The physical and chemical properties were analyzed by Scanning Electron Microscopy (SEM), Fourier Transform Infrared FT-IR, Differential Scanning Calorimetry (DSC), tensile test, Water-Contact Angle (WCA), swelling and gel fraction, release profile, degradation, anti-bacterial activity, and cell viability.

1.2 Objectives

- 1) To fabricate nanofibers of blended polylactic acid (PLA) with Poly(ethylene glycol) containing antibacterial agents and loading with *Centella Asiatica* extracts (CAE) by electrospinning technique

2) To study the physical and chemical properties of blended PLA electrospun nanofibers

3) To investigate the anti-bacterial and cytotoxicity properties of blended PLA electrospun nanofibers

4) To develop the blended PLA electrospun membranes for wound healing

1.3 Scope of studies

1) Determinations of the optimal condition of the blending PLA nanofibers contained chitosan and ZnO nanoparticles and loaded *Centella Asiatica* Extracts (CAE) by electrospinning for suitable formulation

2) Characterizations of the physical and chemical properties of the blended PLA electrospun nanofibers using SEM, FTIR, and WCA

3) Investigations of the antibacterial and cytotoxicity of the blended PLA electrospun nanofibers

1.4 Related Works and Studies

Blended PLA loaded with *Centella Asiatica* extracts (CAE) for antibacterial and anti-inflammatory properties was fabricated via electrospinning. The nanofiber sheets are structurally like the extracellular matrix found in the dermal skin structure. This structure is conducive to the adhesion of growth and the movement of fibroblast cells which causes the formation of skin tissue in the wound area quickly. This research applied the electrospinning technique to generate nanofiber wound dressings as it is suitable for developing into imitation wound dressings for the microenvironment of tissue to help wounds heal faster at the same time, the interconnected pore structure of the fiber sheet also allows oxygen in and out cause inflammation fluid exchange and protection of the wound from dehydration. Previous reports of the development of nanofiber wound dressings from *Centella Asiatica* extract, polycaprolactone [6], and gelatin [7] were used as media for fiber-forming. The research presented here differs from the previous reports by developing nanofibrous polymer mats loaded *Centella Asiatica* extract for wound healing and antibacterial for improving the stability of *Centella Asiatica* extracts and increasing the efficiency of treatment and antibacterial by applying chitosan and ZnO nanoparticles as raw materials because the important

properties of chitosan include antibacterial and anti-inflammatory effects. There is an advantage that these substances have good biological activity with living cells and biodegradability.

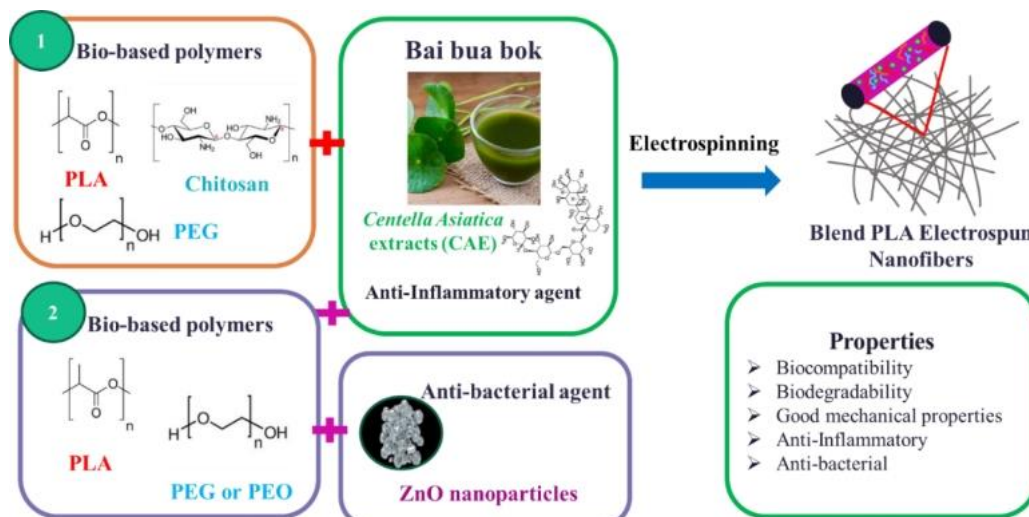


Figure 1. Overall concept of blended PLA electrospun nanofibers loaded CAE via electrospinning for wound healing

1.5 Definitions

PLA = Poly(lactic acid)

LPEG = Low molecular weight Poly(ethylene glycol) (Mw = 4000)

LPEG = Low molecular weight Poly(ethylene glycol) (Mw = 900,000)

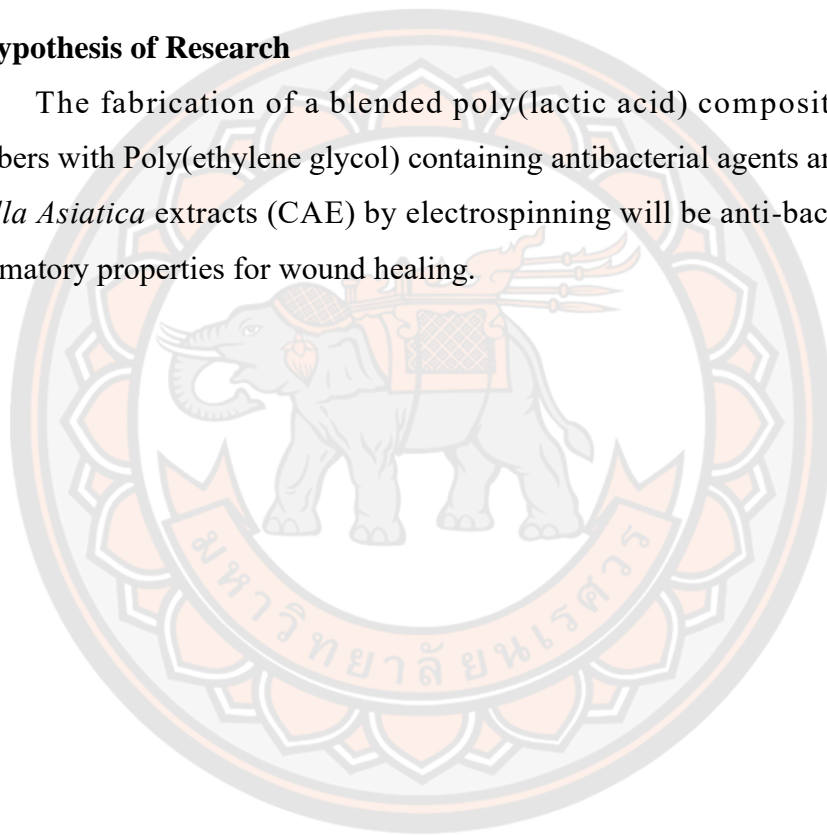
CS = Chitosan

ZnO NPs = Zinc oxide nanoparticles

CAE = *Centella Asiatica* extracts

1.6 Hypothesis of Research

The fabrication of a blended poly(lactic acid) composite electrospun nanofibers with Poly(ethylene glycol) containing antibacterial agents and loading with *Centella Asiatica* extracts (CAE) by electrospinning will be anti-bacterial and anti-inflammatory properties for wound healing.



CHAPTER 2

LITERATURE REVIEWS

2.1 Wound healing

The skin is the human body's largest organ that is exposed to the external environment and protects internal tissues from excessive heat, chemicals, germs, and water loss. Disturbances in the skin's physical structure from wounds are an important problem and require prompt treatment. A wound is defined as an injury or tears on the skin surface by physical, chemical, mechanical, and/or thermal damages. A more scientific definition of a wound is a disruption of normal anatomic structure and function of the skin.

Based on wound healing processes, there are two types of wounds: acute and chronic wounds. Acute wounds are caused by trauma, and the wounds can usually heal within 8 to 12 weeks. These wounds can also be caused by mechanical damage induced by sheer, blunting, and/or stabbing action of hard objects. Acute wounds can also be formed by exposure to extreme heat, irradiation, electrical shock, and/or irritation with corrosive chemicals. The care of these wounds depends on the severity of the wounds. Chronic wounds are injuries produced from specific diseases such as diabetes, tumors, and severe physiological complications. Healing of these wounds might take more than 12 weeks and the recurrence of the wounds is common. Wound healing has generally been simplified by dividing it into phases of hemostasis, inflammation, proliferation, and maturation [9]. Figure 2. shows the sequence of molecular and cellular events in skin wound healing. It is contrary to acute wounds that progress through the various phases of wound healing linearly in healthy individuals, diabetic wounds become stalled, and progression does not occur in synchrony due to diabetes-associated neuropathy and dysfunction of the immune system.

However, chronic wounds unlike the orderly and well-orchestrated process of normal wound healing, chronic wounds are thought to exhibit a persistent pro-inflammatory state that delays or prevents healing. In chronic wounds, a loss of balance between pro-inflammatory cytokines, chemokines, proteases, and their natural inhibitors [9]. Resident neutrophils and activated macrophages in the chronic

wound release proinflammatory cytokines (TNF-alpha, IL-1beta) that increase MMP production and reduce the synthesis of TIMP, which results in the degradation of ECM, impaired cell migration, and reduced fibroblast proliferation and collagen synthesis [10].

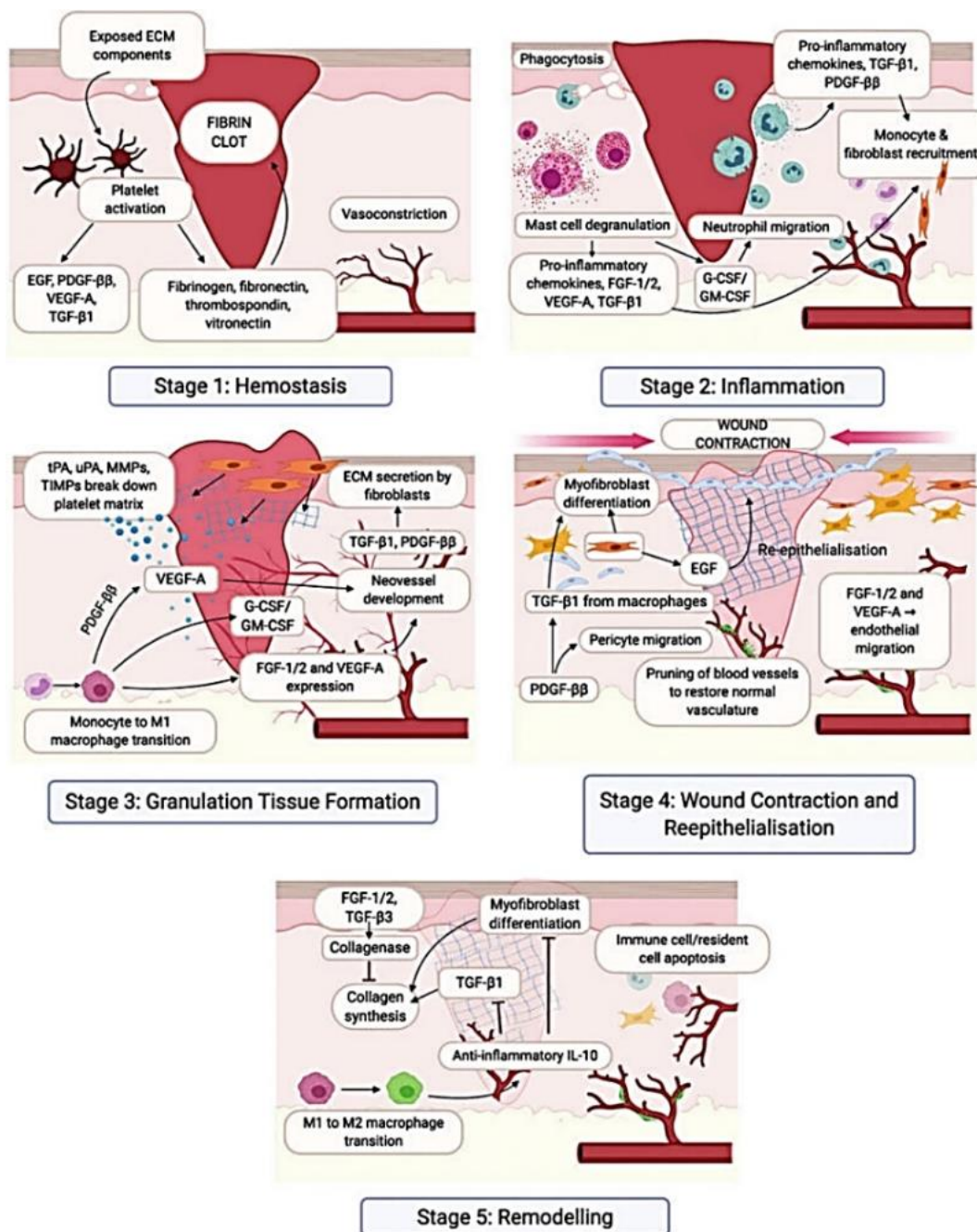


Figure 2. Wound healing response of the skin [9]

Diabetic ulcers are an example of a disorder that tends to slow wound healing. because there is a loss of collagen synthesis. The incidence of atherosclerosis and the process of eating pathogens is reduced. HPEGple with diabetes have atherosclerosis resulting to decrease blood flow, as a result, tissues that receive oxygen and nutrients are reduced. It also affects the nervous system that controls the wound healing process is obstructed resulting in dilation of blood vessels and decreased perception of pain. In addition, the high sugar content of the wound promotes the growth of bacteria, fungi, and yeast [11].

The infection causes the wound to be inflamed which lasts longer, causing it to heal more slowly than usual. Excessive movement of the wound site slows healing. Foreign objects inside the wound will stimulate the body to remove it causing the wound to become inflamed longer than usual. The higher the temperature of the wound, the different chemical reactions. The inside of the cell increases and requires more oxygen. Therefore, the lack of oxygen will cause the wound to heal slowly. To form the granulation tissue, a sufficient supply of oxygen and nutrient is required by blood vessels. A new network of blood vessels is replaced by the damaged one by the process of angiogenesis, formation of extra cellular matrix and collagen generates. With the formation of the granulation tissue damaged mesenchymal cells are converted into the fibroblast cells which acts as a bridge for the movement of the cells around the affected area. In healthy wound, these fibroblasts start to appear within 3 days of the injury and liberate liquids and collagen which help to strengthen the wound site. The wound continues to grow stronger in the proliferation phase with the reorganization of the fibroblast cells and help in the formation of new tissue and accelerate the wound healing process [12].

Standard wound care methods include (1) debridement, or removal of inactive or necrotic tissue to promote cell proliferation, (2) the use of cotton wool or gauze to clean the wound site to treat infection, and (3) wound dressing both to prevent infection and enhance healing [3]. Gauze is currently the most available material for dressing wounds as it is inexpensive and readily for use. However, the gauze material has several disadvantages, for example, highly absorbent, dehydrate the wound (dehydration), and rapidly growing of bacteria. Moreover, it can also cause injury to the newly formed epithelium when the gauze is removed [15]. Several

dressing materials are currently being developed to make them more effective in healing, such as foams, hydrogels, films, and hydrocolloids including nanofiber sheets. Many strategies have been adopted for repairing tissue. Choosing the right dressing is one of the most suitable and convenient way to help the wound heal faster [13-14].

2.2 Biomaterials for wound healing

Polymeric materials offer excellent physical support and enhance biological activity. Recently years had evident extraordinary growth of research and applications of biopolymer materials for new applications in the field of biomedicine and wound healing.

2.2.1 Polylactic acid (PLA)

PLA is a renewable, biocompatible, and biodegradable polymer that has good mechanical and optical properties and is one of the most widely used bioplastics. PLA is obtained either by ring-opening polymerization (ROP) or by direct polycondensation of lactic acid monomer. The monomer is a chiral molecule, existing as d- and l-LA isomers, and can be easily biologically or chemically obtained.

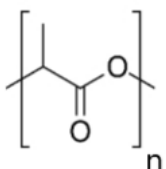


Figure 3. Chemical structure of PLA

PLA can degrade into innocuous lactic acid, making it suitable for use as medical implants in the form of anchors, screws, plates, pins, rods, and mesh. Depending on the type used, it breaks down inside the body within 6 months to 2 years. This gradual degradation is desirable for a support structure because it gradually transfers the load to the body (e.g., to the bone) as that area heals. The strength characteristics of PLA and PLLA implants are well documented. Thanks to its biocompatibility and biodegradability, PLA found interest as a polymeric scaffold for drug delivery purposes [15].

2.2.2 Poly(ethylene glycol) (LPEG)

PEG is a polyether compound derived from petroleum with many applications, from industrial manufacturing to medicine. LPEG is also known as polyethylene oxide (PEO) or polyoxyethylene (POE), depending on its molecular weight. The structure of PEG is commonly expressed as $\text{H}-(\text{O}-\text{CH}_2-\text{CH}_2)_n-\text{OH}$ [3] as displayed in Figure 2.3. PEG is a hydrophilic molecule as it contains hydroxyl group making it a suitable synthetic dressing material for wound healing. The low-toxic PEG macromers are well-bonded advanced textiles for wound care with growth factor-like EGF and can be delivered at the wound site [16]. The mechanical stability of PEG can be enhanced by blending with chitosan and PLGA. Blending also increases the thermal stability and crystallinity of the polymer. PEG-based dressings have been widely used to treat a diabetic wound by promoting and inducing the growth of skin cells and collagen deposition. It also reduces scar formation [16]. The injectable hybrid hydrogel dressing system is developed from PEG-based hyperbranched multiacrylated co-polymer and HA in combination with adipose-derived stem cells to support the viability of cells *in vitro* and *in vivo*. It prevents wound contraction and enhances angiogenesis by acting as a temporary hydrogel wound-healing purpose.

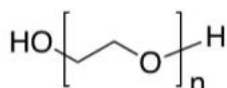


Figure 4. Chemical structure of poly(ethylene glycol) or polyethylene oxide

2.2.3 Chitin-Chitosan (CS)

Chitin is a biodegradable biopolymer. It is found in the exoskeleton of invertebrates such as crab shells, crustaceans, or cell walls of fungi and yeast. Chitin is a polysaccharide composed of N-acetyl-D-glucosamine and D-glucosamine that are connected by $\beta(1\rightarrow4)$ glycosidic bonds (see Figure 2.4). Chitosan is a chitin derivative found only in some fungi in nature. Deacetylation of chitin D-glucosamine is more than 50%. Furthermore, the main difference between chitin and chitosan is their solubility. Chitin is insoluble in aqueous substances. While chitosan is soluble in acidic systems.

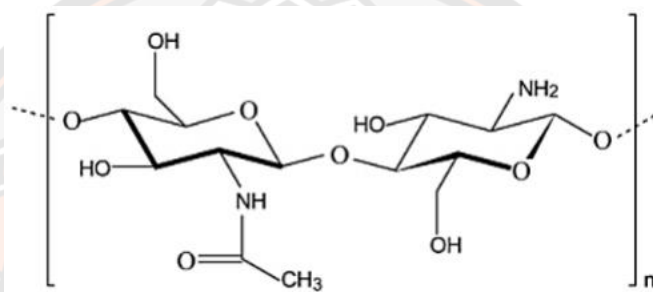


Figure 5. N-acetyl-D-glucosamine and D-glucosamine linking by $\beta(1\rightarrow4)$ glycosidic bonds of chitin and chitosan [8]

Chitosan is extensively used as a functional biomaterial for wound treatment due to its hemostatic effect in the early stages and the ability to inhibit microbial growth and accelerate wound healing [36][17]. The cytotoxicity of two chitosan with similar degrees of deacetylation (DDA) but different molecular weights (120 and 5 kDa) per human keratinocyte cell line HaCaT has been reported [8]. Chitosan was found to induce the release of inflammatory cytokines by HaCaT cells depending on the incubation period and concentration but it did not affect cell viability and proliferation of HaCaT. Chitosan 120 kDa and 5 kDa induce apoptosis mediated by the activation of effect or caspases 3/7. Howling et al. [18] investigated the effects of chitin and chitosan at different DDA but similar molecular weights to the proliferation of human skin cells and cells. In vitro keratinocytes, chitosan with relatively high DDA (89%) was found to strongly stimulate fibroblast proliferation, while subjects with lower DDA showed less activity. The stimulating effect on fibroblast proliferation required serum to be present in the culture medium, indicating that

chitosan may interact with the growth factors present in the serum. In contrast to its stimulating effect on fibroblast, chitosan inhibits human keratinocyte mitogen. These data demonstrate that high-DDA-containing chitosan can pretreat human epidermal cells in vitro.

2.3 Metal and Metal oxide nanoparticles for anti-bacterial

Several types of nanoparticles have received great attention for their potential antimicrobial effects. Metal nanoparticles such as Ag, silver oxide (Ag_2O), titanium dioxide (TiO_2), silicon (Si), copper oxide (CuO), zinc oxide (ZnO), Au, calcium oxide (CaO), and magnesium oxide (MgO) were identified to exhibit antimicrobial activity. ZnO is an interesting material for dose in the nanofiber because of the safety of ZnO and its compatibility with human skin making it a suitable additive for textiles and surfaces that encounter the human body [19,20].

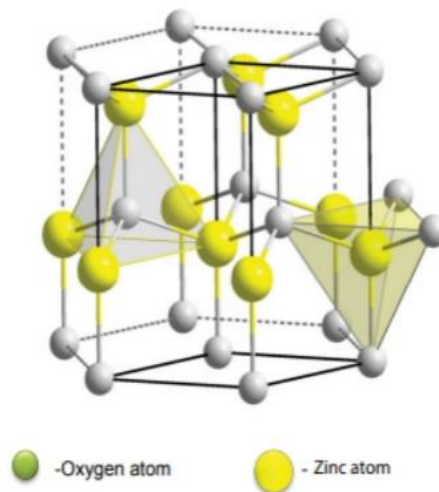


Figure 6. ZnO crystal structure [21]

The unit cell of ZnO is wurtzite (Figure 6.) having a $\text{\AA}c = 3.296$ and $\text{\AA} 5.2065$ with space group $4 C6v$ [22]. However, these lattice parameters may change due to lattice strain, and doping [23]. In the Wurtzite structure, Zn^{2+} and O^{2-} ions are stacked alternately along the c-axis. The top surface is terminated with Zn^{2+} ions while the bottom face is terminated with O^{2-} ions.

ZnO nanoparticles showed Anti-microbial effects on Gram-positive and Gram-negative bacteria as well as the spores which are resistant to high temperature

and high pressure [24]. The improved antibacterial activity of ZnO nanoparticles compared to its microparticles was related to the surface area enhancement in the nanoparticles [25,26].

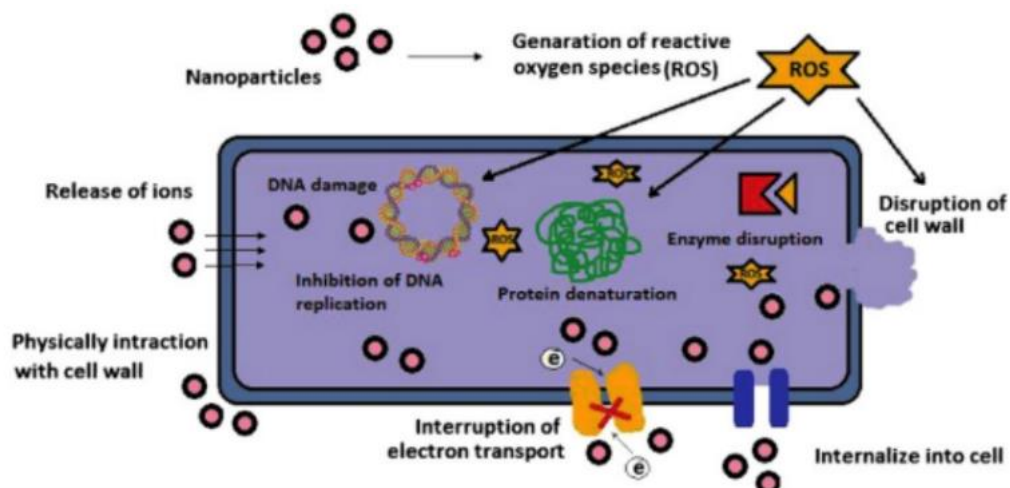


Figure 7. Various mechanisms of anti-microbial activity of the metal and metal oxide nanoparticles [27]

In gram-negative bacteria the cell wall is bi-layer type: the outer membrane is thick while the inner one is a thin (~7-8 nm) plasma membrane of peptidoglycan. However, the cell wall of Gram-positive bacteria consists of a thick (~50 nm) peptidoglycan multilayer. Within the cell wall, the fluid (cytoplasm) content has several complexes of cellulose with 80% water and soluble ions, salts, and nucleic acids. Due to the presence of these ions, the effective charge of the bacteria is usually negative. Cytoplasm controls the production of replica cells- its growth and metabolism and electrical conductivity of the cell. Nanoparticles of particle size ~50 nm can be used to penetrate the cell wall, thus penetrating the cell and affecting the conductivity of the cytoplasm of the bacteria [27].

Padmavathy et al. investigated the antibacterial activity of ZnO nanoparticles with various particle sizes. Their results demonstrated that the bactericidal efficacy of ZnO nanoparticles increased by decreasing particle size [26].

Azam et al. reported a comparative investigation of the antimicrobial activity of ZnO, CuO, and Fe₂O₃ nanoparticles against Gram-negative (*E. coli* and *P. aeruginosa*) and Gram-positive (*S. aureus* and *Bacillus subtilis* (*B. subtilis*)) bacteria.

According to their results, the most bactericidal activity was reported for the ZnO nanoparticles while Fe₂O₃ nanoparticles exhibited the least anti-bacterial effect [24]. ZnO reduces the bacteria viability. However, the exact mechanism of its antibacterial activity has not been well understood so far. One proposed possibility is the generation of hydrogen peroxide as a main factor of the antibacterial activity. It is also believed that the accumulation of the particles on the bacteria's surface due to the electrostatic forces could be another mechanism of the antibacterial effect of ZnO particles [28].

Campylobacter jejuni et al. suggested that the antibacterial mechanism of ZnO nanoparticles might be due to the disruption of the cell membrane and oxidative stress in *C. jejuni*. Their results signified that ZnO nanoparticles caused morphological changes, measurable membrane leakage, and an increase (up to 52-fold) in oxidative stress gene expression in *C. jejuni* [25]. Ag nanoparticles showed antibacterial activity even in ultra-low concentrations; however, the antibacterial activity of ZnO nanoparticles depended on the concentration and surface area. Thus, ZnO nanoparticles in higher concentrations and larger surface areas displayed better antibacterial activity.

Hosseini-Khani et al. investigated the antibacterial characteristics of ZnO nanoparticles against *Shigella dysenteries*. Based on their results, a considerable decrease in the bacteria number was observed because of particle size reduction [29].

Emami-Karvani et al. investigated the antimicrobial activity of ZnO nanoparticles against Gram-negative (*E. coli*) and Gram-positive (*S. aureus*) bacteria. They evaluated the effects of concentration and particle size reduction on the antibacterial activity of ZnO nanoparticles. They found that the antibacterial activity of ZnO nanoparticles increased with decreasing particle size and enhancing powder concentration; nonetheless, ZnO bulk powder showed no significant antibacterial activity [30].

2.4 Gotu kola (*Centella Asiatica (Linnaeus) Urban*) for wound healing



Figure 8. Gotu kola or Asiatic pennywort

Gotu kola or Asiatic pennywort, scientific name *Centella Asiatica (Linnaeus) Urban* is a plant in the family Umbelliferae (Apiaceae). Native names include Phak Wan (South) and Phak Nok (North). Gotu Kola is a tropical and temperate plant native to South Africa. There are distribution areas from Africa, America, Australia, and Asia. which in Asia is found mostly in East Asia and Southeast Asia. The chemical structure of these substances is shown in Figure 9.

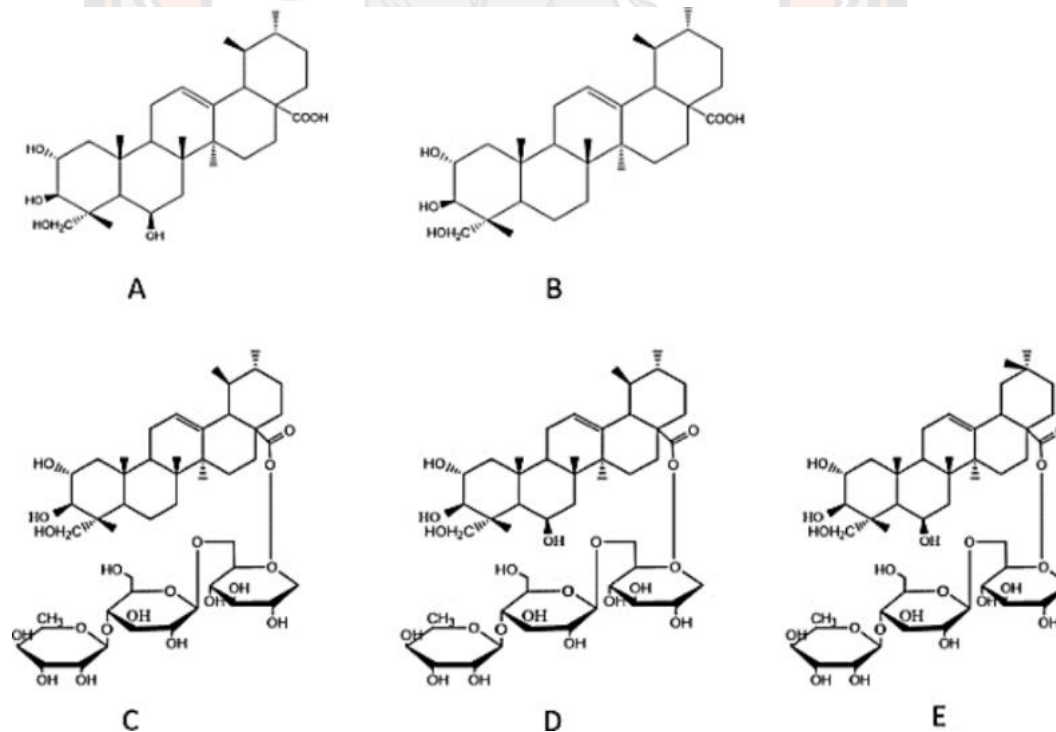


Figure 9. Chemical structure of essential substances in *Centella Asiatica*, madecassic acid (A), asiatic acid (B), asiaticoside (C), madecassoside (D), asiaticoside B (E)

In Thailand, Gotu Kola can be found everywhere in every region. Gotu Kola is an herbaceous plant that is many years old. Some stems spread along the soil surface and have joints. According to the article, roots are inserted into the soil to help hold the stems. In addition, the buds will grow into long branches parallel to the ground, which will grow new roots and stems. The leaves of *Centella Asiatica* are single green leaves in clusters at the base of the plant. The leaf shape is kidney-shaped or rather round, 1-7 cm wide, 1-4 cm long, serrated, or serrated edge, and petiole 5-40 cm long. Leaves and stalks of *Centella Asiatica* are shown in Figure 4. Small flowers, flattened, extended. Propagated by seeds or cuttings with roots and sprouts, can be planted in general. It grows well in clay or loamy soil. The area is wet, but the water does not flood. Can grow well both in the shade and the open air with a lot of sunlight. above-ground plant and fresh leaves Used to eat as a vegetable or to make a drink. Cure heat in fatigue, tonic and can also be applied to fresh wound areas to help heal wounds [31].

The most common substance in *Centella Asiatica* is Triterpenoids (Triterpenoid), which consists of four main substances, including Madecassoside. (Madecassoside) acetone (Asiaticoside), Asiatic acid (Asiatic acid), and madecassic acid (Madecassic acid) [32].

Centella Asiatica has pharmacological effects such as anti-pyretic, anti-bacterial, anti-inflammatory, analgesic, anti-histamine, anti-histamine effects, anti-fungal effect, neuroprotective effect, brain nourishing effects, astringent effect, etc. In the wound healing field, Gotu Kola can be used as an external topical and oral medication to treat wounds. The World Health Organization (WHO) recommended oral dosage of Gotu kola (dose) is 0.33-0.68 g three times a day [32]. Azis et al. In vitro and in vivo, Methanol-extracted Gotu kola extracts contained approximately 2.4% asiaticoside. Results of cytotoxicity by MTT (methyl thiazol tetrazolium) assay on human dermal fibroblast (HDF) and human dermal keratinocyte cells. (HaCaT) No IC50 was found in the extract at concentrations ranging from 100 µg/mL to 0.19 µg/mL. All concentrations tested (0.19–100 µg/mL concentrations) resulted in cell viability greater than 90%, that is, at a high level of cell viability. Concentration 0.19–100 µg/mL, almost no effect. to cytotoxicity. In the scratch assay, parts of Gotu kola

extract extracted with methanol at concentrations of 0.2 µg/mL and 100 µg/mL showed significant effects on HDF and HaCaT cells compared to control samples. An in vivo test showed that a methanol-extracted section of Gotu kola induces collagen synthesis.

Several studies have investigated the healing efficacy of Gotu kola, such as a study by Amin Saeidinia et al., looking at the healing efficacy of superficial burns between ointments prepared from Gotu kola extract and silver sulfadiazine. It is a common antibiotic used to treat burns. Tested on several patients, it was found that the patients who used Gotu kola ointment had better results for burns than the group treated with silver sulfadiazine. when assessed by the elasticity of the wound capillary formation pigment on the skin and visual assessment. In addition, the rate of epithelial formation around the wound Re-epithelialization in the Gotu kola ointment group occurred faster than the silver sulfadiazine group. significantly including making the wound heal faster the mean healing days for Gotu kola ointment was 14.67 ± 1.78 days while for silver sulfadiazine. Can heal wounds completely in 21.53 ± 1.65 days. wound healing faster than using silver sulfadiazine [33].

Weraya Phaocharoen (2010) [31] conducted a randomized controlled study on the efficacy and side effects of Gotu kola extract in treating ulcers in diabetic patients. In 170 diabetic patients who came to be treated at the Department of Surgery, Faculty of Medicine. Thammasat University divided the patients into two groups: a placebo group and group given 50 mg of Gotu kola extract capsules of Asiaticoside extract, 2 capsules 3 times a day after meals for 21 days, for both groups. was treated for diabetes and ulcers as well. Physical examination and wound healing were performed on days 7, 14, and 21. The results showed that the wound healing in the Gotu kola extract group was faster than in the placebo group. No adverse side effects were observed in either group. The results showed that Gotu kola extract accelerated the healing of diabetic wounds and reduced scar formation. without experiencing any side effects or adverse reactions [31].

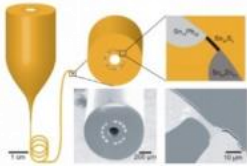
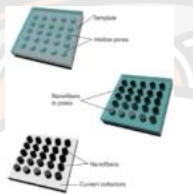
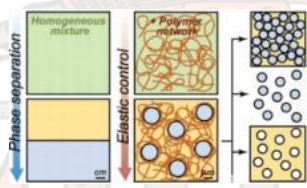
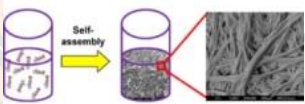
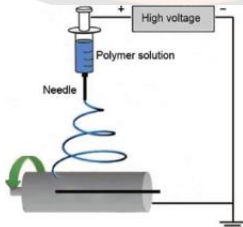
Weerasinghe Muangman (1984) [34] studied the treatment of separating surgical wounds and inflammatory wounds by applying 1 percent Gotu Kola cream to post-surgical inflammation in 14 patients with urinary tract disease, divided twice a day.

2.5 Fabrication techniques of nanofibers

Several processes for nanofiber fabrication such as drawing, template synthesis, phase separation, self-assembly, and electrospinning have been used to prepare nanofibrous polymer in recent years. The drawing is a process like dry spinning in fiber industrial which creates one by one long continuous fiber. However, only viscoelastic material can incur strong deformations while being cohesive enough to support the stresses of developing to creating nanofibers through this process.

- Template synthesis is the process that uses a nanoporous membrane as a template to create nanofibers of solid or hollow shape. This method may build nanotubes and fibrils of various materials that are the most important feature of template syntheses such as electrically conducting polymers, metals, semiconductors, and carbons that can be fabricated but cannot create continuous nanofibers.
- The phase separation consists of dissolution, gelation, and extraction using a different solvent, freezing, and drying that resulted in nanoscale porous foam. This process is a transferring of solid polymer into the nano-porous foam which takes a relatively long period.
- Self-assembly is a process in which individual, pre-existing components organize themselves into desired patterns and functions. However, similarly to phase separation and self-assembly is time-consuming in processing continuous fibrous polymer. Thus, electrospinning seems to be the method that can be further developed for mass production of one-by-one continuous nanofibers from various polymers. Each processing technique has different advantages and disadvantages as illustrated in Table 1.

Table 1. Various processing techniques of nanofiber fabrication

| Techniques | Schematics | Advantages | Disadvantages |
|--------------------|---|---------------------------------|-----------------------------|
| Drawing |  | Minimal equipment requirement | Discontinuous process |
| Template synthesis |  | Easy to vary the small diameter | Discontinuous fiber |
| Phase separation |  | Directly fabricate nanofiber | Limit to a specific polymer |
| Self-assembly |  | Good for obtaining small fiber | Complex process |
| Electrospinning |  | Cost-effective, Simple process | Jet instability |

The most interesting technique belongs to the electrospinning process demonstrated by data that over 200 universities and research institutes worldwide are studying various aspects of the electrospinning process as the nanofibers it produces based on electrospinning have grown in recent years.

2.6 Nanofiber preparation by electrospinning process [35]

Electrospinning is a simple technique for preparing ultrafine fibers from 10 nm to several μm . and very popular process for developing a scaffold in wound healing. It is a method of applying an electric current to a polymer solution or molten polymer of appropriate concentration and viscosity. forming a nanometer to micrometer-scale fiber sheet It has a high surface area and porosity which is beneficial for the development of a wound dressing, i.e., a high surface area material enhances cellular adhesion, enabling faster wound healing. And thanks to the spongy structure, there is good air circulation around the wound. They also found that the nanofiber scaffolds closely resemble the three-dimensional structure of the collagen fiber bundles found in the cell coating. It has been reported in the past that scaffold features strongly influence cellular behaviors such as adhesion and proliferation, the scaffold response. Therefore, the nanoscale fiber structure is a good template for determining the behavior of cell growth.

This technique composes three main important parts a polymer solution or melt, a high voltage power, and a collector. In the electrospinning process, high voltage is applied to a capillary containing a polymer solution or the molten polymer precursor. A droplet of the polymer solution then forms at the tip of the capillary, creating a point known as the “Taylor cone” (the electrostatic force = surface tension). When electrostatic forces overcome the surface tension of the polymer solution, the solution is ejected from the apex of the Taylor cone. The charged jets of polymer solution move towards a collector, the solvent rapidly evaporates, and a non-woven fiber mat was collected on the collector.

The electrospinning process could divide into 6 stages for easy of description: droplet generation; Taylor’s cone formation; launching of the jet; elongation of the straight segment; development of whipping instability and solidification into a fiber.

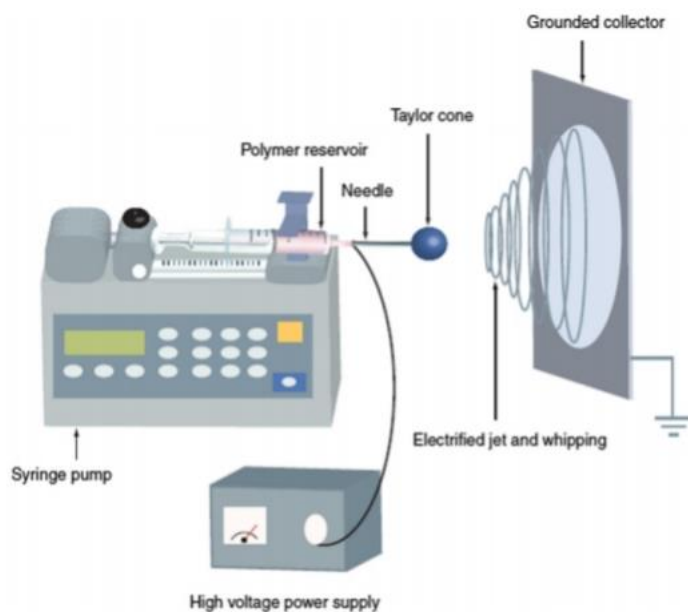


Figure 10. Simple electrospinning process step by step

A droplet of polymer accumulates the charge when the charge increases equal to the surface tension Taylor's cone is observed. Since the electrical force is over than the surface tension of the solution the jet initially launched from the tip of a Taylor cone. The jet of polymer solution is stretched along the electrical field. Many forces such as electrical field, Coulombic force, viscoelastic, gravimetric, etc. cause instability of the jet and as it bends, the jet becomes an invariable series of loops of decreasing diameter, spiraling down to the collector. The whipping instability occurs, the solvent rapidly evaporates, and dried fiber is collected on the collector.

Many varieties of polymer nanofibers have been prepared by electrospinning techniques, such as synthetic and natural polymers, ceramics, and composite materials. Over the years, more than 200 polymers have been electrospun successfully from several natural and synthetic polymers.

In the electrospinning process, there are many parameters that affect fiber formation and structure. The parameter can be classified into solution parameter, process parameter, and environment parameter. Electrospinning parameters and their effects on fiber morphology are shown in Table 2.

The concentration and molecular weight of the polymer influence the viscosity of the solution. If the concentration of polymer increases the solution viscosity will increase.

Table 2. Electrospinning parameters and their effects on fiber morphology [36]

| Parameter | Effect on fiber morphology |
|-----------------------|--|
| Solution parameters | |
| Viscosity | Low-bead generation, high-increase in fiber diameter, disappearance of beads. |
| Concentration | Increase in fiber diameter with increased concentration. |
| Molecular weight | Reduction in the number of beads and droplets with increased molecular weight. |
| Surface tension | No conclusive link with fiber morphology, high surface tension results in the instability of jets. |
| Conductivity | Decrease in fiber diameter with an increase in conductivity. |
| Processing parameters | |
| Applied voltage | Decrease in fiber diameter with an increase in voltage. |
| Distance | Generation of beads with too small and too large distances, The minimum distance required for uniform fibers. |
| Flow rate | Decrease in fiber diameter with a decrease in flow rate, generation of beads with too high flow rate. |
| Needle configuration | 3 types of configurations; single configuration, side-by-side configuration and coaxial configuration. |
| Collector | Influence configuration,,orientation depends on the type of collector |

| Environment parameters | |
|------------------------|---|
| Temperature | An increase in temperature results in a decrease in fiber diameter. |
| Humidity | High humidity results in circular pores on the fibers. |

An important property of wound dressing materials is their antibacterial properties. Past reports suggest that interactions between positively charged chitosan molecules and negatively charged microbial membranes lead to microbial membrane disturbances, and subsequently causing the leakage of proteins and other elements within the cell. Drugs can be loaded into nanofibers by dissolution in polymer solution; suspension in polymer solution, from emulsion with polymer solution, and the use of coaxial electrospinning technique to incorporate drug in inner fiber or coated drug with polymer fibers.

Differentiations of loading methods influence the drug's location in nanofibers. When a drug dissolves in a polymer solution it should be completely dissolved in the polymer matrix at the molecular level. Alternatively, a drug does not dissolve in a polymer solution its crystals can be dispersed in the polymer matrix. Drug emulsified or co-axial spin with polymer solution is enclosed in the polymer matrix yielding a core of the drug encapsulated by a polymer layer. The preparation and drug incorporation affect the release characteristic of the drug from electrospun nanofibers. Many studies have investigated the release of drugs from nanofibers and showed the rapid release (burst release) within the first hours. Experimentally, the fraction of drug released by the polymer matrix (M_t/M_∞) at time t is the quantity most convenient method. The mechanisms of drug release from matrices containing swellable polymers are complex and not completely understood. Some systems may be classified as either pure diffusion or erosion control, while most systems exhibit a combination of these mechanisms.

Andri Hardiansyah et al, (2015) [37], studied chitosan-blended polylactic acid (PLA) nanofibers which were fabricated via an electrospinning process by using a solvent composed of chloroform, water, acetic acid, and ethanol. In particular, the

introduction of ethanol made acetic acid/water and chloroform miscible. The resultant chitosan-blended PLA nanofibers were subject to characterization including scanning electron microscope (SEM), UV-visible spectroscopy, fluorescence microscope, and Fourier transform infrared (FTIR) spectroscopy. The average diameter of chitosan-blended PLA nanofibers decreased with increasing chitosan content. The minimum inhibitory concentration (MIC) of chitosan-blended PLA nanofibers against *Escherichia coli* was 0.015 g/mL when the chitosan to PLA ratio was 4 wt%. Furthermore, chitosan-blended PLA nanofibers exhibited no cytotoxicity to the L-929 cells, suggesting cytocompatibility. These results show that chitosan and PLA can be blended without using highly toxic solvents and the electrospun chitosan-blended PLA nanofibers can potentially be employed for biomedical applications.

Jianming Zhang et al., (2017) [38], studied Polylactic acid (PLA) blended with chitosan (CS) to fabricate electrospun-aligned PLA-CS nanofibers. These prepared nanofibers were aligned using a novel collector made of parallel blades which is designed to increase the transversal electric field across the gap. SEM images show that the fiber diameter mostly ranges between 150 ± 60 nm and Fourier Transform Infrared Spectroscopy (FTIR) analysis confirms the presence of PLA and CS. X-ray diffraction (XRD) studies explain the amorphous nature of electrospun PLA-CS nanofibers, suitable for faster degradation. Degradation studies confirmed that PLA-CS nanofiber has enhanced degradation than pure PLA fibers. Cell studies with human dermal fibroblasts (HDF) show the orientation of cells along the direction of fiber alignment. The results indicate that the prepared PLA-CS-aligned nanofibers are promising materials for skin tissue engineering.

2.7 Drug delivery application of electrospun nanofibers

Electrospun nanofibers possess a high surface area to volume or mass ratio, small inter-fibrous pore size with high porosity, and vast possibilities for surface functionalization. The simplicity of the electrospinning process itself can also provide the ability to conveniently incorporate therapeutic compounds into the electrospun fibers for preparing useful drug delivery systems. Merin Sara Thomas et al., 2018, studied fabricating novel materials for biomedical applications that mostly require the use of biodegradable materials. polylactic acid (PLA) and chitosan (CHS) were used for designing electrospun mats by the electrospinning technique using a mixed solvent system. The addition of chitosan into PLA offered a decrease in fiber diameter in the composites with uniformity in the distribution of fibers with an optimum at 0.4wt% CHS. The fiber formation and the reduction in fiber diameter were confirmed by the SEM micrograph. The current findings are very important for the design and development of new materials based on polylactic acid-chitosan composites for environmental and biomedical applications. [35] The properties of drug and polymer properties are very important and affect the release profile of added drugs. Various methods have been used to load drugs into electrospun nanofibers (see Figure 11).

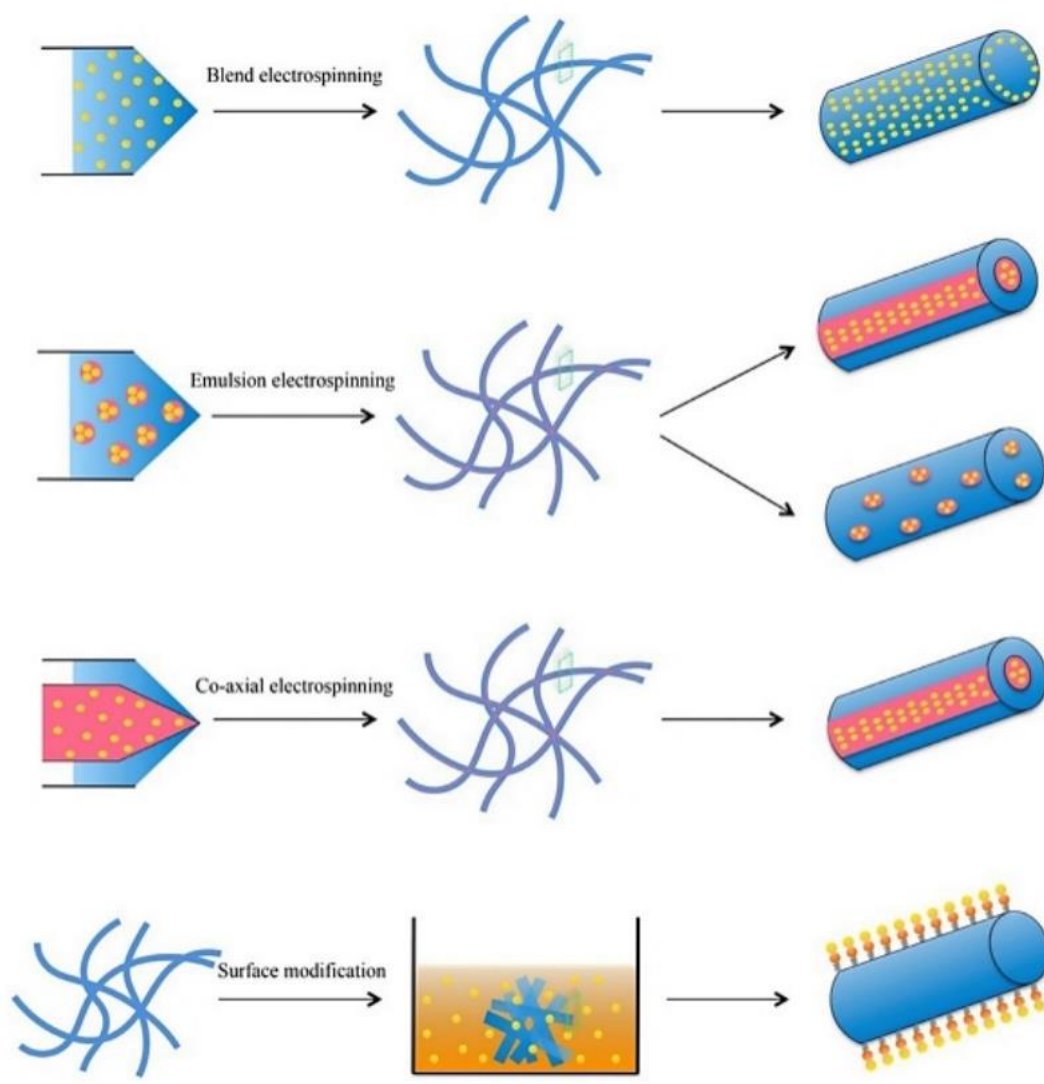


Figure 11. Various adopted methods for inclusion of drug into nanofibers [35]

CHAPTER 3

EXPERIMENTAL

3.1 Chemicals and Materials

1. Polylactic acid (PLA) Mw 150,000 g/mol (Luminy Lx105) Corbion
2. Poly(L-lactide) (PLA) (medical grade) Inherent viscosity 1.67 dl/g from Bioplastic Production Laboratory, Chiang Mai University
3. Poly(ethylene glycol) Mw 4000 Da (LPEG), Merck
4. Chitosan (CS) BIO21
5. Polyethylene oxide HPEG, Mw 900,000 Da (HPEG), Sigma aldrich
6. *Centella Asiatica* extracts (CAE) ECA233
7. Zinc Oxide nanoparticles (ZnO NPs)
8. Chloroform (CF) (99.7%) AR RCI Labscan
9. Acetone (AT) 99.5% AR, RCI Labscan
9. Ethanol (Eth) 95% AR, RCI Labscan
10. Formic acid (FA) 98/100% AR, RCI Labscan
10. Syringe pump
12. Cylinder 1-3 ml
13. Needle
14. Rotational collectors
15. Power supply (high voltage 1-60 kV)
16. Foils
16. Stencil paper
17. Digital weightier

3.2 Experimental

This work was separated into 3 parts including:

1. Preparation of blended PLA with LPEG4000 and chitosan-contained CAE via electrospinning
2. Development of blended PLA electrospun nanofibers with LPEG4000 and HPEG various ratios dissolved in chloroform and acetonitrile for improving flexibility and hydrophilicity
3. Effect of loaded ZnO nanoparticles as antibacterial agents and CAE in the best condition from 2 for the wound dressing.

3.2.1 Fabrication of blended polylactic acid (PLA) electrospun nanofibers with LPEG or HPEG, or Chitosan (CS) loaded *Centella Asiatica* extracts (CAE) via electrospinning

3.2.1.1 Preparation of PLA/LPEG/CS/CAE solution

PLA and LPEG were dissolved in a mixed solvent system between chloroform (CF) and formic acid (FA) (2:1 v/v). First, the 15%PLA solution was prepared in optimized conditions using a mixed solvent including formic acid (FA)/chloroform (CF)/acetone (AT) (3:2:1 v/v/v). Then, LPEG 10% w/w of PLA was added to the 15%PLA solution dissolved with chloroform. CS3.4% wt of PLA was prepared to dissolve in formic acid before being mixed in PLA/LPEG solution and stirred until a well-mixed solution. After that, CAE was added to PLA/LPEG/CS solutions at the concentration range of 0.05-0.4% (w/w) with respect to the polymer content then added ethanol to a concentration of 4.2% v/v to be miscible as shown in Figure 12. This experiment was adapted from K. T. Shalumon et al (2017) [38].

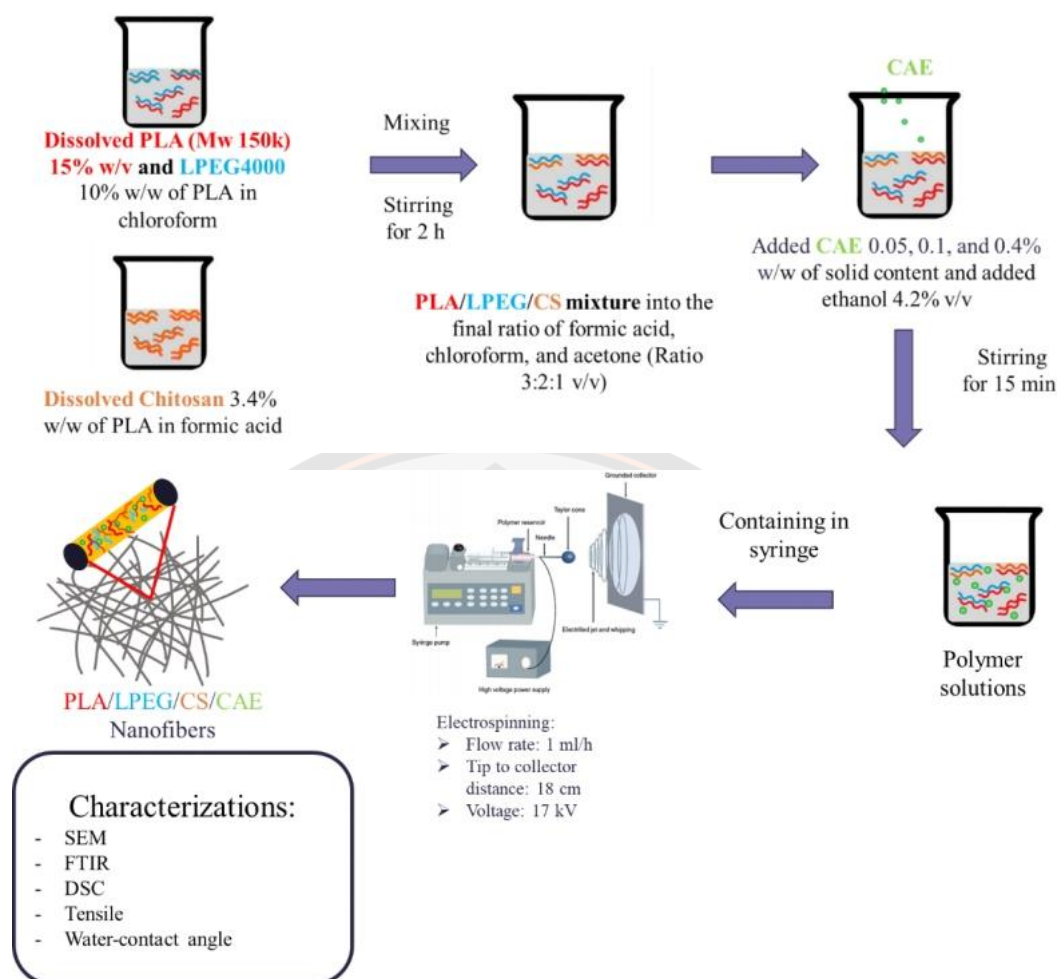


Figure 12. Scheme of preparation of blended PLA nanofibers with LPEG4000 and CS loaded on CAE processing

3.2.1.2 Preparation of blended PLA electrospun nanofiber membrane

All electrospun nanofiber membranes were fabricated using the electrospinning apparatus operating at a feed rate of 1.0 ml h^{-1} using an electric voltage of 17 kV, a distance to the collector of 18 cm. The experiments were performed at relative humidity and temperature, respectively (Figure 13.).



Figure 13. Setting up of electrospinning system

3.2.1.3 Preparation of blend PLA with LPEG or HPEG, ZnO and CAE composite electrospun nanofibers

Polymer solutions were prepared to dissolve in the mixture solvent system between trichloromethane and acetonitrile by the ratio of 60:40 v/v following Table 3. First step, the polymer mixture of poly(L-lactide) (PLA) (Inherent viscosity 1.67 dl/g) and polyethylene oxide (HPEG, M w 900,000 g/mol) was dissolved in trichloromethane. Then the final polymer solution is 7% w/v. and ZnO nanoparticles was prepared 2% w/w of polymers to dispersed in acetonitrile and sonicated for 15 min and adding *Centella Asiatica* extract (CAE, ECA233) 0.7-2.7% w/w of polymers was dissolved in ethanol (98% AR) in the volume ratio of 1:15 v/v (Ethanol: total solvent) before adding in PLA solutions. Afterward, it was stirred for 30 min then sonicated for 30 min. After that, all electrospun nanofiber membranes were prepared using the electrospinning apparatus operating at a feed rate of 1.0 ml h⁻¹ using an electric voltage of 15 kV, a distance to the collector of 15 cm. The experiments were performed at relative humidity and temperature, respectively as shown in Figure 14-15.

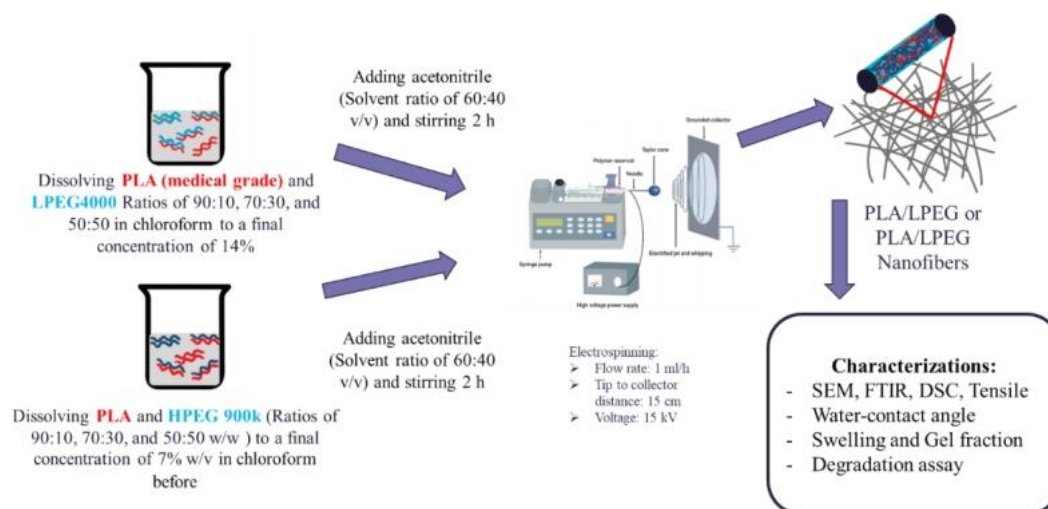


Figure 14. Schematic drawing of blended PLA/LPEG or PLA/HPEG electrospun nanofibers processing

Table 3. Preparation of blended PLA solutions

| NO. | Samples | Polymer concentration (%w/v) | Ratios (PLA : PEG) | ZnO NPs (%w/w) | CAE (%w/w) |
|-----|--------------------------|------------------------------|--------------------|----------------|------------|
| 1 | PLA | 14 | 100:0 | - | - |
| 2 | 90PLA/10LPEG | 14 | 90:10 | - | - |
| 3 | 70PLA/30LPEG | 14 | 70:30 | - | - |
| 4 | 50PLA/50LPEG | 14 | 50:50 | - | - |
| 5 | 90PLA/10HPEG | 7 | 90:10 | - | - |
| 6 | 70PLA/30HPEG | 7 | 70:30 | - | - |
| 7 | 50PLA/50HPEG | 7 | 50:50 | - | - |
| 8 | 70PLA/30HPEG/2ZnO | 7 | 70:30 | 2 | - |
| 9 | 70PLA/30HPEG/2ZnO/0.7CAE | 7 | 70:30 | 2 | 0.7 |
| 10 | 70PLA/30HPEG/2ZnO/1.4CAE | 7 | 70:30 | 2 | 1.4 |
| 11 | 70PLA/30HPEG/2ZnO/2.8CAE | 7 | 70:30 | 2 | 2.8 |

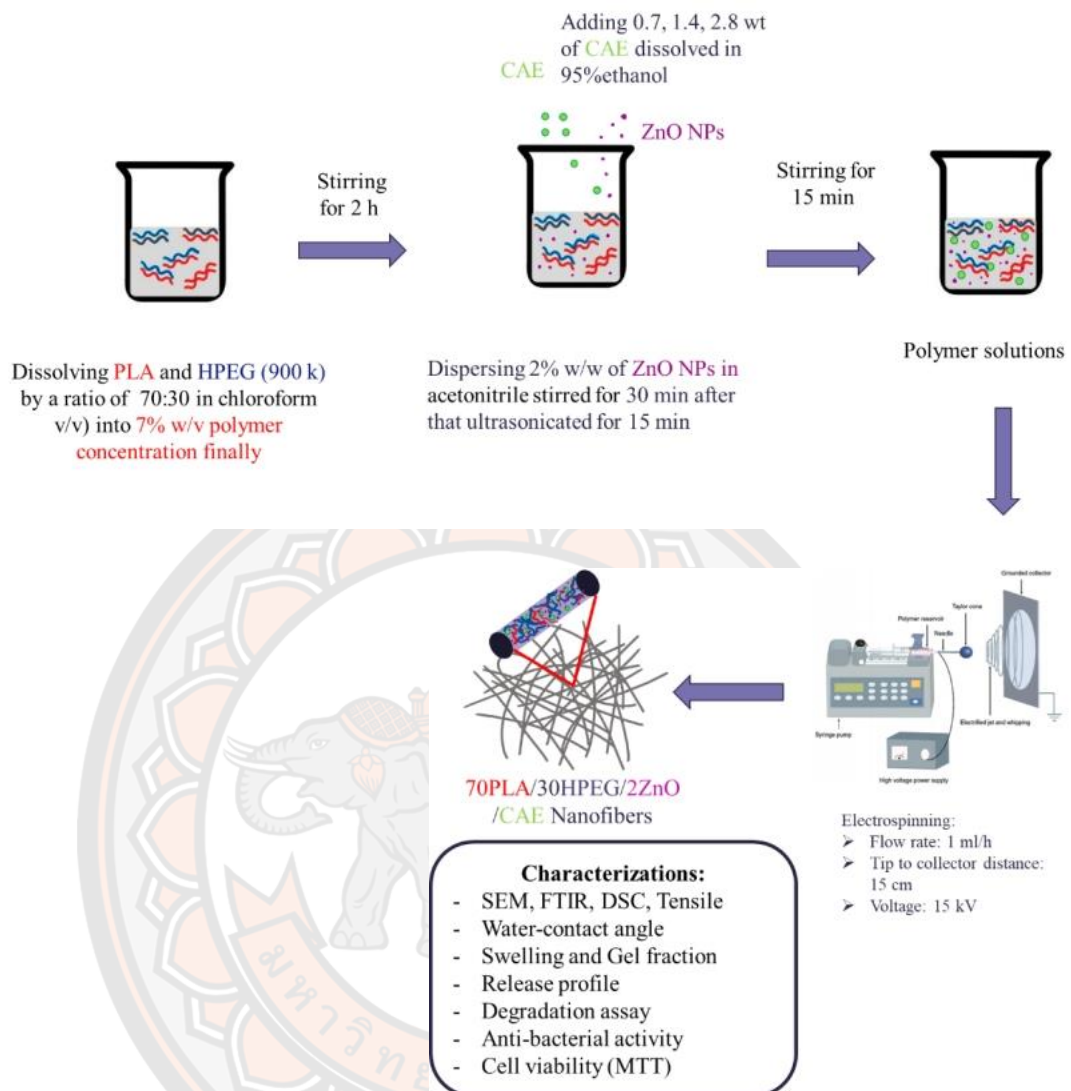


Figure 15. Schematic drawing of blended 70PLA/HPEG electrospun nanofibers loaded 2%ZnO and 0.7-2.8% CAE processing

3.2.2 Characterization of physical and chemical properties of blended PLA electrospun nanofiber loaded *Centella Asiatica* extract (CAE) via electrospinning

3.2.2.1 Morphology and size of the electrospun nanofibers by Scanning Electron Microscopy (SEM)

Samples were cut into a rectangular shape ($0.5 \times 0.5 \text{ cm}^2$), placed onto carbon tape on an aluminum holder, and coated with gold and were taken by Field Emission Scanning Electron Microscope (FESEM) to evaluate surface morphology and the nano-electrospun fiber diameters were measured by ImageJ program (National Institutes of Health version 1.48v). The elemental analysis was measured by energy-dispersive X-ray spectroscopy (EDS, model SAMx) at an accelerating voltage of 100 kV.

3.2.2.2 Analysis of functional group by Fourier Transform Infrared (FTIR)

The FTIR spectra of samples were collected in ATR mode scanning on 4000 cm^{-1} to 400 cm^{-1} .

3.2.2.3 Thermal properties analysis by Differential Scanning Calorimetry (DSC)

All Samples amount of $\sim 10 \text{ mg}$, were cooled down to $25 \text{ }^\circ\text{C}$ and heated up to $250 \text{ }^\circ\text{C}$. After the first heating run, all samples were kept for 2 min at $250 \text{ }^\circ\text{C}$ and then cooled down to $0 \text{ }^\circ\text{C}$ with a cooling rate of $10 \text{ }^\circ\text{C}/\text{min}$ and heated again for a second run up to $250 \text{ }^\circ\text{C}$ with a heating rate of $10 \text{ }^\circ\text{C}/\text{min}$. An empty crucible was used as a reference under a nitrogen atmosphere. The degree of crystallization was determined from the first heating scan thermogram which DH_{mPLA} is the heat of fusion of 100% crystalline PLA (93 J/g) [6], DH_m is the melting enthalpy, DH_{cc} is the cold crystallization enthalpy, and W is the weight fraction of PLA in blended polymers. Calculated following equation 1.

$$\%X_c = \frac{\Delta H_m - \Delta H_{cc}}{\Delta H_m(\text{PLA}) \times W} \times 100 \quad (1)$$

3.2.2.4 Mechanical properties by Tensile testing

Electrospun nanofiber samples were prepared by cutting the rectangular shape of 1x5 cm using load cell 50 N and were measured under the extension rate of 10 mm/min by the Universal Testing Machine (Instron model 4502) according to ASTM D5034.

3.2.2.5 Hydrophilicity analysis by water contact angles (WCA)

Electrospun nanofiber samples were cut into a rectangular shape and placed on a glass slide. The water-contact angle was analyzed on a contact angle illustration (droplet 5 μ L) measured by the CA program and Swelling and Gel fraction test, they were cut into 1.5x1.5 cm and were immersed in DI water 10 ml for 1-7 days calculated by %swelling Eq. 2 and Gel fraction Eq.3

$$\% \text{Swelling} = \frac{W_s - W_d}{W_d} \times 100 \quad (2)$$

where W_s is the weight of swollen samples after soaked already

W_d is the weight of insoluble dried gel which the swollen sample was dried in the oven at 50 °C for 24 h

$$\% \text{Gel fraction} = \frac{W_g}{W_i} \times 100 \quad (3)$$

where W_g is the weight of a before dissoluble sample, W_i is the weight of insoluble dried gel.

3.2.3 Release Profile

The release profile study (*in vitro*) of CAE from PLA/HPEG/ZnO electrospun nanofibers was carried out in a phosphate saline solution (PBS) simulated blood plasma conditions and/or exudate from a wound [33]. The electrospun nanofibers (~100 mg) were immersed in 10 ml of PBS (0.1 mol L⁻¹, pH 7.4) at 37°C under stirring. Then 2 ml of the solution was taken at specific time intervals and analyzed by Microplate reader (MR) at 290 nm. Meanwhile, the same volume of PBS solution was

added to keep the volume constant. The amount of CAE released over time was calculated using the prebuilt calibration curve for CAE in the PBS buffer (pH 7.4). The presented data were average values from three measurements. The cumulative release was calculated using Eq.4.

$$\text{Cumulative Release (\%)} = \frac{M_t}{M_0} \times 100 \quad (4)$$

where M_t (mg) is the mass of CAE released at a certain time (t)

M_0 (mg) is the CAE mass encapsulated in the nanofibers.

The release mechanism was considered based on the value obtained from the Korsmeyer-Peppas model fitting curve [39]. The value was determined considering the portion of the release curve that satisfied the Korsmeyer-Peppas equation [40] and was used to describe the CAE release profile as follows:

$$kt^n = \frac{M_t}{M} \quad (5)$$

where M_t (mg) and M (mg) are the mass of CAE released at an arbitrary time and at equilibrium respectively, k is the release rate constant, and indicates the release exponent suggesting the nature of the release mechanism [35]. Data acquired from drug release studies (*In vitro*) were plotted as log cumulative percentage drug release versus log time.

2.3.4 Degradation assay

Hydrolytic degradation of the electrospun nanofibers was carried out in phosphate buffer solution (pH 7.4, 37°C) for up to 7 weeks, according to the methodology described in [41]. At fixed times, i.e., 7, 14, 21, and 36 days, the electrospun nanofibers were taken out from the medium and characterized regarding morphological changes and weight loss after washing with distilled water and drying.

3.2.5 Analysis of the antibacterial activity of blended PLA electrospun nanofiber membranes

Antibacterial activity (JIS L 1902 (Quantitative)) tested by NSTDA Characterization and Testing Service Center (NCTC), The PLA/HPEG/ZnO and PLA/HPEG/ZnO/CAE electrospun nanofibers (0.1 g) were put into the tube after exposing them to UV- radiation for 15 min. Then, 1 mL of bacteria (*Pseudomonas aeruginosa* ATCC27853 and *Staphylococcus aureus* ATCC6538) suspensions with a concentration of 1.5×10^8 CFU. mL⁻¹ was added to the nutrient broth and was incubated at 37 °C for 18 h afterward, it was added saline and shacked to pour on an agar plate and then was counted to calculate % Reduction absolute and % Reduction relative by Eq.6.

$$\% \text{Reduction} = \frac{N_c - N_t}{N_c} \times 100 \quad (6)$$

Where N_c is the number of organisms recovered from the control

N_t is the number of organisms recovered from the treated sample) / the number of organisms recovered from control.

3.2.6 Analysis of cytotoxicity using cell viability by MTT assay

Cell viability assay of different nanofibrous polymer mats was assessed by the MTT ([3-(4,5-dimethyl- thiazol-2-yl)-2,5-diphenyl tetrazolium bromide]) assay. The cell number and viability were evaluated by measuring the mitochondrial-dependent conversion of the yellow tetrazolium salt MTT. The human foreskin fibroblast (HFF1) cells were cultured using Dulbecco's modified Eagle's medium (DMEM), 10% fetal bovine serum, and 1% penicillin-streptomycin solution. The nanofibrous polymer mates were seeded in 96-well plates at a density of 5×10^4 cells per well and incubated with 5% CO₂ at 37 °C. After 24 and 48 h, the medium of each well was replaced by 10% (v/v) MTT solution and incubated for 4 h. Then, the formed formazan crystals were dissolved in dimethyl sulfoxide, and the optical density was measured with a microplate reader at the wavelength of 570 nm which was calculated from the ratio between the number of cells treated with the nanofibers and that of nontreated cells (control). The samples were then dehydrated through a series of graded ethanol solutions and subsequently dried at room temperature.

CHAPTER 4

RESULTS AND DISCUSSION

This work was separated into 3 parts including:

1. Preparation of blended poly (lactic acid) (PLA) with poly(ethylene glycol) (Mw = 4,000 Da) (LPEG) and Chitosan (CS) and *Centella Asiatica* extracts (CAE)
2. Development of the blended PLA with low and high Mw PEG denoted as LPEG and HPEG, respectively
3. Effect of doping zinc oxide nanoparticles (ZnO NPs) into the blended PLA from the best condition of 2 and loaded *Centella Asiatica* extracts (CAE)

4.1 Results of blended PLA with LPEG and CS and *Centella Asiatica* extracts (CAE)

4.1.1 Solubility of polymer solutions of blended PLA with LPEG and CS

A blended polymer was dissolved in a mixture of solvents with formic acid, chloroform, and acetone. Blended PLA nanofiber with LPEG and chitosan can be prepared in various solvents such as trifluoroacetic acid (TFA) based on the previous reports [18, 19], HCOOH/CHCl₃/acetone (60:20:20) [14, 6], TFA/CH₂Cl₂ (80:20) [26], and TFA/ CH₂Cl₂/DMF (1:1:1) [27]. However, some solvents influence the environment and are highly toxic after processing of spun fiber. Normally, Chitosan can be dissolved only in dilute acid, but the solution cannot be spun into fibers by electrospinning. A concentrated acetic acid solution could dissolve chitosan for electrospinning [45] but it could not dissolve PLA. In this case, the mixture of solvents (HCOOH/CHCl₃/acetone) (3:2:1) and adding ethanol were applied to dissolve all materials simultaneously. Thus, finding proper solvents to dissolve both chitosan and PLA became challenging work. That's why the electrospinning of PLA/LPEG/CS blended has never been reported. It was found that pure PLA is homogeneous with good stability. PLA/LPEG forms emulsion gel resulting from the effect of formic acid. LPEG cross-linking causes the separation layer between polymers with a little solvent. The yellow solution of PLA/CS is from chitosan color

and PLA/LPEG/CS is a separation layer of chitosan on the top after 2 hours because of the effect from LPEG gel as can be seen in Table 4.

Table 4. Solubility and stability of blended PLA with LPEG and CS solution








| No. | Sample name | Solubility | stability | color | Pictures |
|-----|----------------------|--------------|---------------------------------------|---------|---|
| 1. | PLA | Homogeneous | Good | Clear |  |
| 2. | PLA/LPEG | Emulsion gel | small separated LPEG | Brittle |  |
| 3. | PLA/CS | Homogeneous | Good | Yellow |  |
| 4. | PLA/LPEG/CS | Emulsion gel | separated CS layer on top for 3 hours | Yellow |  |
| 5 | PLA/LPEG/CS /0.05CAE | Emulsion gel | separated CS layer like PLA/LPEG/CS | Yellow |  |

Table 5. Solubility and stability of blended PLA with LPEG and CS solution (continued)

| No. | Sample name | Solubility | stability | color | Pictures |
|-----|------------------------|-----------------|--|--------|---|
| 6. | PLA/LPEG/CS/ 0.1CAE | Emulsion gel | separation of layers like PLA/LPE G/CS | Yellow |  |
| 7. | PLA/LPEG/CS/ 0.4CAE | Emulsion gel | separation of layers like PLA/LPE G/CS | Yellow |  |

The solubility and stability of polymer solution are important for the fabrication of electrospun nanofiber because the miscible solution can generate a polymer jet continuously into the collector. Therefore, it is necessary to determine the suitable solvents and the optimum ratio of mixing polymers in the ternary phase of miscible polymer solution. In this work, we try to prepare a mixture of formic acid, chloroform, and acetone at the ratio of 3:1:1 and ethanol for dissolving CAE which is lower toxic than using TFA or fluorine component solvent. The concentration of polymer solution apparently affected the spinnability of the electrospun fiber during spinning.

4.1.2 Morphology of blended PLA electrospun nanofibers with LPEG and CS by Scanning Electron Microscope (SEM)

The morphological identification of electrospun fiber of pure PLA nanofibers and blended PLA/LPEG/CS/CAE nanofibers was measured by SEM as shown in Figure 16 and the comparison of average diameter sizes was illustrated in Figure 17.

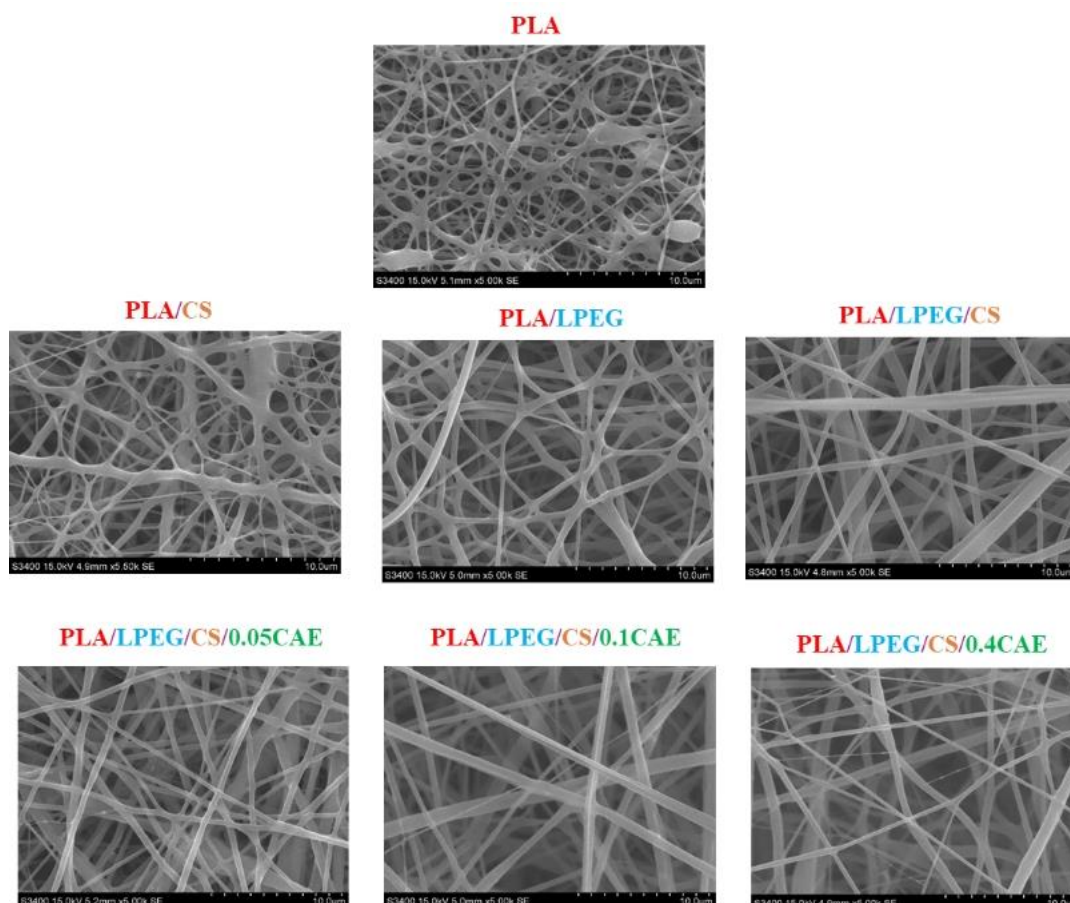


Figure 16. SEM illustration of blended PLA nanofibers with LPEG and CS-loaded CAE (5 kX)

The average diameters of the PLA nanofibers decreased with adding LPEG and chitosan content. PLA nanofibers look like a net. When PLA was added with LPEG, it shows continuous fiber compared to pure PLA fiber. When chitosan was added into PLA, the solution became acidic solution due to the amino group that carries positive charges. This leads to an increase in the charge density of the polymer jet, reflecting the increase in viscosity and conductivity during electrospinning of the

blended PLA/CS. The higher charge density on the surface of the ejected jet was obtained by imposing higher elongation forces on the jet under the electric field. This is because the electric force is proportional to the charge density on the jet, resulting in thinner fibers with smaller diameters due to higher charge density. This is in accordance with the previous study that confirmed the incorporation of LPEG and chitosan with PLA would increase the nanofiber form [17, 42].

Table 6. Average diameter size of blended PLA/PEG/CS/CAE electrospun fibers

| Samples | Average diameter | |
|--------------------|------------------|-----|
| | size (nm) | SD |
| PLA | 413 | 158 |
| PLA/PEG | 662 | 215 |
| PLA/CS | 467 | 184 |
| PLA/PEG/CS | 709 | 364 |
| PLA/PEG/CS/0.05CAE | 549 | 174 |
| PLA/PEG/CS/0.1CAE | 747 | 245 |
| PLA/PEG/CS/0.4CAE | 541 | 283 |

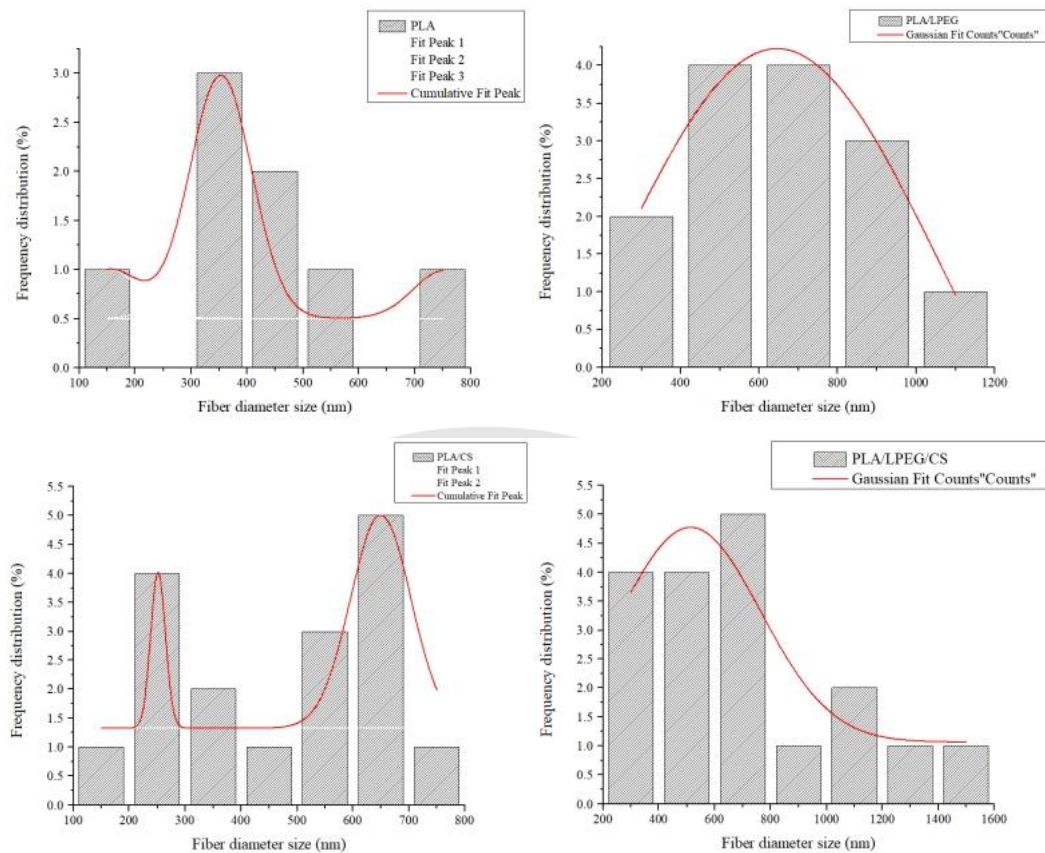


Figure 17. Diameter size distribution of PLA, PLA/LPEG, PLA/CS, and PLA/LPEG/CS

Comparing the average diameter sizes of PLA, PLA/LPEG, PLA/CS, PLA/LPEG/CS, and PLA/LPEG/CS loaded CAE, 0.05, 0.1, and 0.4 % wt were shown in Figure 4.2. It was found that blended PLA and LPEG always give a large size and CS in PLA/LPEG generates the largest size. However, the addition of CAE can reduce the fiber size which can also be affected by adding ethanol and changing some parameters of the polymer solution such as viscosity, conductivity, and boiling point of the mixture solvents. Adding LPEG, CS, and CAE displays better than size distribution that is a slim curve comparing PLA, PLA/LPEG, PLA/CS, and PLA/LPEG/CS

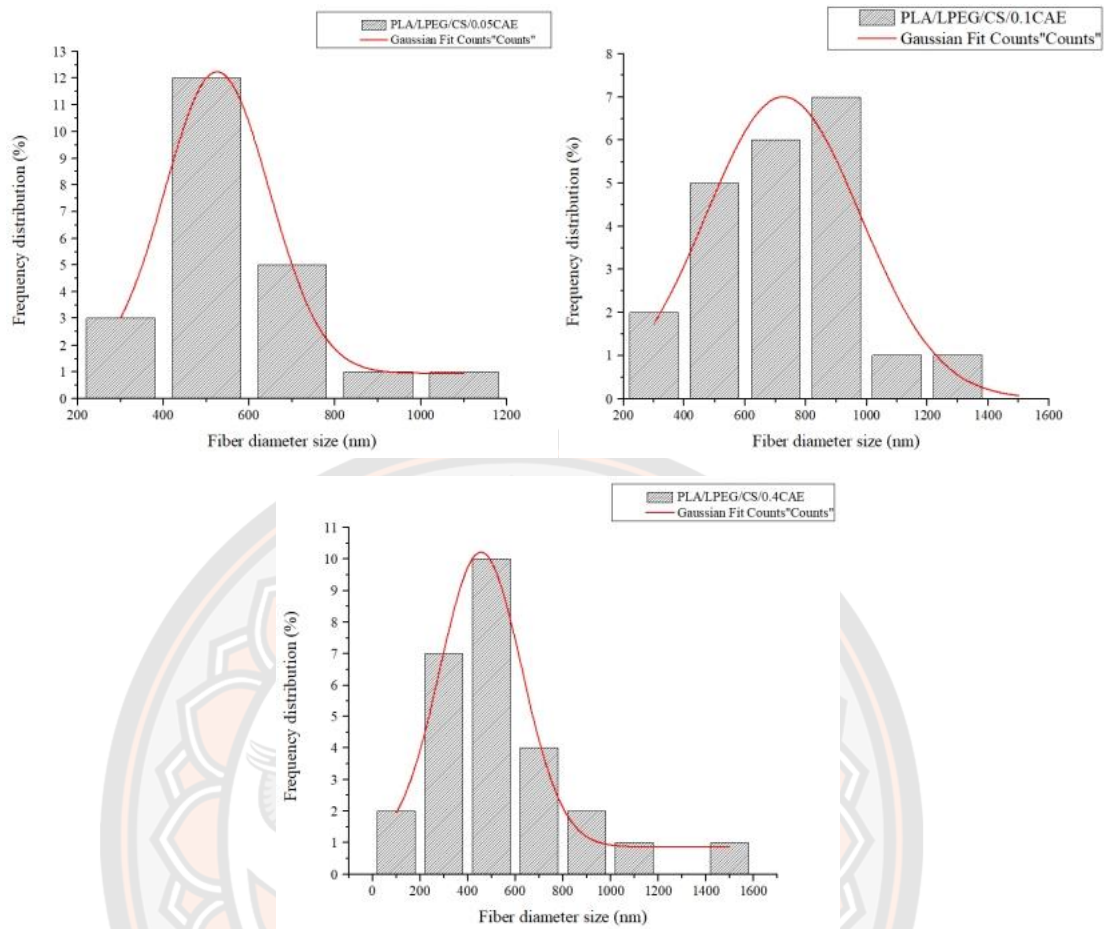


Figure 18. Diameter size distribution of PLA/LPEG/CS loaded 0.05, 0.1 and 0.4% wt of CAE

4.1.3 Water-Contact Angle analysis of the blended PLA electrospun nanofiber with LPEG and Chitosan loaded CAE

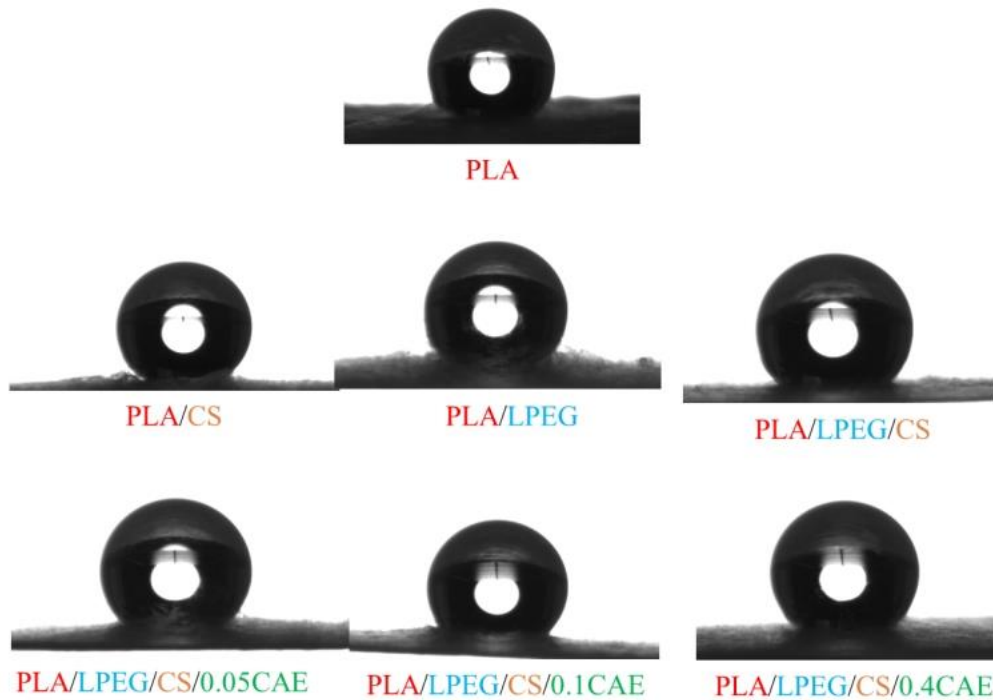


Figure 19. Contact angle images of blended PLA nanofibers with LPEG and CS-loaded CAE

In Figure 19., the contact angle images of all samples show hydrophobicity with a contact angle greater than 90° . The nanofibers have the characteristics of the lotus effect phenomenon which has the appearance of small pore spaces as evidenced from SEM image. This might be due to the influence of PLA as based polymer which is hydrophobic and it might be possible that the low ratio of LPEG which gives a small area of the fiber surface could affect the hydrophobic fibers of each sample as follows: PLA 118.9° , PLA/LPEG 117.9° , PLA/CS 133.6° , PLA/LPEG/CS 130° , PLA/LPEG/CS/0.05CAE 133° , PLA/LPEG/CS/0.1CAE 133.6° , and PLA/LPEG/CS/0.4CAE 130.7°

In addition, it does not show a wettability on the surface of electrospun fiber membranes even the fibers contain many hydroxyl -OH groups on the fiber surface through adding LPEG, CS, and CAE. Thus, all samples of blended PLA with 10%LPEG4000 and 3.4 CS are not hydrophilic materials.

4.1.4 Chemical analysis for Functional group by Fourier transform infrared (FTIR)

The functional groups of blended PLA nanofibers confirmed the polarity of the fibers as the apparency of hydroxyl group (-OH) of LPEG and amino group (-NH₂) of CS by the Fourier Transform Infrared (FTIR).

a) Adding LPEG in PLA nanofiber

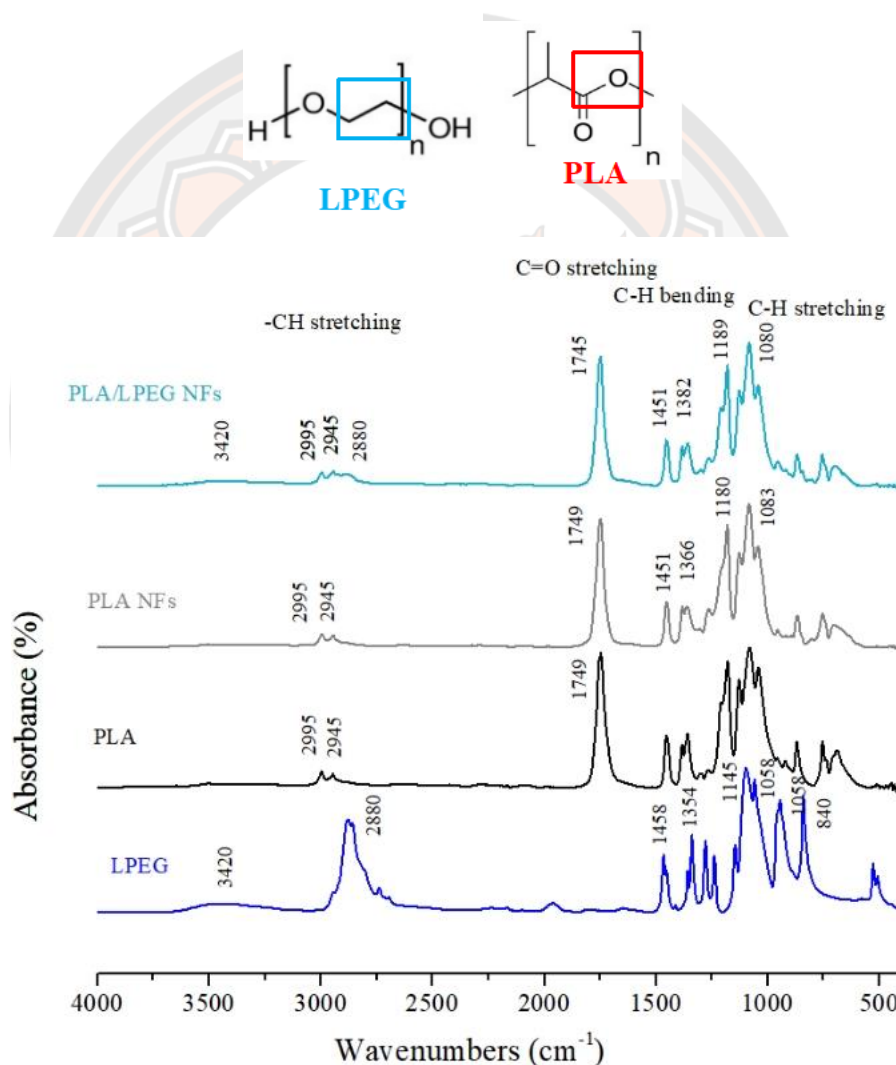


Figure 20. FTIR spectra of the PLA, PLA/LPEG electrospun fibers

As displayed in Figure 20., the FTIR spectroscopy of the PLA, LPEG4000, pure PLA electrospun, and blended PLA electrospun nanofibers with LPEG. The

FTIR spectrum of neat PLA depicted characteristic absorption bands at 1747 and 2997 cm^{-1} that was due to the characteristic C=O and C-H vibrations and the peaks at 1179, 1128, and 1082 cm^{-1} represented the C-O-C linkage of the backbone ester group of PLA. The PLA nanofibers (PLA NFs) displayed at 2995, 1749, 1180, 1127 and 1083 cm^{-1} respectively. LPEG4000 displayed strong characteristic absorption peaks of C-O, C-C stretching, CH₂ rocking, CH₂ rocking, CH₂ twisting C-O, C-C stretching, CH₂ rocking, C-O, C-C stretching, C-O stretching, CH₂ rocking, CH₂ twisting, CH₂ wagging and CH₂ scissoring at 840, 945, 1058, 1097, 1145, 1229 and 1278, 1340 and 1465 cm^{-1} respectively. Obviously, in the blended PLA/LPEG electrospun nanofibers, the peak position of these spectra almost changed. The characteristic peak of PLA was weak because PLA does not have enough -OH groups to form hydrogen bonds with -OH groups of 3420 cm^{-1} when added LPEG which displays the peaks at 2880, and 1745 cm^{-1} with relatively lesser intensity corresponding to the absorption values of C-O of the carboxylic group of PLA whereas those at 2945, and 1382 cm^{-1} correspond to the asymmetric bending of CH and acyclic C-C.

b) Adding CS in PLA and PLA/LPEG nanofiber

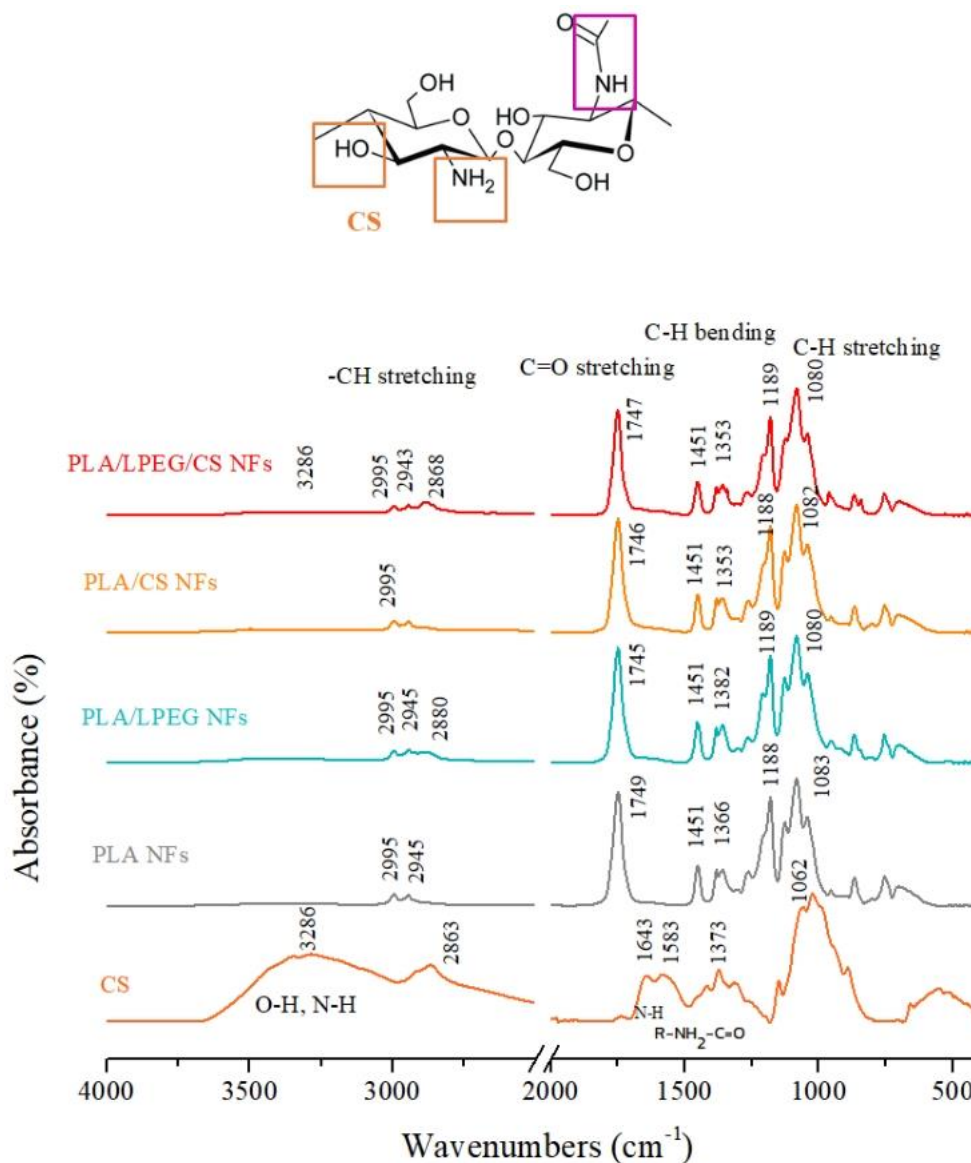


Figure 21. FTIR spectra of the CS, PLA, PLA/LPEG, PLA/CS, and PLA/LPEG/CS electrospun fibers

Chitosan depicted characteristic absorption bands at 3286 cm^{-1} corresponding to the N–H stretching vibrations and those at 1643 , 1583 , and 1318 cm^{-1} which correlates to the amide I and II and a weak peak at 1373 cm^{-1} is the amide III characteristic absorption bands respectively. FTIR spectra of the blended PLA/CS and PLA/LPEG/CS electrospun nanofibers show the peak position of these spectra that may explain the molecular interaction between LPEG, chitosan, and PLA was

weak because PLA does not have enough $-OH$ groups to form hydrogen bonds with $-OH$ groups and $-NH_2$ groups in chitosan. The samples added with LPEG reveals the peaks at 2880, and 1745 cm^{-1} with relatively lesser intensity resulting from the absorption values of C-O of the carboxylic group of PLA whereas those at 2945, and 1382 cm^{-1} relate to the asymmetric bending of CH and acyclic C-C, amide II of CS presented in PLA/CS. All these results confirm the existence of PLA, LPEG, and CS in PLA/LPEG/CS electrospun nanofibers.

c) Adding CAE in PLA/LPEG/CS nanofiber

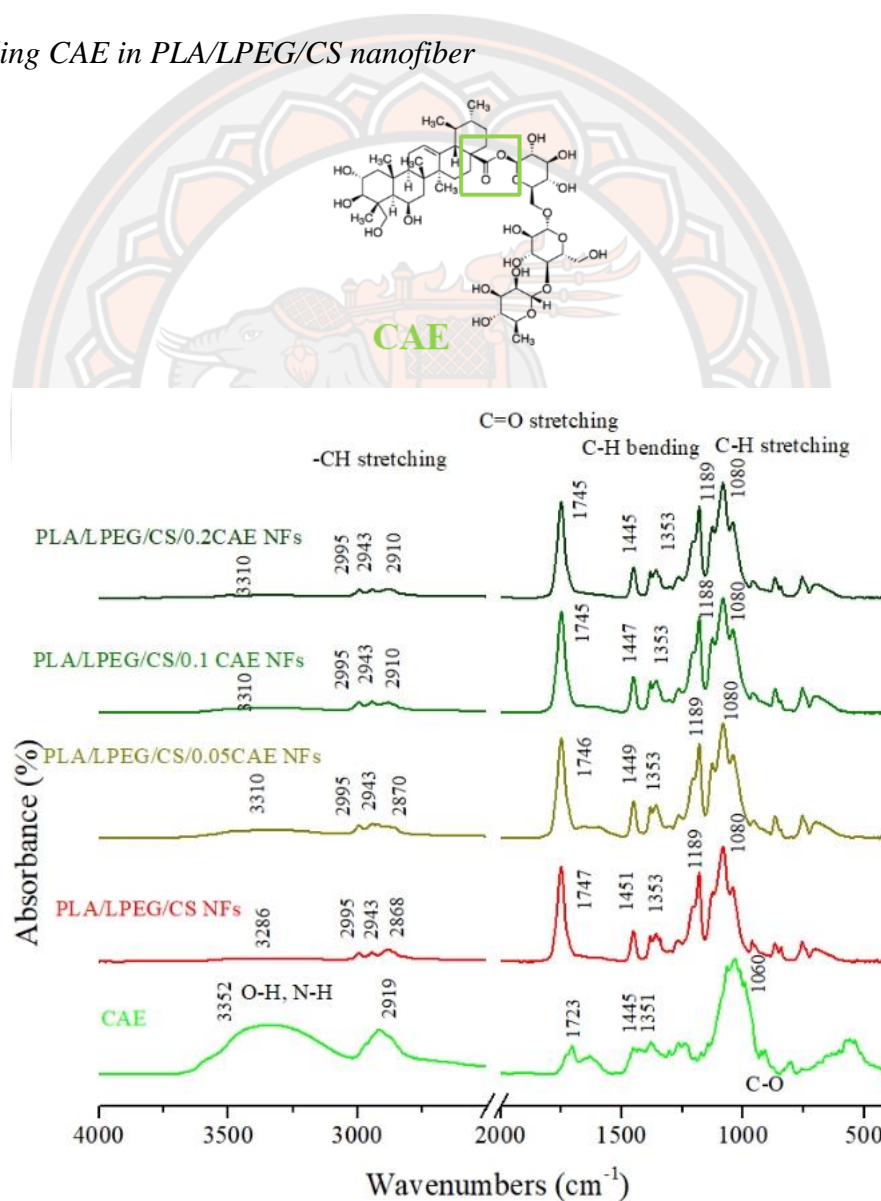


Figure 22. FTIR spectra of the CS, PLA, PLA/LPEG, PLA/CS, and PLA/LPEG/CS electrospun fibers

CAE shows the peaks at 3352, 2919, 1633, 1445 and 1060 cm^{-1} which are the possible functional groups of -OH, -CH stretching, R-NH₂-C=O, C-H bending, and C-O, respectively. All samples adding CAE show the broad peak at 3352 cm^{-1} and the peak at 2868 cm^{-1} is shifted to 2870, 2910, 2910 cm^{-1} in PLA/LPEG/CS/0.05CAE, PLA/LPEG/CS/0.1CAE and PLA/LPEG/CS/ 0.4CAE, respectively.

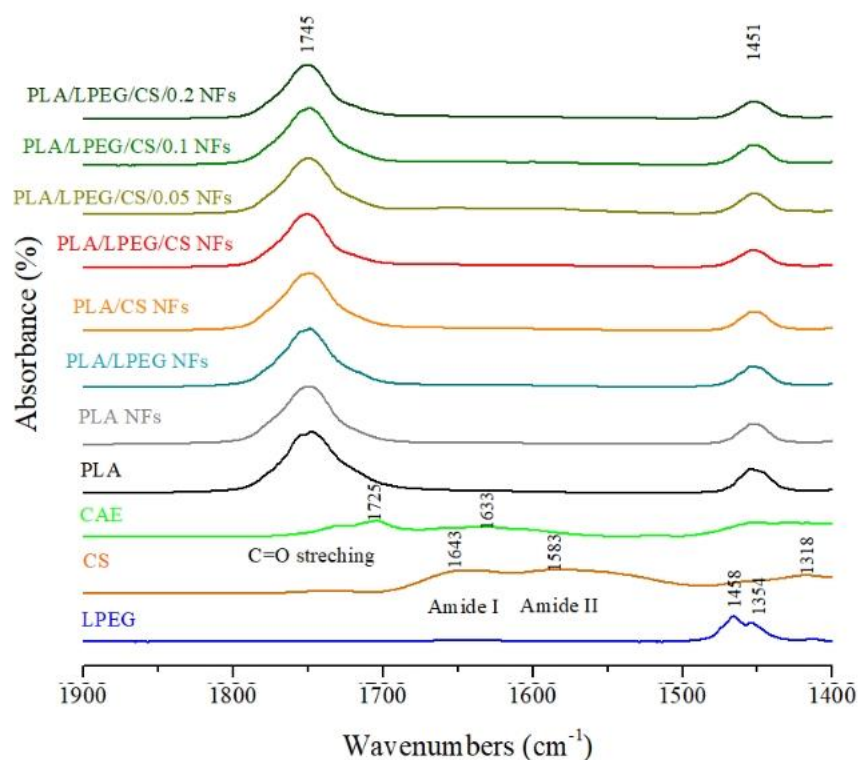


Figure 23. FTIR spectra at wavenumbers in the range of 1,900-1,400 cm^{-1} of the CS, PLA, PLA/LPEG, PLA/CS, and PLA/LPEG/CS and PLA/LPEG/CS/CAE electrospun fibers

Figure 23. shows the relation of the peak position in the range of 1,900-1,400 cm^{-1} that is N-H stretching vibrations on chitosan at 1643, 1583, and 1318 cm^{-1} which corresponds to the amide I and II and a weak peak at 1373 cm^{-1} represents the amide III characteristic absorption bands, and 1633 corresponds to R-NH₂-C=O in CAE while in the blended PLA of all samples do not displays the peak of CS and CAE because of the low intensity of peak. This can be concluded that polymer solution with low solubility could not provide the quality of spinnability.

4.1.5 Thermal Properties blended PLA electrospun nanofibers with LPEG and CS loaded CAE by Differential Scanning Calorimetry (DSC)

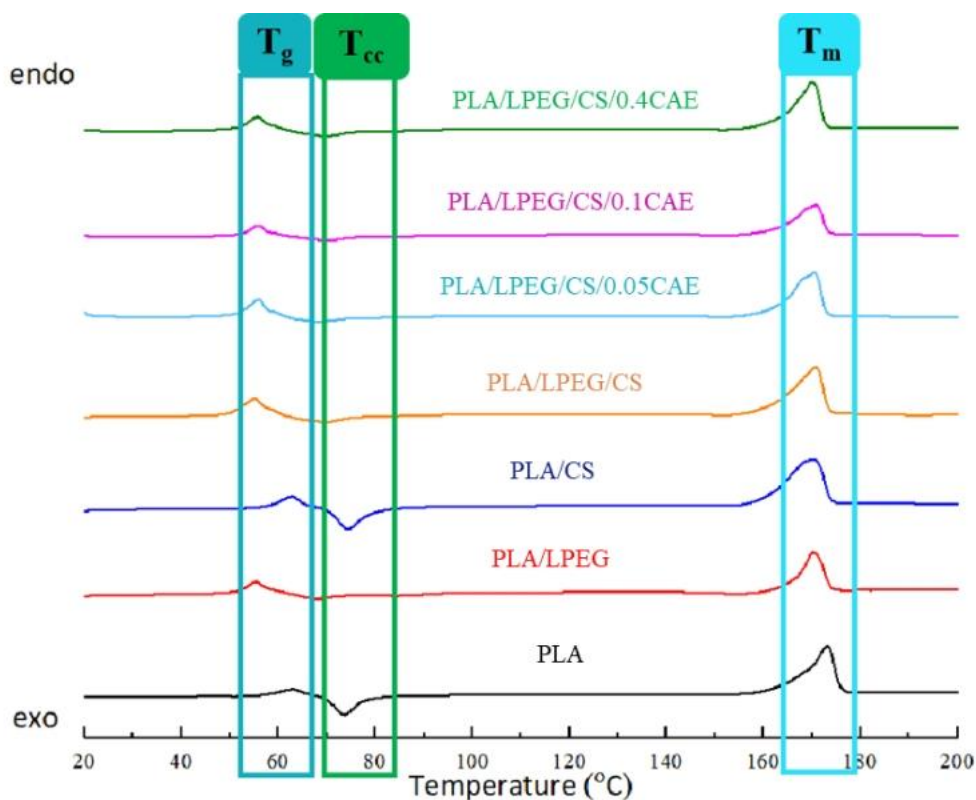


Figure 24. DSC thermogram of electrospun fibers: PLA, PLA/LPEG, PLA/CS, PLA/LPEG/CS, PLA/LPEG/CS/0.05CAE, PLA/LPEG/CS/0.1CAE, and PLA/LPEG/CS/0.4CAE

DSC technique was used to analyze thermal properties of electrospun nanofibers. The DSC thermograms in Figure 24. were obtained from the first heating scan. The nanofibers showed a glass transition temperature (T_g), a cold crystallization temperature (T_{cc}), and a melting temperature (T_m) typical peak of PLA and PLA blended with LPEG and CS. Degree of crystallinity (X_c) are listed in Table 7. It can be observed that the T_g of PLA significantly decreased after the addition of 10 wt% of LPEG4000 to the blended because LPEG acted as a plasticizer to improve the flexibility of PLA . The T_g of pure PLA nanofiber was ~ 63 °C whereas T_g of PLA/LPEG was ~ 55 °C. When adding Chitosan 3.4 %wt into PLA, T_g of PLA/CS

was ~ 63 °C, PLA/LPEG/CS promoting the plasticization effect of LPEG as T_g of samples decreased with adding LPEG and chitosan content.

This synergy was clearly observed in the PLA/LPEG/CS loaded CAE samples, which showed the lowest T_g of 55 °C for samples, Both LPEG and chitosan acted as nucleating agents by reducing T_{cc} of PLA, PLA NFs, PLA/LPEG and PLA/CS showed T_{cc} at 74 °C while PLA/LPEG/CS, PLA/LPEG/CS/0.05CAE, PLA/LPEG/CS/0.1CAE and PLA/LPEG/CS0.4CAE exists T_{cc} at 70°C. It seemed that a mixture of LPEG and chitosan produced the lowest and it significantly dropped approximately ~ 4 °C after mixing with chitosan and LPEG and CAE. The occurrence of cold crystallization affected the melting enthalpy of PLA. In this case, ΔH_m in the DSC thermogram was a result of the initial crystallinity of PLA and the crystallinity during heating in DSC analysis (ΔH_{cc}). By excluding ΔH_{cc} , X_c represented the original degree of crystallization of samples. LPEG and chitosan affect the crystallinity of PLA nanofiber that X_c was decreased with adding LPEG and was increased by adding LPEG and CS. This might affect the mechanical properties of PLA/LPEG/CS nanofibrous polymers.

Table 7. T_g , T_{cc} , T_m , Enthalpy, and X_c of blended PLA with LPEG, CS loaded CAE

| Samples | T_{gPLA} (°C) | T_{cc} (°C) | T_{mPLA} (°C) | W_{PLA} | DH_m (J/g) | DH_{cc} (J/g) | X_c (%) |
|-------------------------|--------------------|------------------|--------------------|-----------|-----------------|--------------------|-----------|
| PLA | 63 | 74 | 173 | 1.000 | 55 | 19 | 39 |
| PLA/LPEG | 55 | 74 | 170 | 0.909 | 30 | 9 | 25 |
| PLA/CS | 63 | 74 | 170 | 0.967 | 53 | 19 | 38 |
| PLA/LPEG/CS | 55 | 70 | 171 | 0.882 | 51 | 9 | 51 |
| PLA/LPEG/CS/ 0.05CAE | 56 | 69 | 170 | 0.881 | 56 | 10 | 56 |
| PLA/LPEG/CS/ 0.1CAE | 56 | 70 | 171 | 0.881 | 51 | 8 | 52 |
| PLA/LPEG/CS/ 0.4CAE | 56 | 70 | 170 | 0.878 | 51 | 7 | 54 |

4.1.6 Mechanical properties of blended PLA electrospun nanofibers with LPEG and CS loaded CAE

Table 8. Tensile strength, elongation at break, and young's modulus of PLA, PLA/LPEG, PLA/CS, and PLA/LPEG/CS nanofiber

| Samples | Tensile strength (MPa) | Elongation at Break (%) | Young's Modulus (MPa) |
|-------------|---------------------------|----------------------------|--------------------------|
| PLA | 0.63 | 46.00 | 20.50 |
| PLA/LPEG | 0.54 | 84.00 | 30.15 |
| PLA/CS | 0.43 | 75.25 | 35.58 |
| PLA/LPEG/CS | 1.18 | 72.46 | 173.21 |

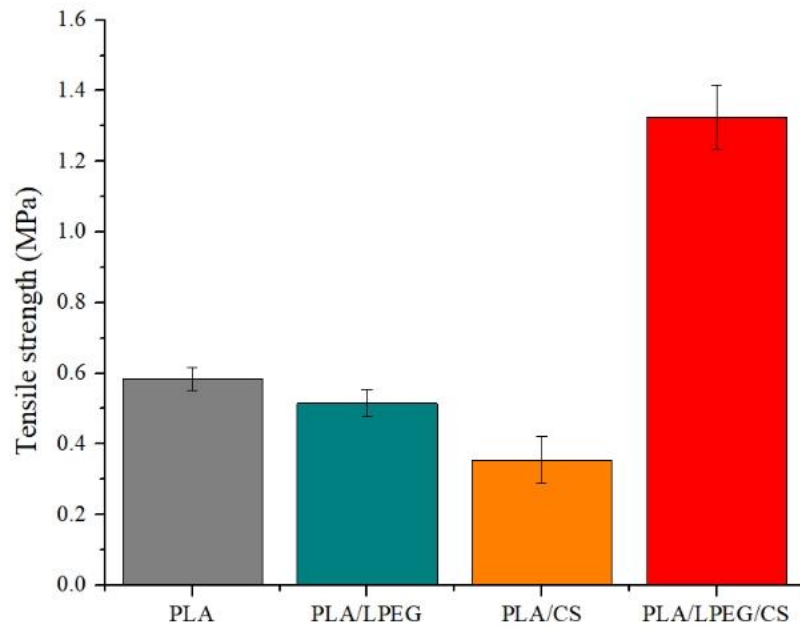


Figure 25. Comparison of tensile strength of PLA, PLA/LPEG, PLA/CS, PLA/LPEG/CS electrospun nanofibers

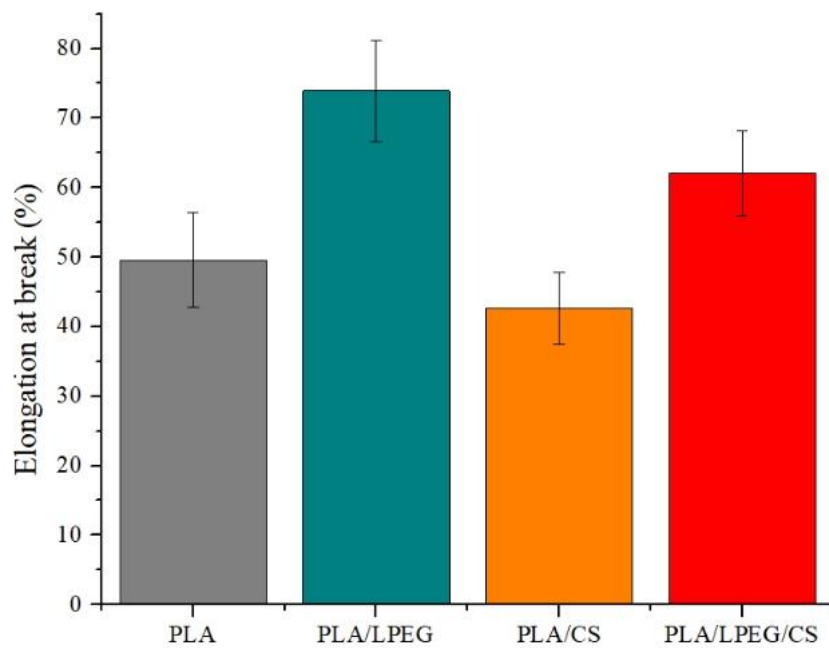


Figure 26. Comparison of elongation at break of PLA, PLA/LPEG, PLA/CS, PLA/LPEG/CS electrospun nanofibers

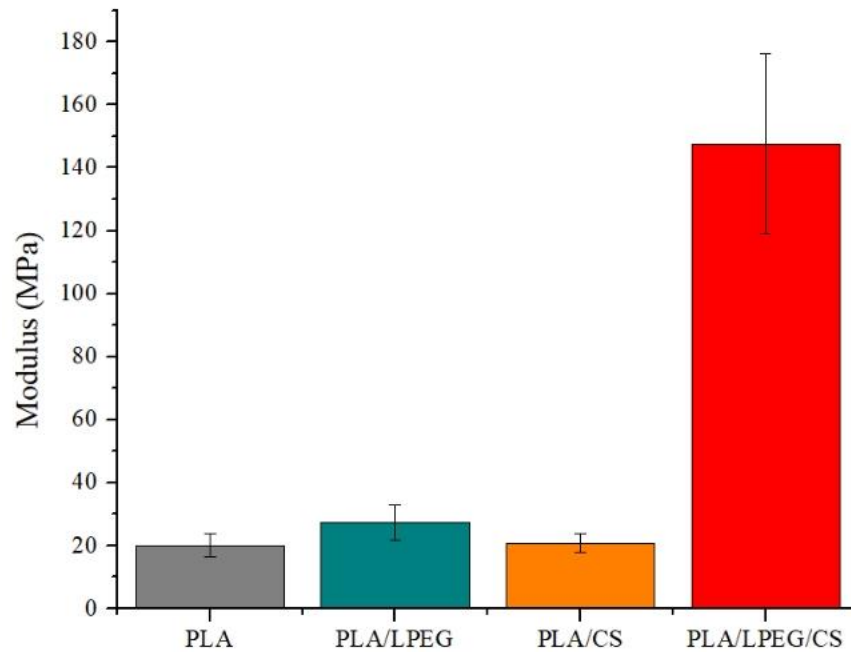
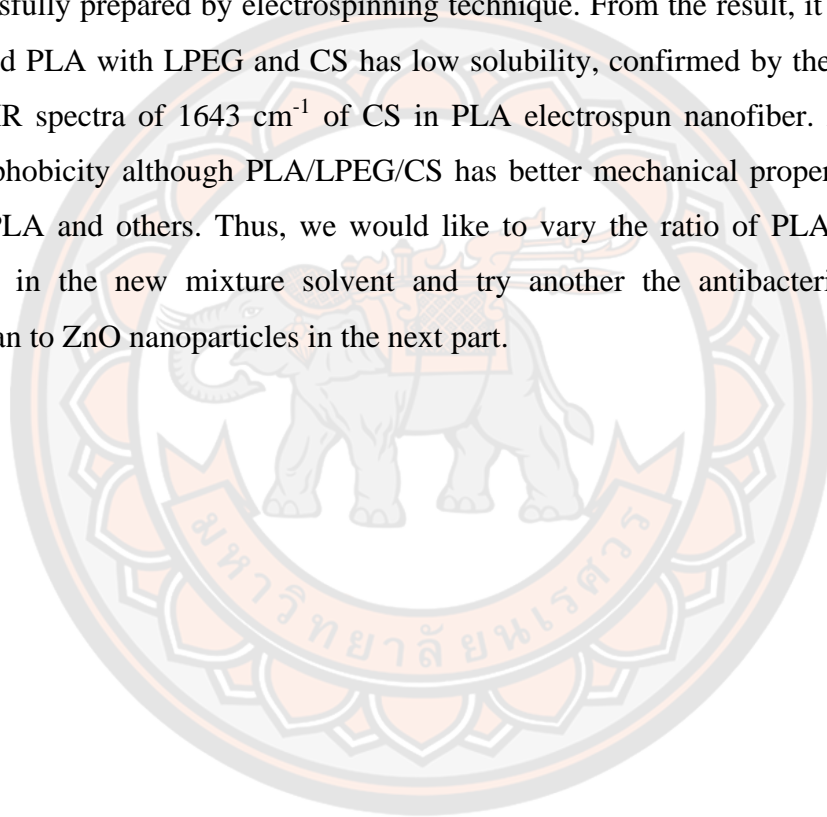


Figure 27. Comparison of modulus of PLA, PLA/LPEG, PLA/CS, PLA/LPEG/CS electrospun nanofibers

Chitosan in the present study was to evaluate the putative bioactivity of chitosan in PLA electrospun fibers and to develop the mechanical properties of PLA by adding LPEG for wound healing applications. Tensile stresses at Maximum Force of 15PLA, 15PLA/10LPEG, 15PLA/3.4CS, and 15PLA/10LPEG/3.4CS are 0.63, 0.54, 0.43, and 1.18 MPa, respectively, reflecting the decrease of the X_c . On the other hand, 15PLA/10LPEG/3.4CS have X_c higher than that of adding LPEG or CS in PLA resulting in high tensile stress and Young's Modulus.

4.1.7 Conclusion of the preparation of blended PLA with LPEG and Chitosan (CS) and Centella Asiatica extracts (CAE)

The fabrication of blended poly (lactic acid) (PLA) electrospun nanofibers was separated to study into 3 parts. The first part was PLA and blended PLA with Poly(ethylene glycol) (LPEG4000) and chitosan (CS) as bio-based polymers (PLA/LPEG/CS NFs) loaded with *Centella Asiatica* extracts (CAE) using the mixture solvents including Formic acid/chloroform/acetone and adding ethanol which were successfully prepared by electrospinning technique. From the result, it was found that blended PLA with LPEG and CS has low solubility, confirmed by the disappearance of FTIR spectra of 1643 cm^{-1} of CS in PLA electrospun nanofiber. And it showed hydrophobicity although PLA/LPEG/CS has better mechanical property than that of pure PLA and others. Thus, we would like to vary the ratio of PLA and LPEG or HPEG in the new mixture solvent and try another the antibacterial agent from chitosan to ZnO nanoparticles in the next part.



4.2 Result of development of Blended PLA with LPEG and HPEG

4.2.1 Morphologies of blended PLA electrospun nanofibers with LPEG and HPEG by Scanning Electron Microscope (SEM) using 5 kX

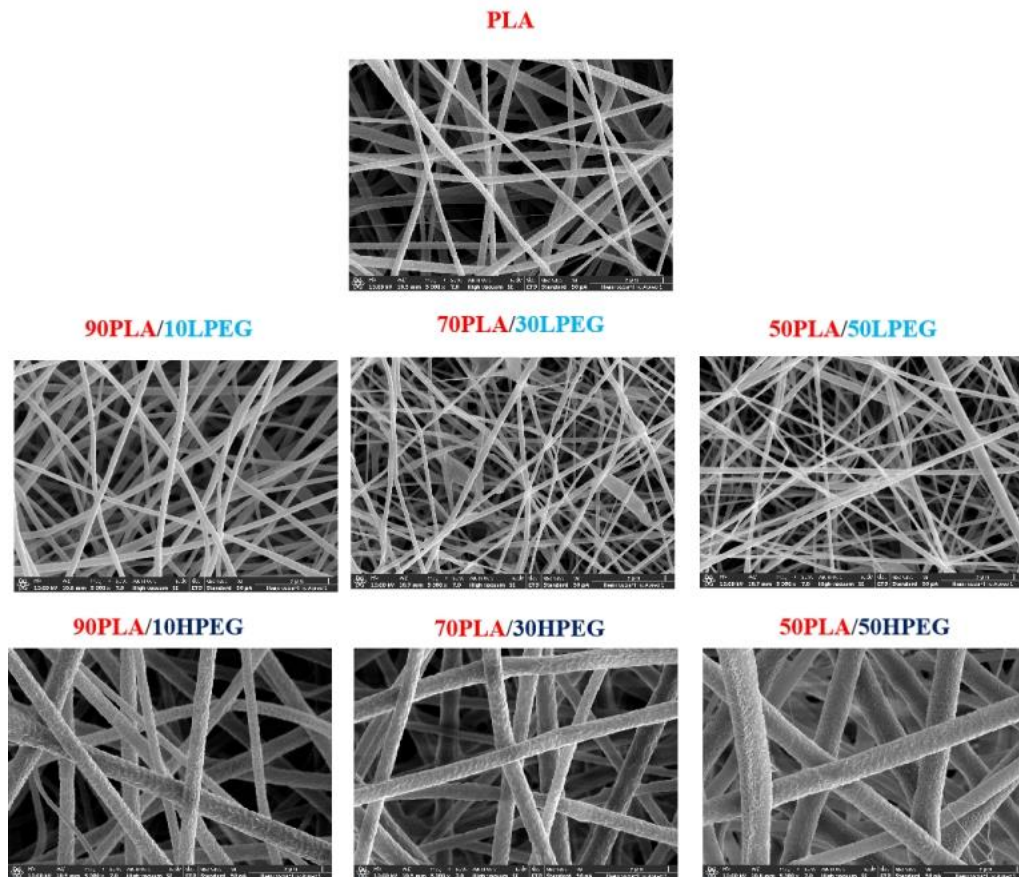


Figure 28. SEM illustrations of blended PLA electrospun nanofibers with LPEG and HPEG (5 kX)

From SEM images shown in Figure 28., pure PLA nanofibers and blended PLA/LPEG and PLA/HPEG. The average diameter of the PLA nanofibers decreased with adding LPEG and increased with HPEG. PLA nanofibers prepared in chloroform/acetonitrile can spin into continuous fibers and porous on the fiber. PLA added with LPEG shows continuous and smooth fibers compared to pure PLA fibers but the increased LPEG content in the ratios of 70:30 and 50:50 is small and has some beads. Adding HPEG displays a large size in microfiber that increases HPEG and also be rough fibers.

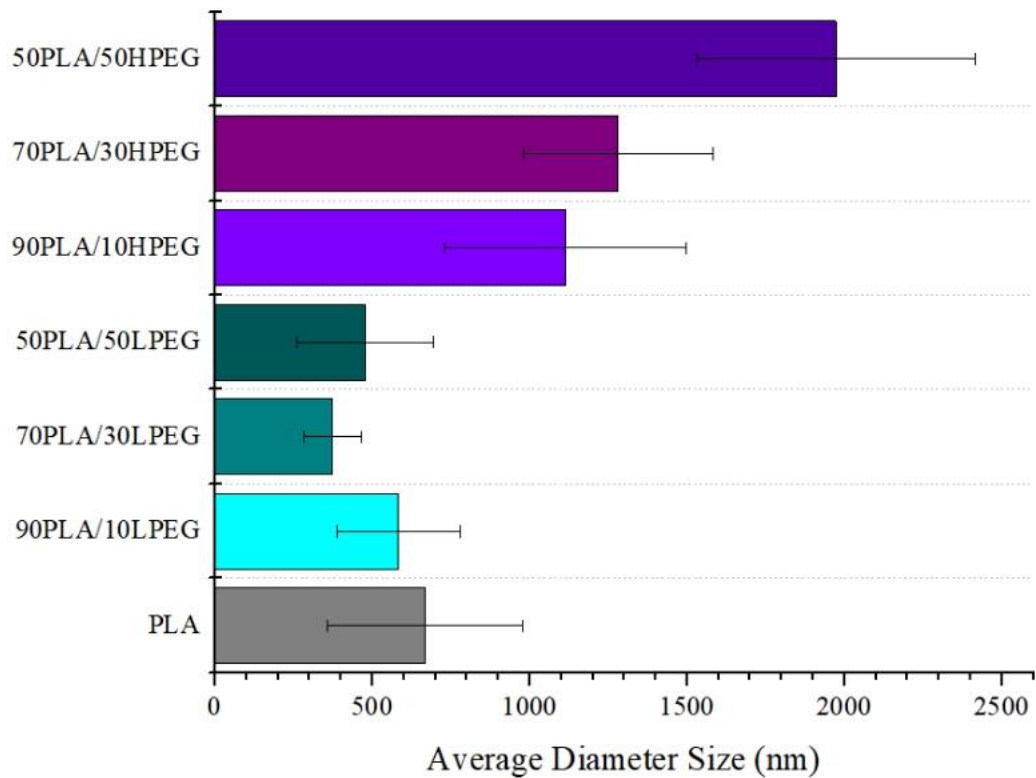


Figure 29. Comparison of average diameter sizes of PLA, PLA/LPEG, PLA/HPEG electrospun nanofibers

A comparison of the effect of LPEG and HPEG in blended PLA electrospun nanofiber for the average diameter size is shown in Figure 29. It was found that blended PLA and LPEG are always a small size compared to pure PLA nanofibers, but PLA/HPEG is the largest size and increases when HPEG contents are high.

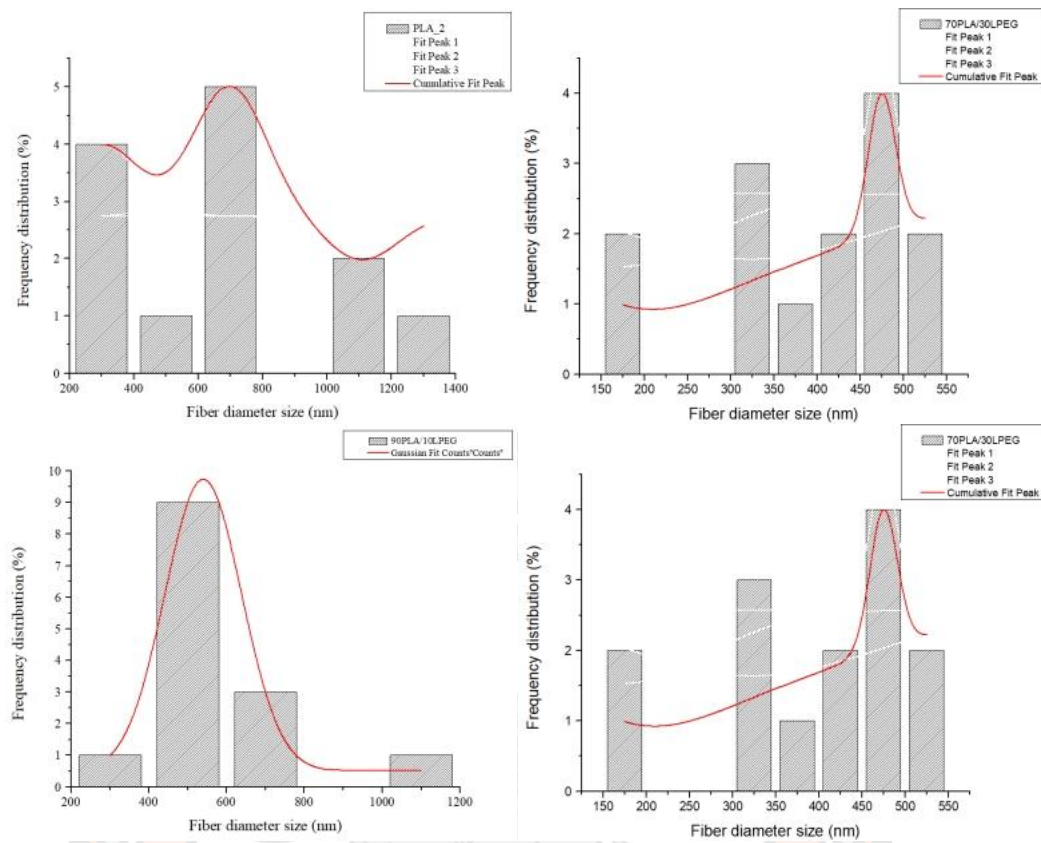


Figure 30. Diameter size distribution of PLA and PLA/LPEG (Ratios of 90:10, 70:30 and 50:50)

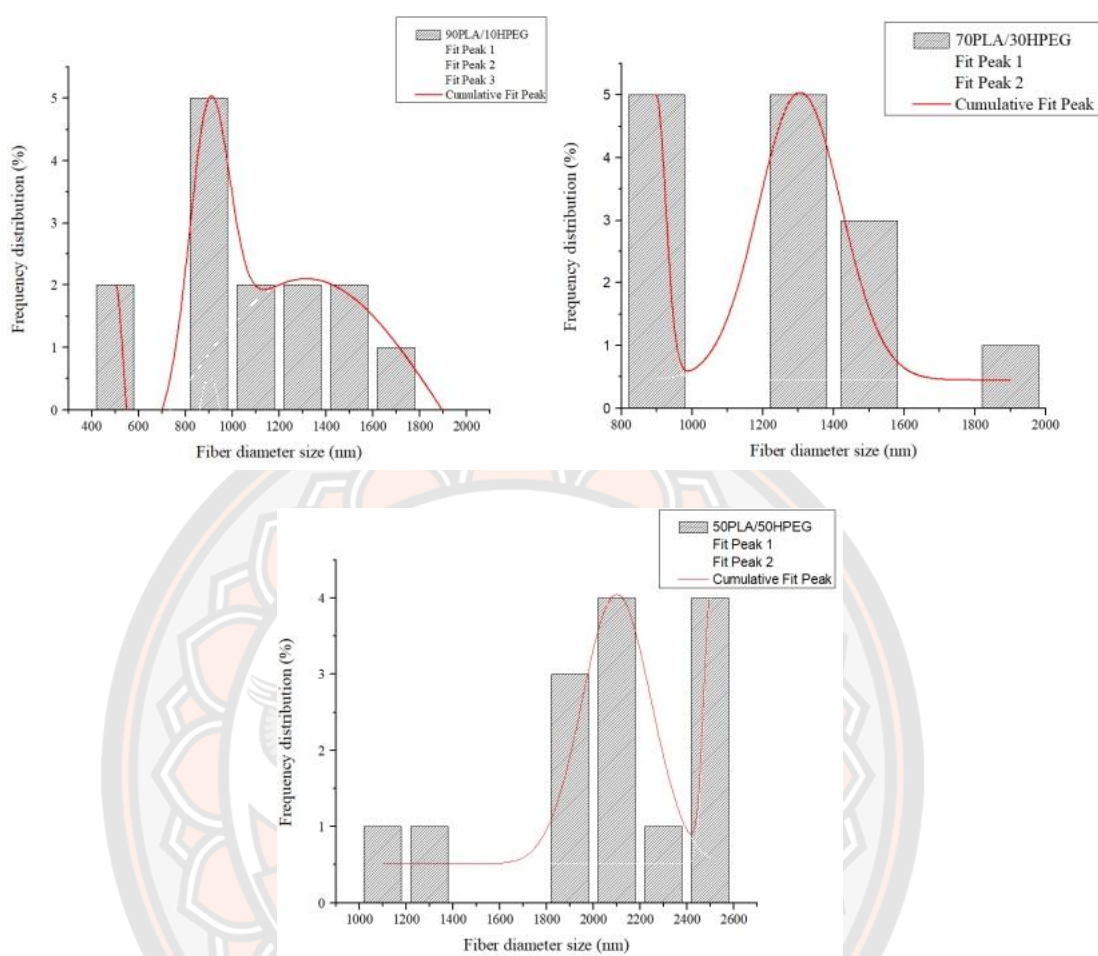


Figure 31. Diameter size distribution of PLA and PLA/HPEG (Ratios of 90:10, 70:30 and 50:50)

Size distribution of adding LPEG is wildly small size but adding HPEG increased comparing PLA.

This can be noticed that the morphology and fiber size might enhance the effect of the wet phenomena on the surface area in the nanofiber membrane like a lotus effect which was confirmed in the water-contact angle.

4.2.2 Water-contact angle analysis of Blended PLA electrospun nanofiber with LPEG or HPEG

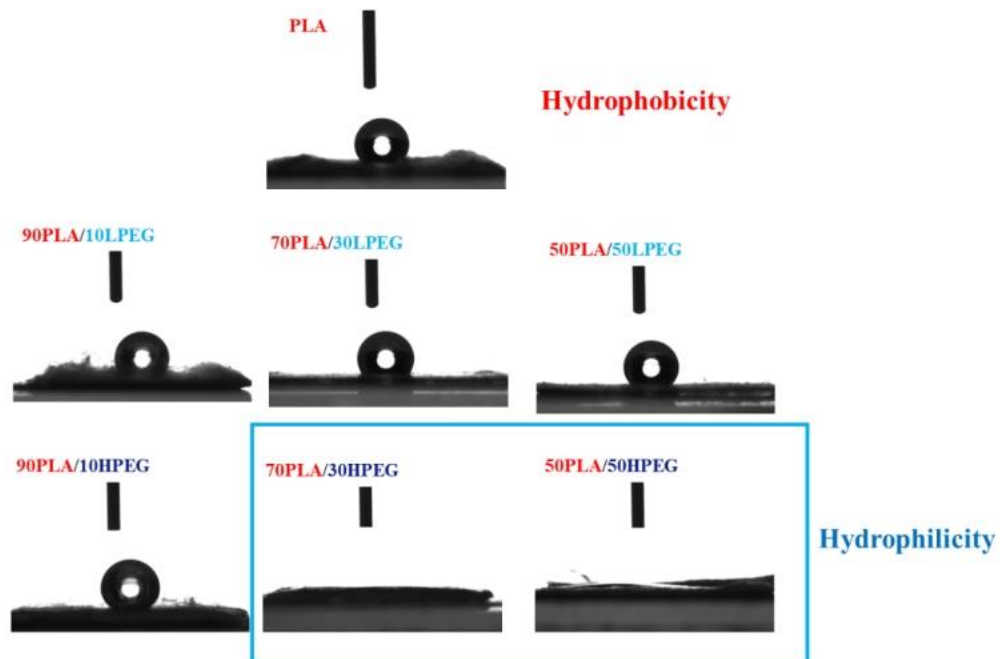
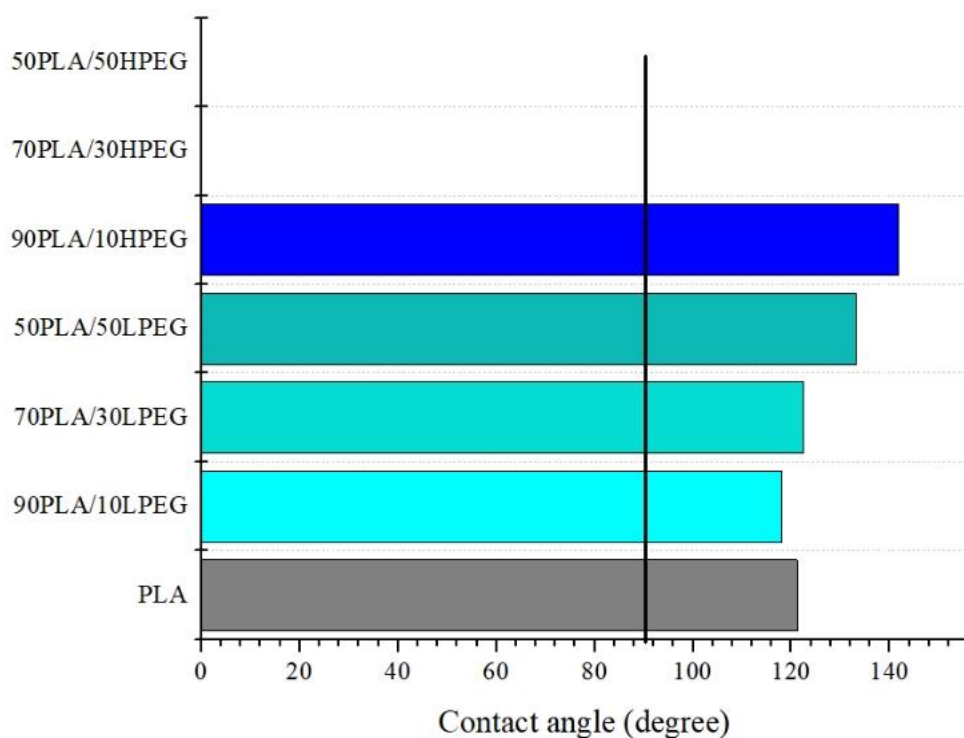


Figure 32. Contact angle images of blended PLA nanofibers with LPEG or HPEG

In Figure 32., The contact angle image of all samples showed hydrophobicity with a contact angle greater than 90 degrees except 70PLA/30HPEG and 50PLA/50HPEG. The nanofibers have the characteristics of the lotus effect phenomenon which has the appearance of small pore spaces and smooth fiber of PLA/LPEG (confirmed by SEM image) and the base of biopolymer used on the fibers was made of polylactic acid which is hydrophobic and is possible of the low ratio of Poly(ethylene glycol) which is a slight area of the fiber surface thus affected the hydrophobic fibers of each sample by shows the contact angle as follows Table 9.

Table 9. Water-contact angles of blended PLA with LPEG or HPEG

| Samples | Water-contact angles (degree) |
|--------------|----------------------------------|
| PLA | 121.1 |
| 90PLA/10LPEG | 118.35 |
| 70PLA/30LPEG | 122.4 |
| 50PLA/50LPEG | 133.05 |
| 90PLA/10HPEG | 141.6 |
| 70PLA/30HPEG | 0 |
| 50PLA/50HPEG | 0 |

**Figure 33.** Comparison of water-contact angle of PLA, PLA/LPEG, PLA/HPEG

Hydrophilicity is one of the most significant features of the surface of the material for wound healing. Measuring the water contact angle determines the surface wettability which moderates hydrophilic surfaces between 30° and 70° of contact angles and has been shown to encourage cells to adhere and expand. Surface hydrophobicity and high hydrophilicity exhibit lower cell adhesion.[51] In the work, the blended PLA/LPEG and 90PLA/10LPEG showed water contact angle values

increased angles more than 90° but 70:30 and 50:50 HPEG like those of super hydrophilic substrates of hydrophilicity around 0° could be attributed to the presence of functional groups such as hydroxyl groups (confirmed by FTIR) which decreased the water contact angle (increased hydrophilicity) due to the presence of hydroxyl groups on its surface. In addition to cell adhesion, hydrophilic biomaterials can also provide the required moisture during wound healing.

4.2.3 Chemical analysis for functional group on blended PLA/LPEG and PLA/HPEG electrospun nanofibers by Fourier transform infrared (FTIR)

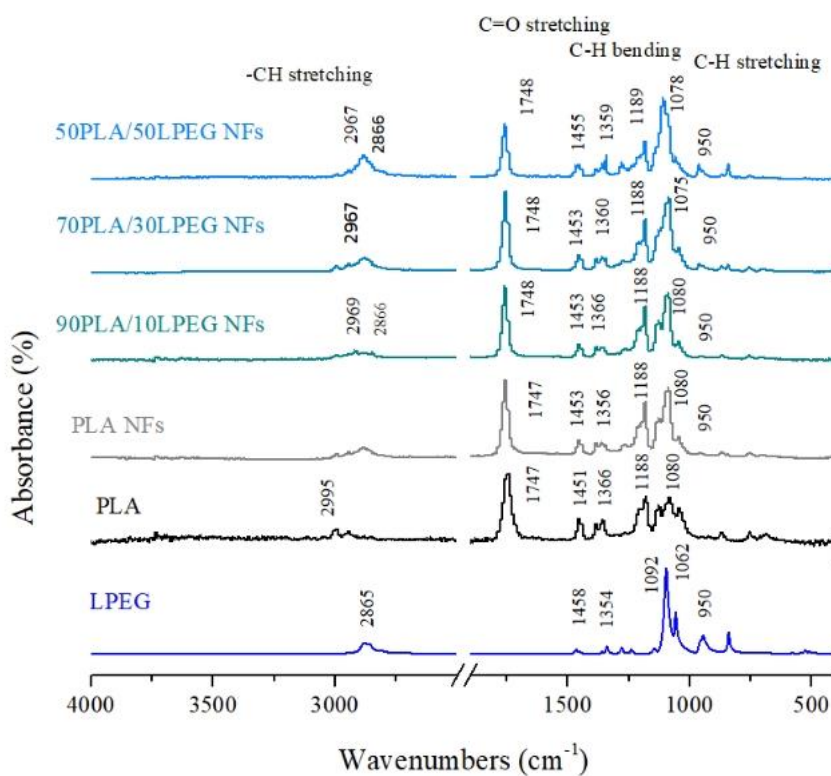


Figure 34. FTIR spectra of the pure PLA, PLA/LPEG electrospun nanofibers various ratios of 90:10, 70:30 and 50:50

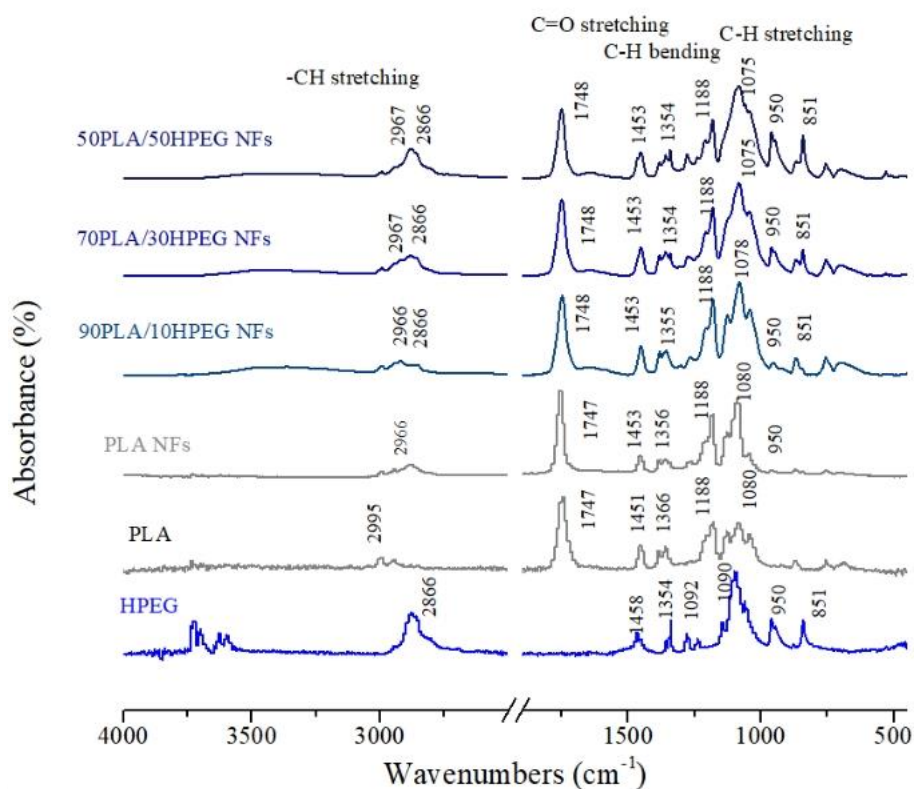


Figure 35. FTIR spectra of the pure PLA, PLA/HPEG electrospun nanofibers various ratios of 90:10, 70:30 and 50:50

In displays, the FTIR spectra of the PLA, LPEG, HPEG, pure PLA electrospun, and blended PLA electrospun nanofibers with LPEG and HPEG (Figure 34 and 35). The FTIR spectrum of PLA depicted characteristic absorption bands at 1747 and 2997 cm^{-1} that was due to the characteristic C=O and C-H vibrations and at 1179, 1128, and 1082 cm^{-1} represented due to the C-O-C linkage of the backbone ester group of PLA and pure PLA electrospun nanofibers displayed at 2995, 1749, 1180, 1127 and 1083 cm^{-1} respectively. LPEG and HPEG displayed strong characteristic absorption peaks of C-O, C-C stretching, CH₂ rocking, CH₂ rocking, CH₂ twisting C-O, C-C stretching, CH₂ rocking, C-O, C-C stretching, C-O stretching, CH₂ rocking, CH₂ twisting, CH₂ wagging and CH₂ scissoring at 840, 945, 1058, 1097, 1145, 1229 and 1278, 1340 and 1465 cm^{-1} respectively. Obviously, in blended PLA/LPEG the increase of LPEG and HPEG was weak because PLA does have enough -OH groups to form hydrogen bonds with -OH groups, and PLA/HPEG shows a high-intensity peak at 3420 cm^{-1} (O-H) compared to PLA/LPEG. Thus, adding HPEG provides O-H and hydrophilic materials.

4.2.4 Swelling and Gel-fraction of PLA, PLA/LPEG

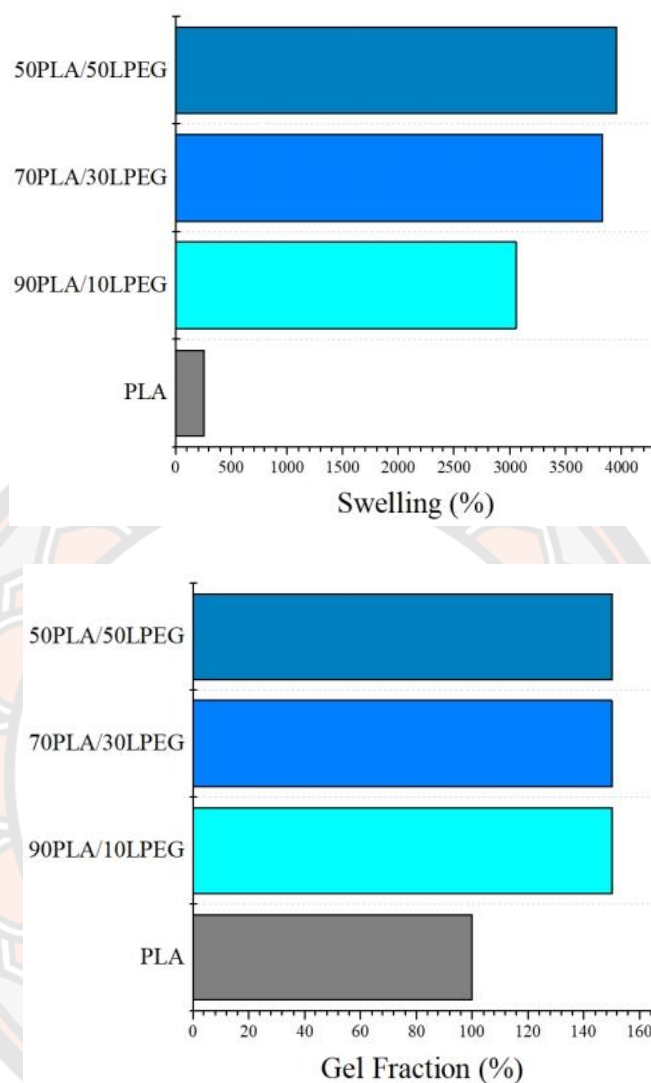


Figure 36. Swelling and gel fraction of adding LPEG in PLA electrospun

Swelling and gel fraction is the important parameter in the control-release mechanism of materials for wound healing and affects the release of various active ingredients. In this work, antibacterial agents (ZnO nanoparticles) and anti-inflammatory (CAE) were added in blend PLA electrospun nanofibers. The effects of this swelling were studied and will also affect the release profile. Adding LPEG into PLA can increase the swelling value further when the amount of LPEG increases.

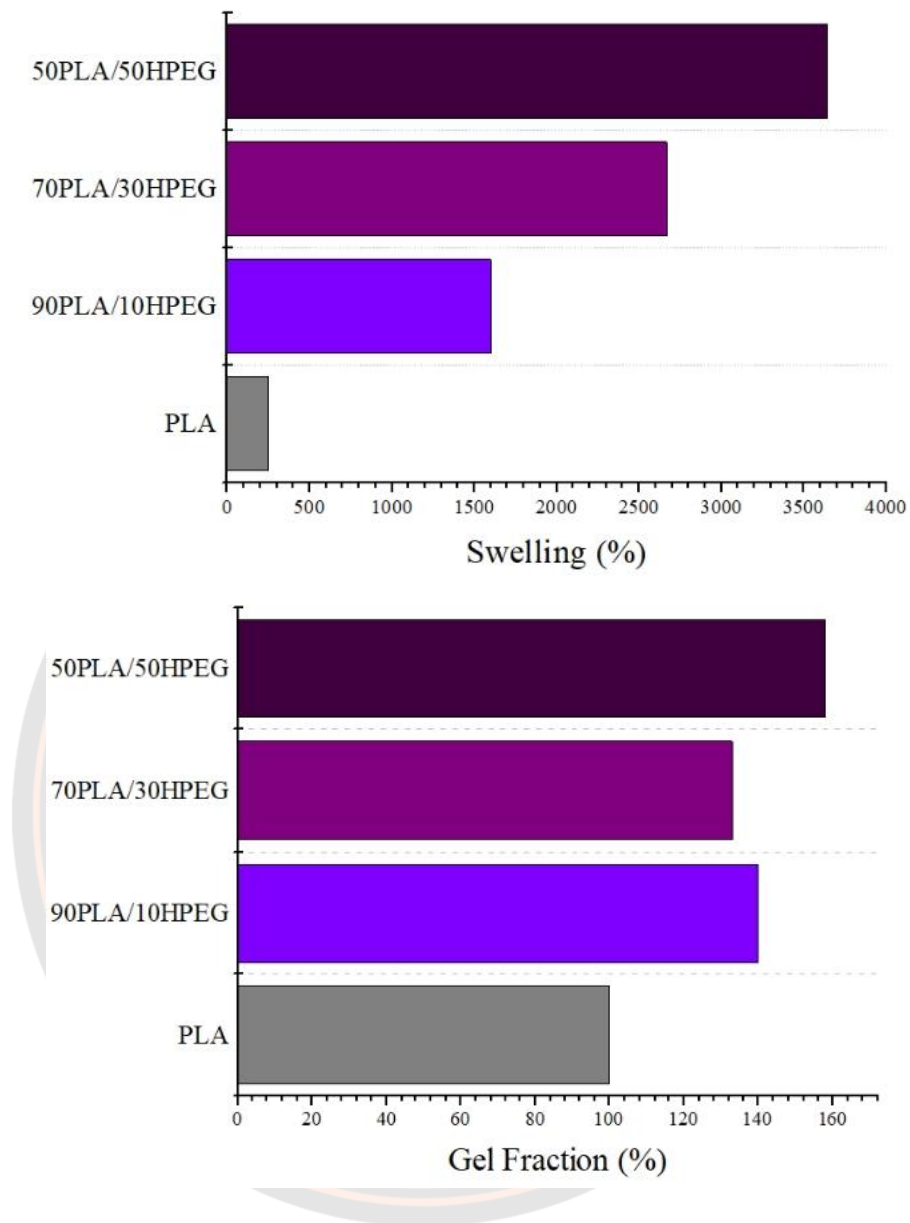


Figure 37. Swelling and gel fraction of adding HPEG in PLA electrospun nanofibers

Figure 37. shows the relationship between swelling and gel fraction. It can be observed that the swelling and gel fraction increase with increasing the ratio of HPEG into PLA as well as adding LPEG because of dissolving with water. Thus, it affects degradation fibers depicted in 4.2.5

4.2.5 Degradation of PLA, PLA/HPEG around 5 weeks

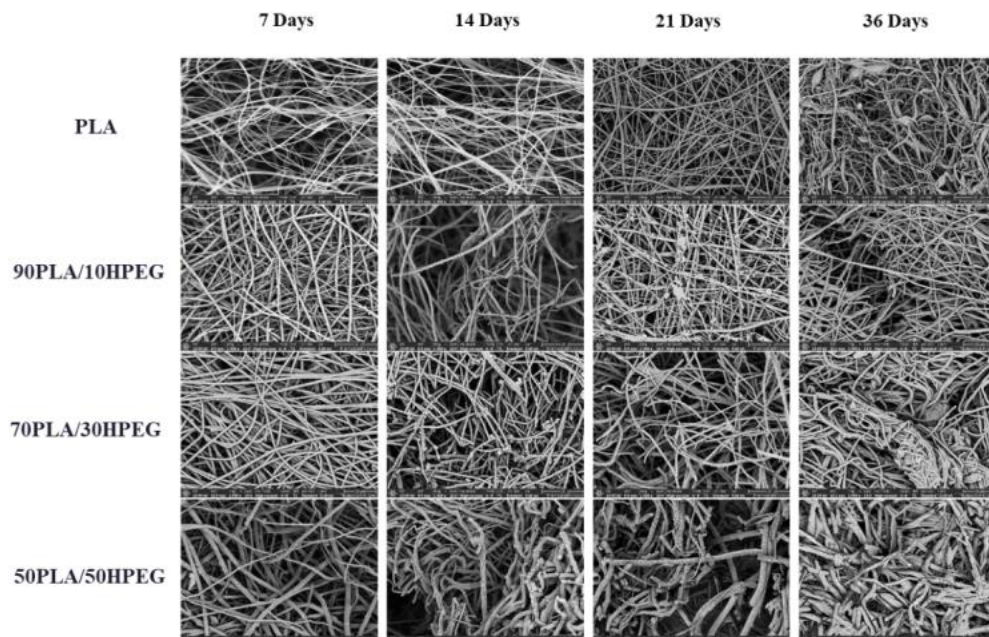


Figure 38. SEM illustrations of degradation of PLA and PLA/HPEG for 36 days

The degradation of PLA, 90PLA/10HPEG, 70PLA/30HPEG, and 50PLA/50HPEG electrospun fibers membrane plays an essential role in cell regeneration, for the rate of fiber degradation should be able to match the rate of new tissue formation which this work is initiated at 7 days to 36 days. In this study, we used one method to test the degradation that was soaked in PBS and incubated at 37°C. So, blended PLA for wound healing applications, is important to understand the mechanism of degradation. We found that the HPEG significantly increased the degradation rate of the electrospun nanofibers when dispersed to the surface of PLA fibers. The result may come from the fact that the degradation rate of PLA is slower than HPEG (Figure 38.). However, we considered that this result may come from the high swelling and displays many fiber breaks for a long time.

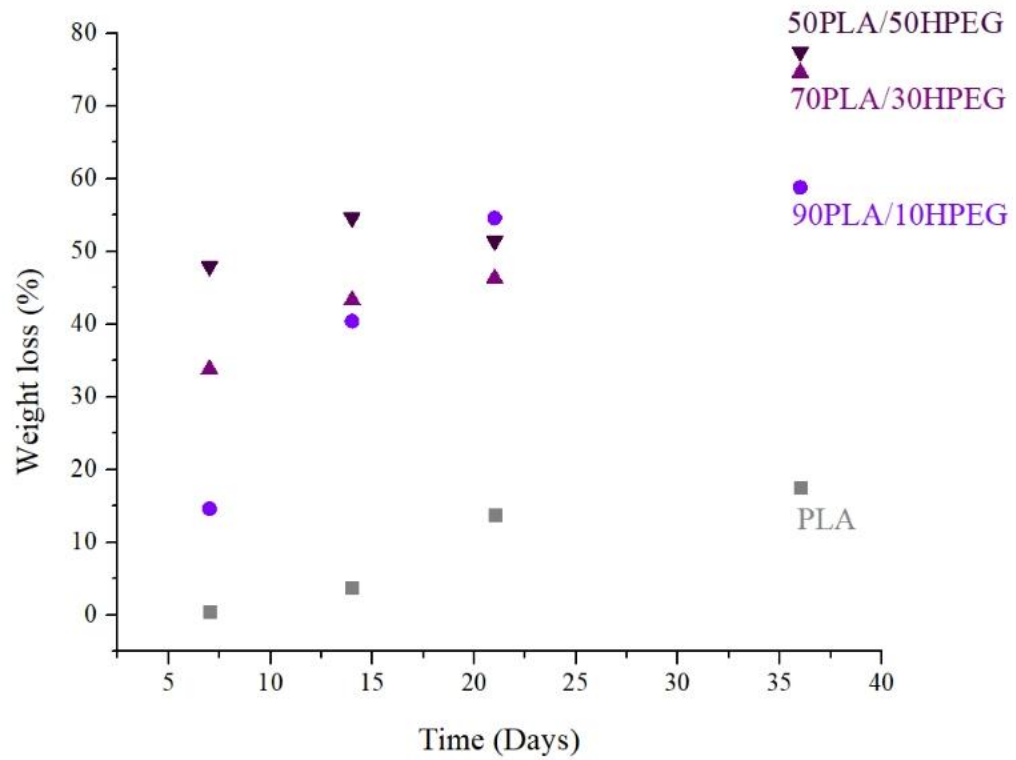


Figure 39. Degradation graph of PLA and PLA/HPEG various ratios

Figure 39. shows comparing %weight loss between pure PLA and blend PLA/HPEG in the ratios of 90:10, 70:30, and 50:50, respectively. It was found that increasing HPEG can increase degradation in 7 days and high degradation in 70:30 as 70%.

4.2.6 Thermal properties of blended PLA/LPEG and PLA/HPEG electrospun nanofibers by Differential Scanning Calorimetry (DSC)

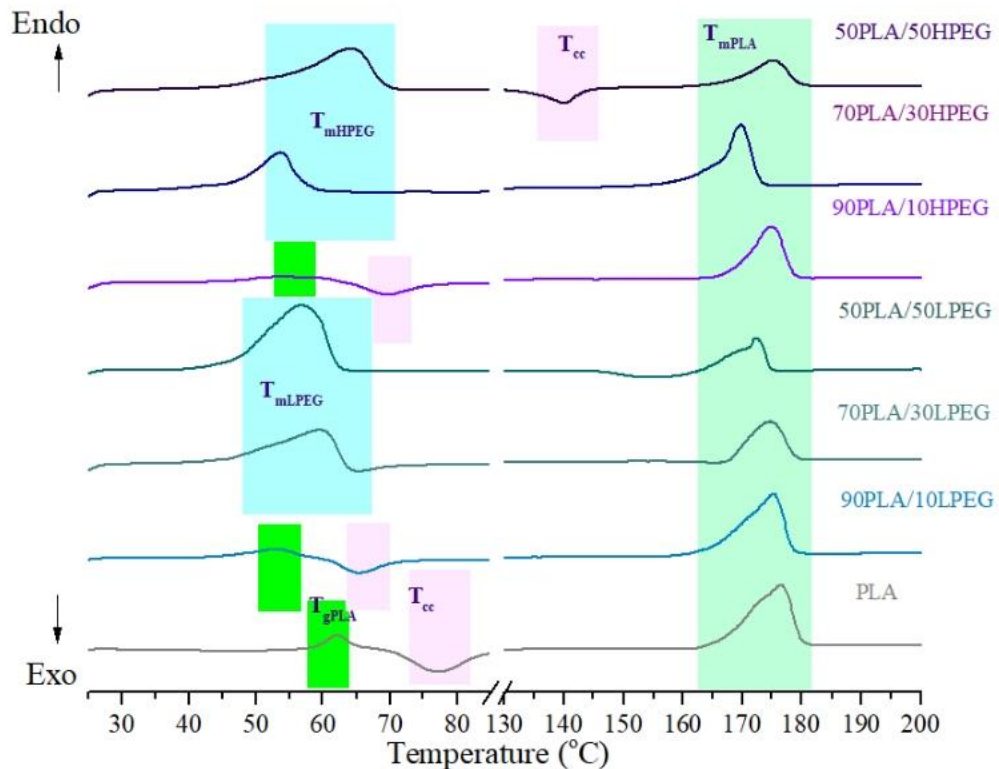


Figure 40. The first heat of DSC thermograms of blended PLA electrospun fibers: PLA, PLA/LPEG, and PLA/HPEG

The first heat of the DSC thermograms of PLA, PLA/LPEG, and PLA/HPEG electrospun nanofiber various ratios showed a glass transition temperature (T_g), a cold crystallization temperature (T_{cc}), the melting temperature (T_m) typical peak of PLA and blended PLA with LPEG and HPEG (Figure 40.) and degrees of crystallinity (X_c) are listed in Table 10. It can be noticed the significant decrease of T_g of PLA with addition of LPEG or HPEG in ratios of 90:10 as it acts as a plasticizer. On the other hand, adding LPEG 70:30 and 50:50 or HPEG to the blended PLA results in inhibiting the movement of the polymer chain of blended PLA and also exists in the second heat because semi-crystalline PEG causes to separate the polymer phase between PLA and PEG. Thus, the T_m and crystallinity of PLA were decreased as shown in Table 10.

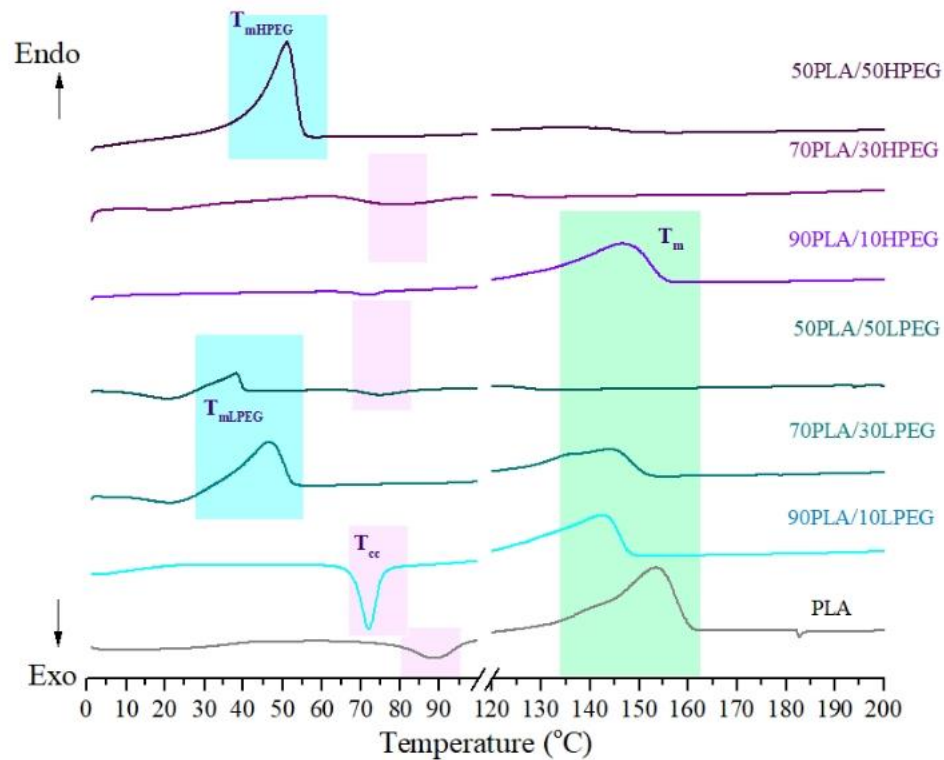


Figure 41. The second heat of DSC thermograms of blended PLA electrospun fibers: PLA, PLA/LPEG, and PLA/HPEG

The second heat of the DSC thermogram shows the T_g and T_{mPLA} reduced when adding LPEG and HPEG. The higher amount of HPEG of 70:30 and 50:50 do not show the peak of T_m but at 50:50 HPEG appears the T_{mHPEG} so it confirmed the interaction of a chain of HPEG because of long-chain and high molecular weight of HPEG ($M_w=900,000$) However, the LPEG and HPEG affected for crystallinity that decreased when increasing LPEG 70:30 and 50:50 but 70PLA/30HPEG increased.

Table 10. T_g , T_{cc} , T_m , enthalpy, and %crystallinity of blended PLA/LPEG or PLA/HPEG NFs

| Samples | T_g (°C) | T_{mLPEG} (°C) | T_{mHPEG} (°C) | T_{cc} (°C) | T_{mPLA} (°C) | W_{PLA} | DH_{mLPEG} (J/g) | DH_{mHPEG} (J/g) | DH_{mPLA} (J/g) | DH_c (J/g) | X_{cPLA} (%) |
|-------------|---------------|---------------------|---------------------|------------------|--------------------|-----------|-----------------------|-----------------------|----------------------|-----------------|-------------------|
| PLA | 62 | | | 77 | 176 | 1.00 | | | 52 | 19 | 36 |
| 90PLA/10PEG | 53 | | | 65 | 175 | 0.90 | 7.24 | | 49 | 14 | 42 |
| 70PLA/30PEG | | 59 | | 65 | 174 | 0.70 | 33.77 | | 24 | 3 | 33 |
| 50PLA/50PEG | | 57 | | | 172 | 0.50 | 80.30 | | 24 | 7 | 36 |
| 90PLA/10PEO | 54 | | | 70 | 175 | 0.90 | | 7.41 | 35 | 12 | 27 |
| 70PLA/30PEO | | | 54 | | 170 | 0.70 | | 32 | 40 | | 62 |
| 50PLA/50PEO | | | 64 | | 175 | 0.50 | | 66.76 | 28 | 17 | 23 |

The occurrence of cold crystallization affected the melting enthalpy of PLA. In this case, DH_m in the DSC thermogram was a result of the initial crystallinity of PLA and the crystallinity during heating in DSC analysis (DH_{cc}). By excluding DH_{cc} , X_c represented the original degree of crystallization of samples. From the results in Table 10., it is noted that addition of LPEG and HPEG affects the degree of crystallinity (X_c) of PLA nanofiber. The X_c was increased with adding 90:10 LPEG and 70:30 HPEG but other ratios of LPEG and HPEG do not assist to improve the crystallinity of PLA. This might be due to obstruction of molecular movement of long-chain polymer. This could also affect to the mechanical properties of PLA/LPEG or PLA/HPEG nanofibrous membranes.

4.2.7 Mechanical properties of blended PLA/LPEG and PLA/HPEG electrospun nanofibers by Tensile (ASTM D5034)

Table 11. Tensile strength, elongation at break, and young's modulus of blended PLA/LPEG and PLA/HPEG electrospun nanofibers

| Samples | Tensile strength | | Elongation at Break | | Modulus | |
|--------------|------------------|------|---------------------|-------|---------|-------|
| | MPa | SD | % | SD | MPa | SD |
| PLA | 0.38 | 0.08 | 77.95 | 1.87 | 6.64 | 0.75 |
| 90PLA/10LPEG | 0.58 | 0.06 | 115.70 | 15.02 | 23.67 | 6.51 |
| 70PLA/30LPEG | 1.58 | 0.11 | 38.85 | 3.33 | 98.68 | 20.52 |
| 50PLA/50LPEG | 0.43 | 0.16 | 4.50 | 2.24 | 42.58 | 11.60 |
| 90PLA/10HPEG | 1.04 | 0.16 | 468.24 | 32.13 | 43.49 | 8.12 |
| 70PLA/30HPEG | 0.69 | 0.03 | 169.47 | 31.21 | 21.07 | 5.40 |
| 50PLA/50HPEG | 1.19 | 0.06 | 510.09 | 14.44 | 21.77 | 2.96 |

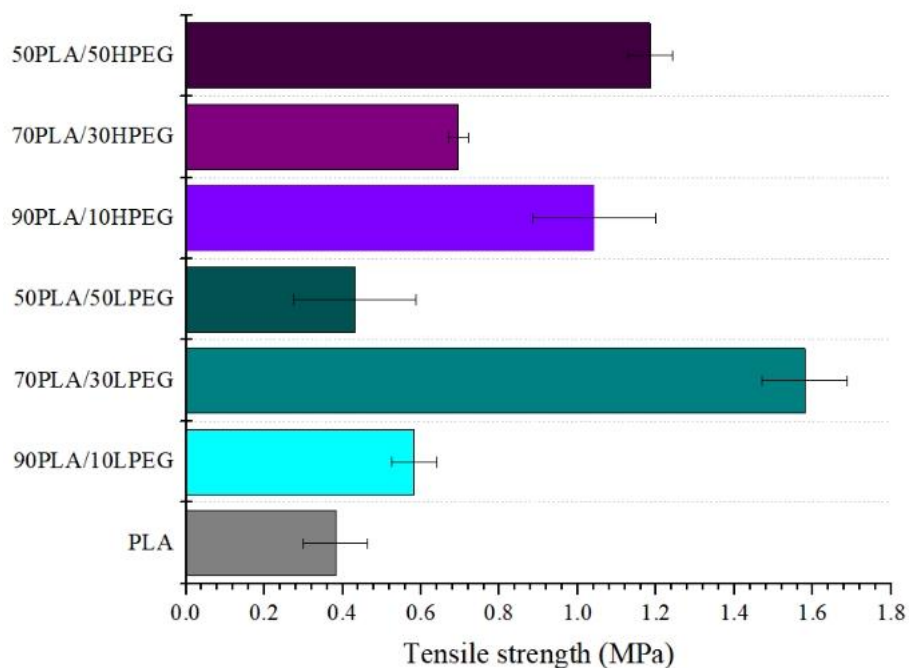


Figure 42. Comparison of tensile strength at break of PLA, PLA/LPEG, PLA/HPEG electrospun nanofibers

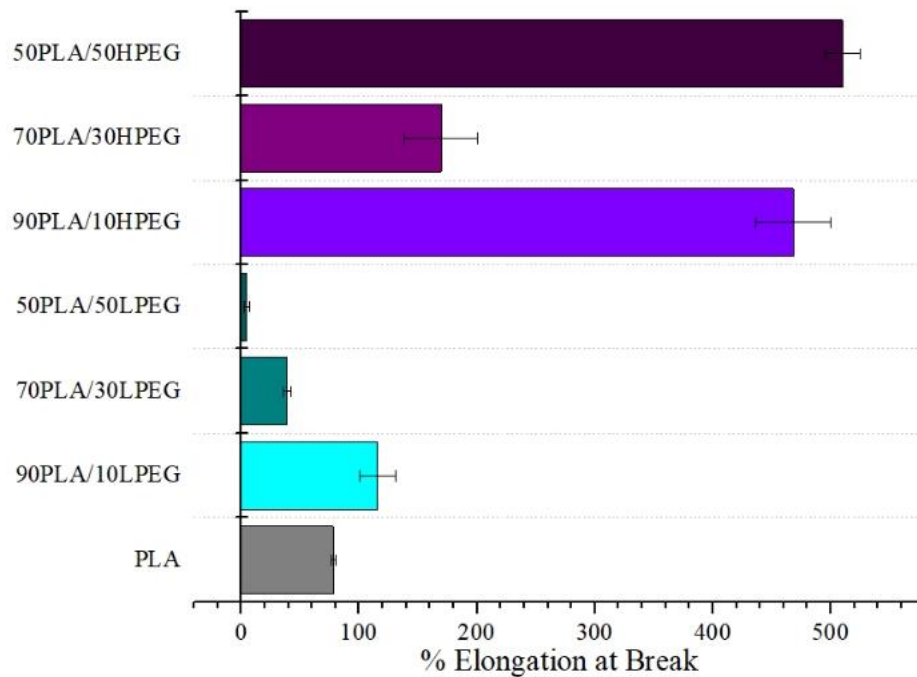


Figure 43. Comparison of elongation at break of PLA, PLA/LPEG, PLA/HPEG electrospun nanofibers

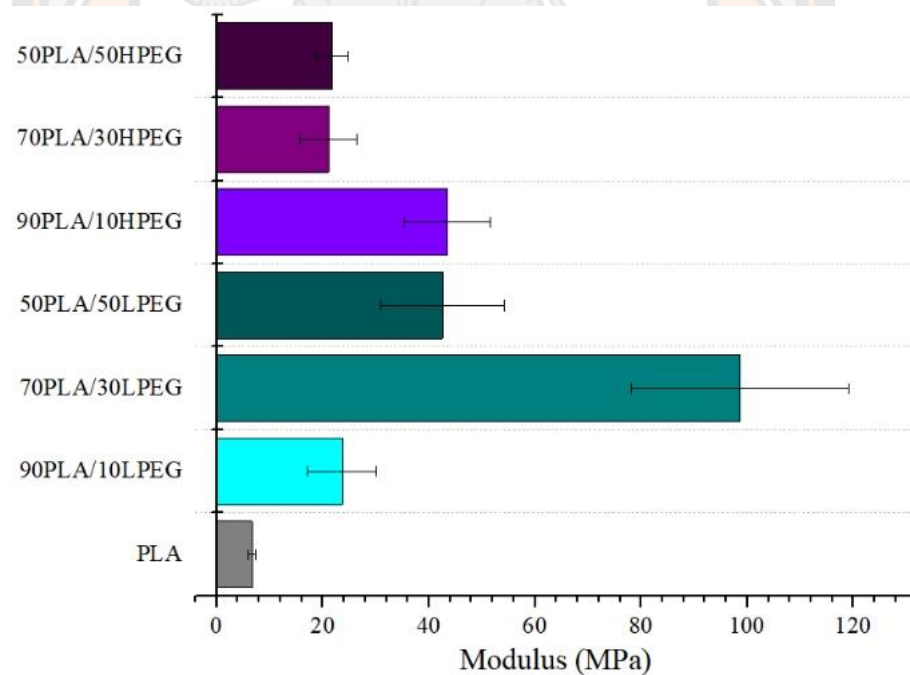


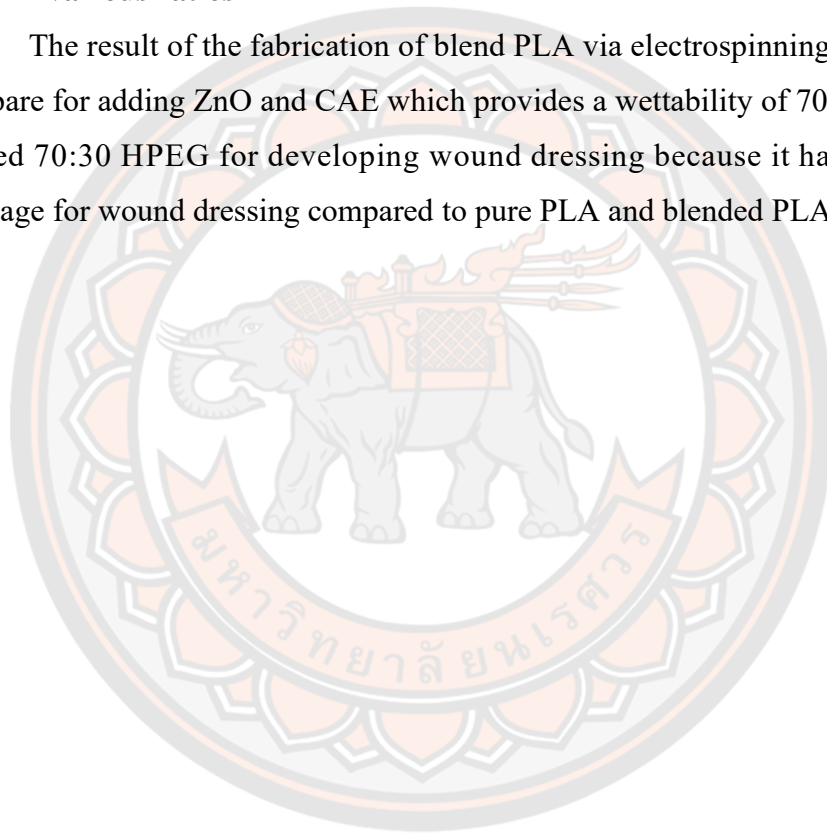
Figure 44. Comparison of modulus at break of PLA, PLA/LPEG, PLA/HPEG electrospun nanofibers

The effect of LPEG and HPEG on mechanical properties of PLA electrospun fibers by tensile strength at maximum force, elongation at break, and modulus, the

result shows the highest tensile strength is 70PLA/30LPEG, the second scanning is 50PLA/50HPEG that the highest elongation is 50PLA/50HPEG, the second scanning is 90PLA/10HPEG and 70PLA/30HPEG which is more than PLA and PLA/LPEG and the highest modulus is 70PLA/30LPEG and the second scanning is 90PLA/10HPEG.

4.2.8 Conclusion of the preparation of blended PLA with LPEG or HPEG various ratios

The result of the fabrication of blend PLA via electrospinning was improved to prepare for adding ZnO and CAE which provides a wettability of 70:30 HPEG. We selected 70:30 HPEG for developing wound dressing because it has a moderated advantage for wound dressing compared to pure PLA and blended PLA/LPEG



4.3 Results of the effect of doped ZnO into the blended PLA from the best condition of 2 and loading *Centella Asiatica* extracts (CAE)

4.3.1 Morphologies of 70PLA/10LPEG loaded 2%ZnO and various CAE by Scanning Electron Microscope (SEM) using 5 kX

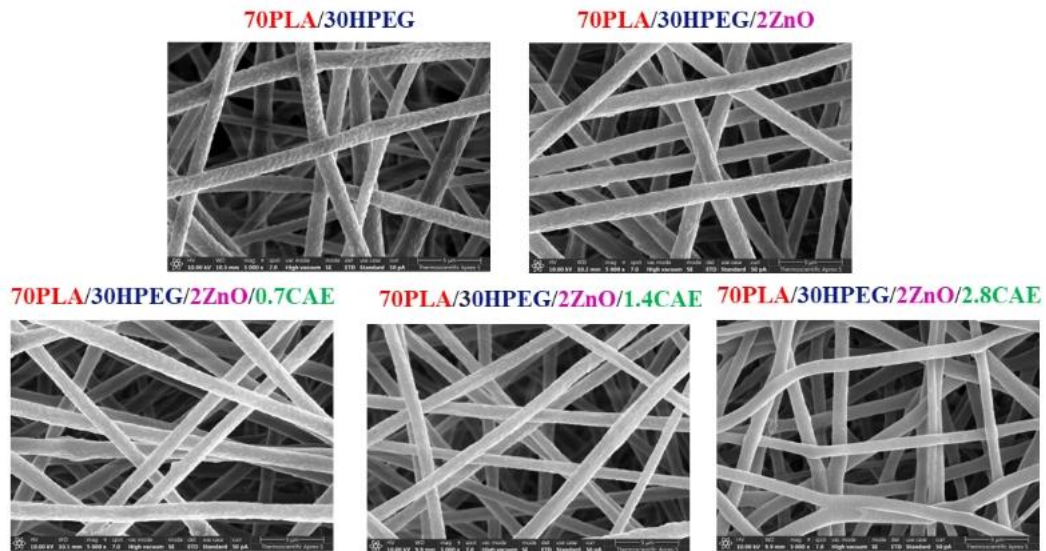


Figure 45. SEM illustrations of 70PLA/10LPEG loaded 2%ZnO and various CAE (5 kX)

From SEM images shown in Figure 45., 70PLA/30HPEG nanofibers and blended PLA/HPEG with ZnO nanoparticles (NPs) and CAE. The average diameter of the 70PLA/30PLA nanofibers increased with adding ZnO NPs and decreased with CAE. (as shown in Table 12) and size distribution of 70PLA/30HPEG is wildly large size but adding ZnO and increased CAE is smaller and high frequency distribution in the range of 1,200 nm. (Figure 46.)

Table 12. Average diameter size of 70PLA/30PLA, 70PLA/30PLA/2ZnO and 70PLA/30PLA/2ZnO/CAE

| Average diameter size | | |
|----------------------------|--------|-------|
| Samples | (nm) | SD |
| 70PLA/30HPEG | 1280.0 | 300.7 |
| 70PLA/30 HPEG /2ZnO | 1470.5 | 235.5 |
| 70PLA/30HPEG /2ZnO/0.7CAE | 1373.0 | 160.0 |
| 70PLA/30 HPEG /2ZnO/1.4CAE | 1219.5 | 181.1 |
| 70PLA/30 HPEG /2ZnO/2.8CAE | 1116.5 | 122.2 |

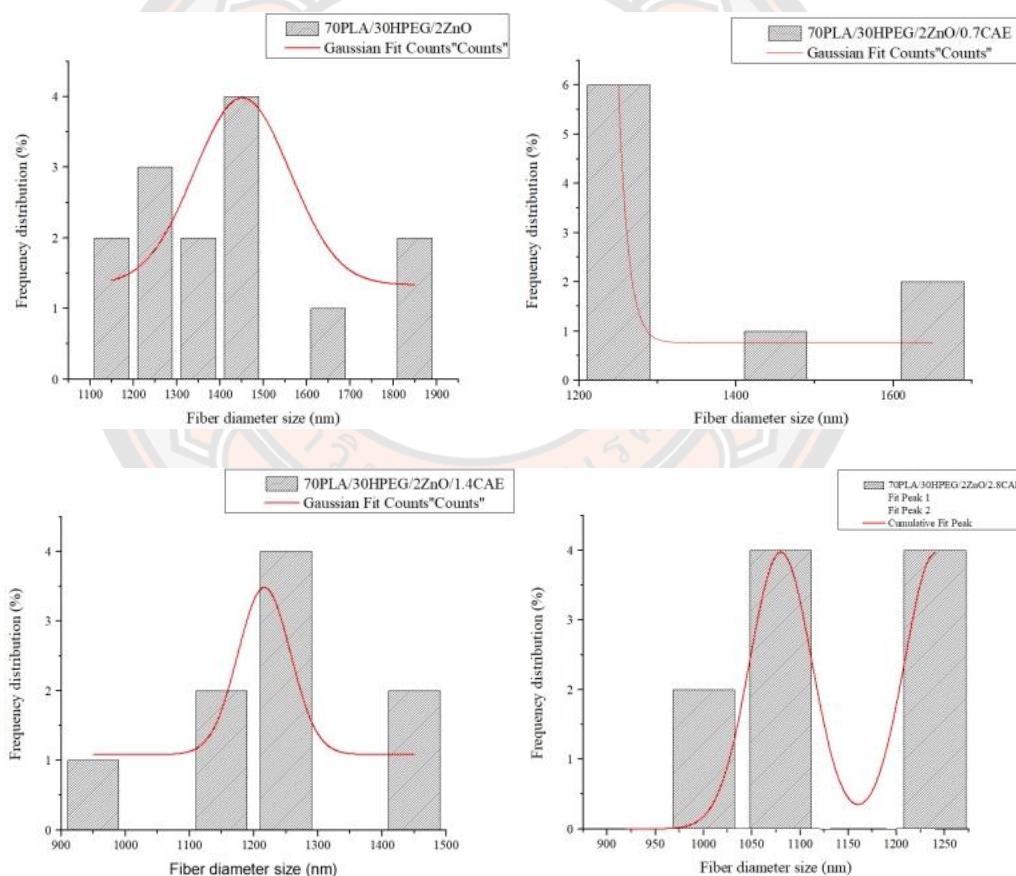


Figure 46. Diameter size distribution of 70PLA/30HPEG/2ZnO and 70PLA/30HPEG/2ZnO loaded CAE (0.7, 1.4 and 2.8 %wt)

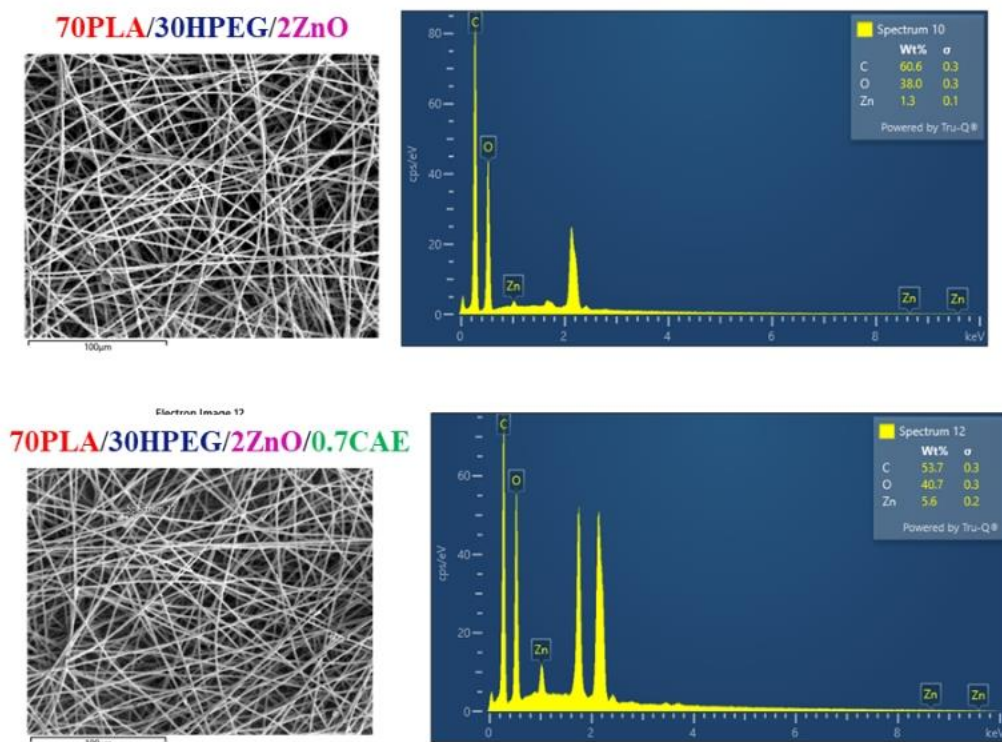


Figure 47. EDS illustrations of 70PLA/10LPEG loaded 2%ZnO and 70PLA/30HPEG/2ZnO/0.7CAE (5 kX)

The SEM image and EDS measurements of 70PLA/30HPEG electrospun fibers with ZnO nanoparticles (2% wt.) are displayed in Figure 47. It is obvious that the sample has uniform and smooth nanofibers with an average size of 1,470 nm diameter without any beads. ZnO nanoparticles were well dispersed in the nanofibrous matrix. Furthermore, the elemental analysis via energy-dispersive X-ray spectroscopy (EDS) showed three main peaks for Zn, O, and C, confirming the successful synthesis of the 70PLA/30HPEG/2ZnO and 70PLA/30HPEG/2ZnO/0.7CAE electrospun fibers. This could be pointed out that CAE is incorporated into nanofibers. In addition, their existence, and distribution can also be described through Fourier transform infrared spectroscopy (FTIR).

4.3.2 Functional group analysis of the blended PLA/LPEG and PLA/HPEG electrospun nanofibers by Fourier transform infrared spectroscopy (FTIR)

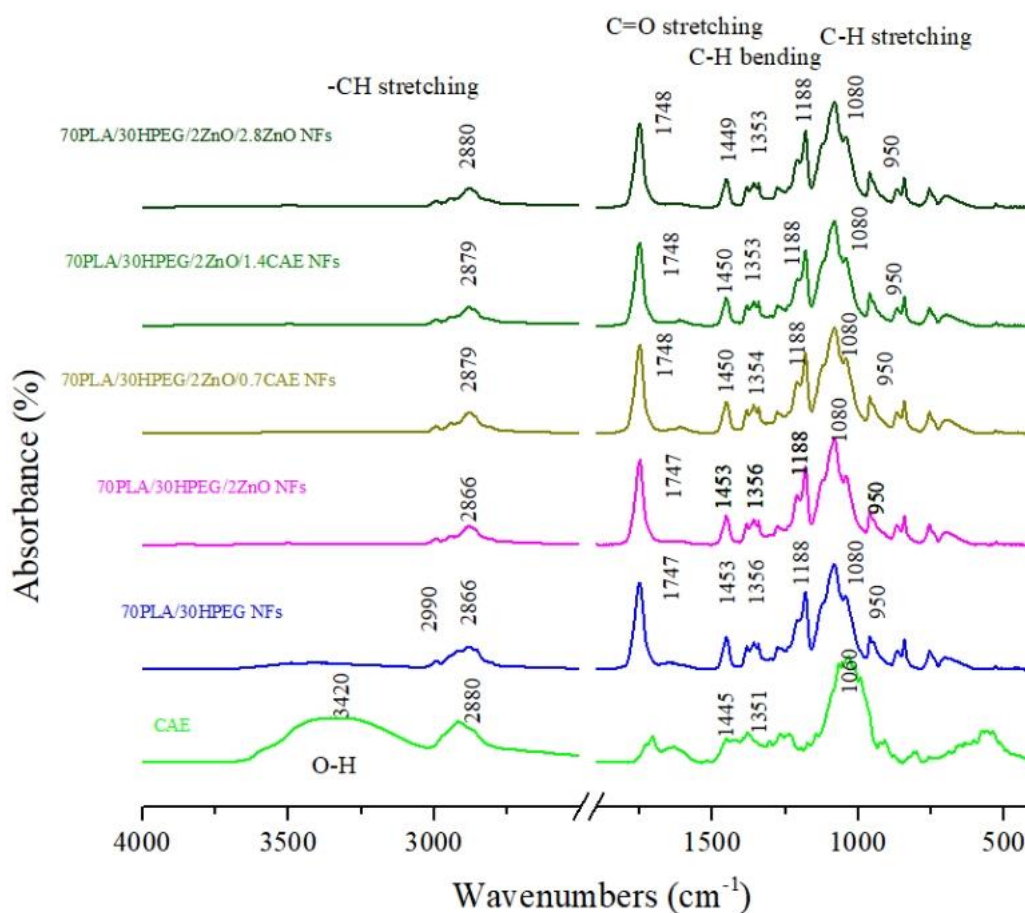


Figure 48. FTIR spectra of the 70PLA/30HPEG electrospun nanofibers loaded 2%ZnO and various contents of CAE

The FTIR spectra of *Centella Asiatica* extracts (CAE) and blended 70PLA/30HPEG electrospun fibers loaded 2%ZnO and 0.7-2.8% CAE depicted characteristic absorption bands at 2995, 1749, 1188, 1127, and 1083 cm^{-1} , respectively that were due to the CH stretching, C=O and C-H bending and C-H stretching and the C-O-C linkage of the backbone ester group of PLA, respectively. Addition of HPEG shows characteristic peaks in the regions of 1453 cm^{-1} , 1356 cm^{-1} , 1180 cm^{-1} , and 845 cm^{-1} that represent different bonds of CH₂ in scissoring, wagging, twisting, and rocking forms. The sharp peak at 287 cm^{-1} is related to CH stretching,

and the smooth peak at 3420 cm^{-1} shows the presence of the OH group. Other peaks at 1141 cm^{-1} , 1095 cm^{-1} , and 950 cm^{-1} are related to C–O–C stretching, which is responsible for the semi-crystalline phase of HPEG. The spectrum of the 70PLA/30HPEG/2ZnO/CAE displays the characteristic peaks of ZnO-NPs and CAE at 3420 cm^{-1} (OH groups on the surface), 528 cm^{-1} (Zn–O bond)

4.3.3 Swelling and gel-fraction of 70PLA/30HPEG and 70PLA/30HPEG/2ZnO loaded 0.7-2.8% CAE

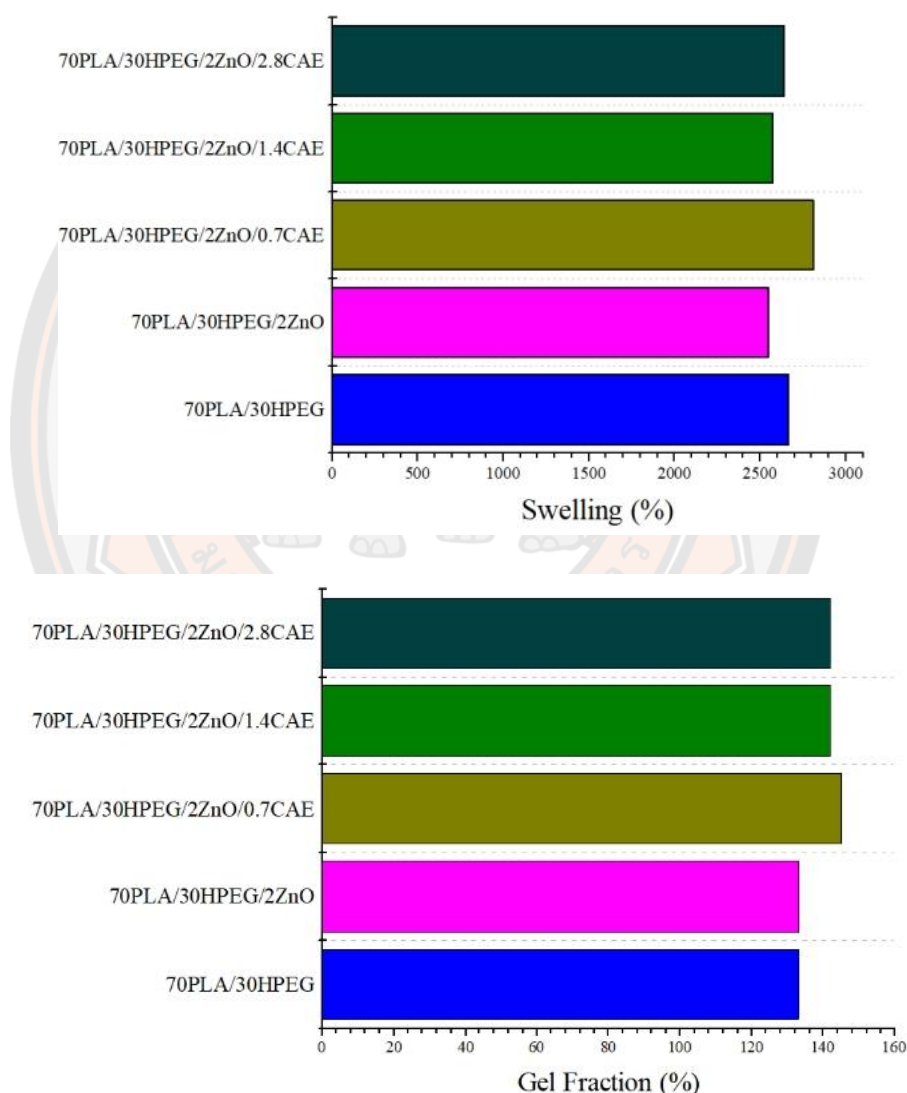


Figure 49. Swelling and gel fraction of adding ZnO and CAE in 70PLA/30HPEG electrospun nanofibers

Adding HPEG into PLA can increase the swelling and gel fraction value further when the amount of HPEG increases. However, adding ZnO and CAE does

not affect swelling and gel fraction. Furthermore, the samples of blended 70PLA/30HPEG electrospun fibers loaded ZnO NPs and CAE affect to the higher degradation compared to pure PLA nanofibers about 36 days.

4.3.4 Thermal properties of blended 70PLA/30HPEG electrospun nanofibers loaded ZnO and CAE by Differential Scanning Calorimetry (DSC)

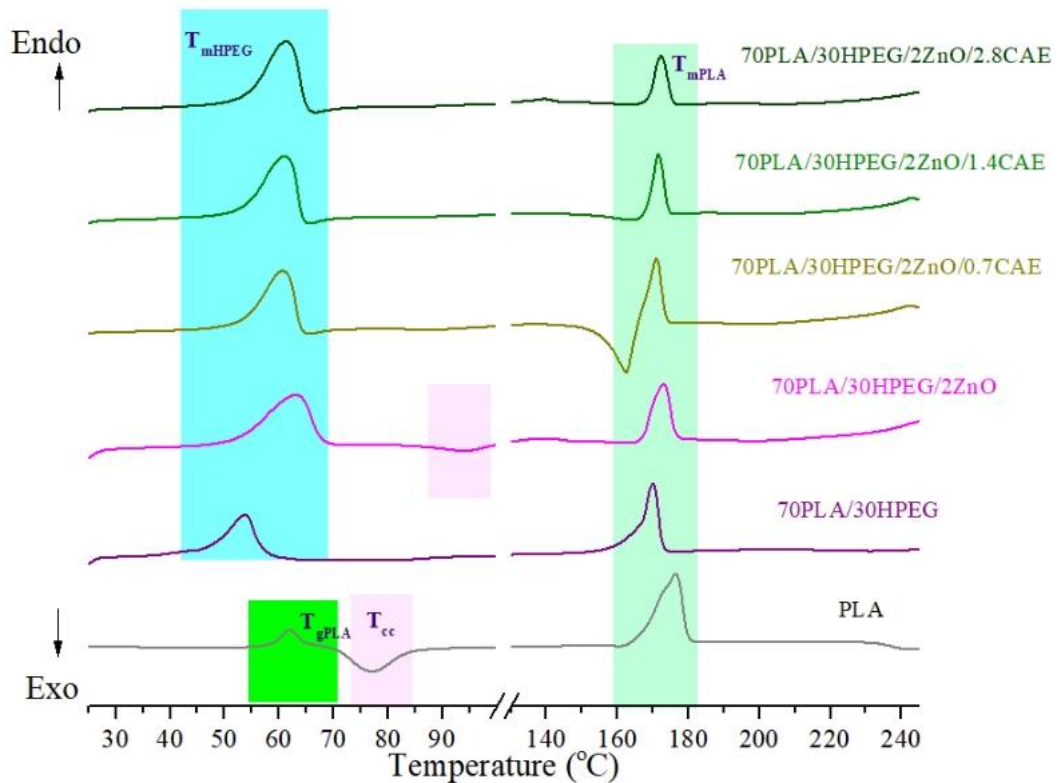


Figure 50. The first heat of DSC thermograms of blended PLA electrospun fibers: PLA, 70PLA/30HPEG, 70PLA/30HPEG/2ZnO, and 70PLA/30HPEG/2ZnO loaded various contents of CAE

From Figure 50., the peaks of T_{mHPEG} , T_{cc} , and T_{mPLA} were clearly observed in the 70PLA/30HPEG nanofibers, which showed the lowest T_{mHPEG} at 54 °C when adding ZnO NPs. T_{mHPEG} are increased. This might be due to the nucleating effect from ZnO NPs. The 70PLA/30HPEG/2ZnO loaded CAE results in decreasing T_{mPLA} and crystallinity of PLA. It is important to note that semi-crystalline phase in HPEG inhibited the crystallization of PLA leading to separate both phases of polymers between PLA and HPEG. Thus, it influences to mechanical properties such strength and elongation because of reducing flexibility of HPEG by ZnO.

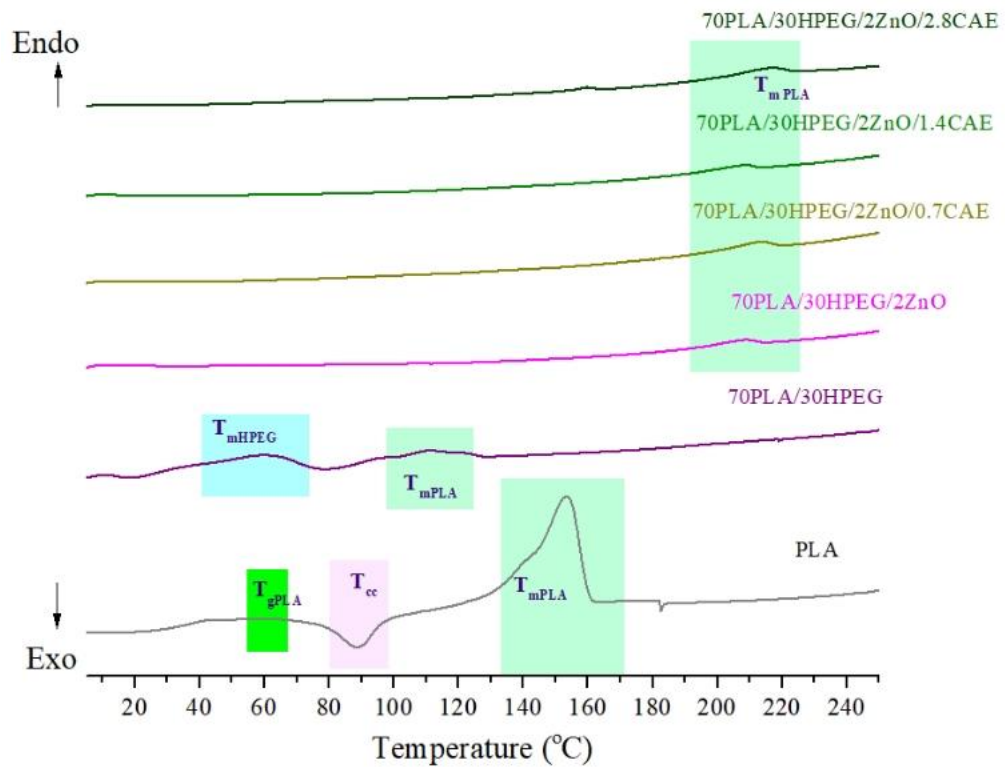


Figure 51. The second heat of DSC thermograms of blended PLA electrospun fibers: PLA, PLA/LPEG, and PLA/HPEG

In the second heat of DSC thermograms confirmed the effect of ZnO-inhibited T_g and induced T_m and reduced the %crystallinity of 70PLA/30HPEG and decreased when CAE increased

Table 13. Thermal properties of the blended 70PLA/30HPEG NFs loaded ZnO and CAE

| Samples | T_g | T_{mHPEG} | T_{cc} | T_{mPLA} | W_{PLA} | DH_{mHPEG} | DH_{mPLA} | DH_{cc} | X_{cPLA} |
|------------------------------|-------|-------------|----------|------------|-----------|--------------|-------------|-----------|------------|
| | (°C) | (°C) | (°C) | (°C) | | (J/g) | (J/g) | (J/g) | (%) |
| PLA | 62 | | 77 | 176 | 1 | | 52 | 19 | 36 |
| 70PLA/30LPEG | | 54 | | 170 | 0.7 | 32 | 40 | 3 | 62 |
| 70PLA/30HPEG/2ZnO | | 63 | 94 | 173 | 0.69 | 38 | 29 | 5 | 37 |
| 70PLA/30HPEG/2ZnO/ 0.7CAE | | 67 | 90 | 171 | 0.68 | 44 | 25 | 2 | 37 |
| 70PLA/30HPEG/2ZnO/ 1.4CAE | | 61 | | 171 | 0.68 | 45 | 19 | | 30 |
| 70PLA/30HPEG/2ZnO/ 2.8CAE | | 61 | | 171 | 0.67 | 47 | 17 | | 27 |

* W_{PLA} = weight fraction of PLA

4.3.5 Mechanical properties of blended PLA/LPEG and PLA/HPEG electrospun nanofibers by Tensile (ASTM D5034)

Table 14. Tensile strength, elongation at Break, and young's modulus of blended 70PLA/30HPEG NFs loaded ZnO and CAE

| Samples | Tensile strength | | Elongation at Break | | Modulus | |
|------------------------------|------------------|------|---------------------|-------|---------|-------|
| | MPa | SD | % | SD | MPa | SD |
| PLA | 0.38 | 0.08 | 77.95 | 1.87 | 6.64 | 0.75 |
| 70PLA/30HPEG | 0.69 | 0.03 | 169.47 | 31.21 | 21.07 | 5.40 |
| 70PLA/30HPEG/2ZnO | 0.48 | 0.07 | 22.40 | 9.52 | 22.20 | 6.19 |
| 70PLA/30HPEG/2ZnO/ 0.7CAE | 0.08 | 0.05 | 15.60 | 15.60 | 9.04 | 0.72 |
| 70PLA/30HPEG/2ZnO/ 1.4CAE | 0.23 | 0.12 | 34.40 | 12.03 | 17.20 | 12.00 |
| 70PLA/30HPEG/2ZnO/ 2.8CAE | 1.27 | 0.20 | 36.60 | 20.56 | 84.30 | 7.59 |

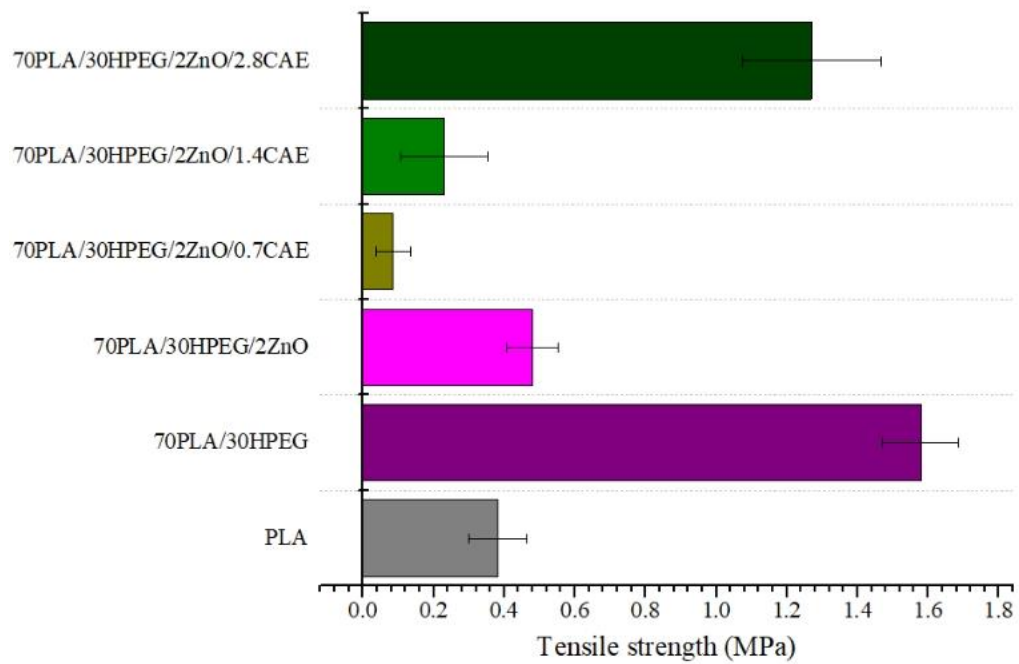


Figure 52. Comparison of tensile strength of 70PLA/30HPEG/2ZnO and 70PLA/30HPEG/2ZnO loaded various CAE

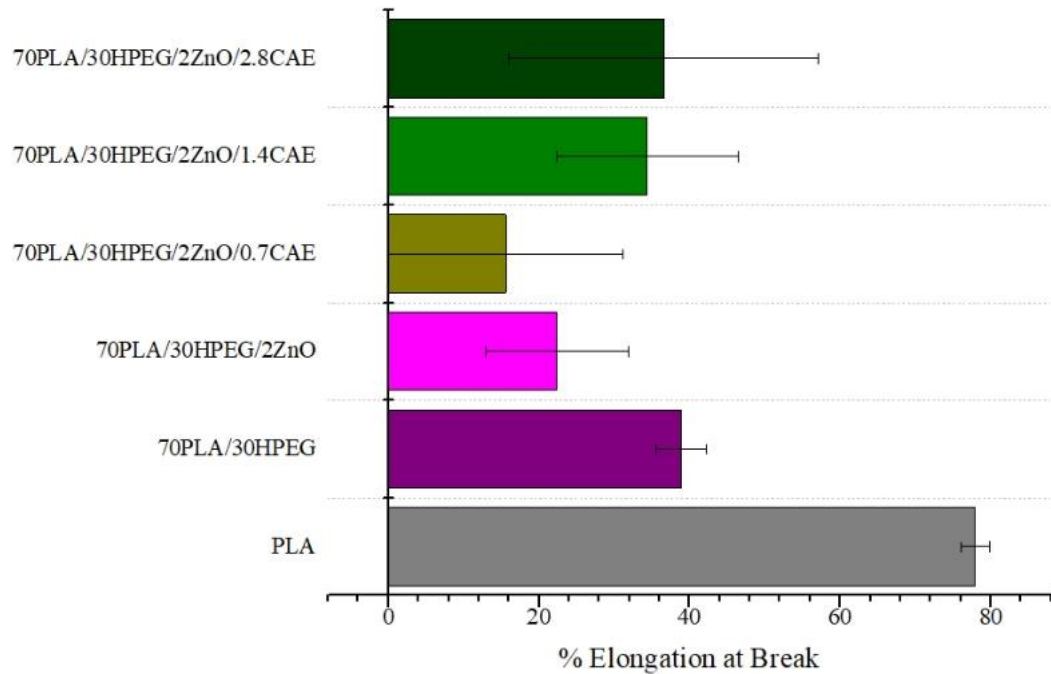


Figure 53. Comparison of elongation at break of PLA 70PLA/30HPEG/2ZnO and 70PLA/30HPEG/2ZnO loaded various CAE

The effect of ZnO NPs on mechanical properties of 70PLA/30HPEG electrospun fibers by tensile strength at maximum force, elongation at break, and modulus, the result shows the tensile decreased when adding ZnO NPs and lowest adding 0.7%CAE when the amount of CAE increased to induce tensile as same as elongation.

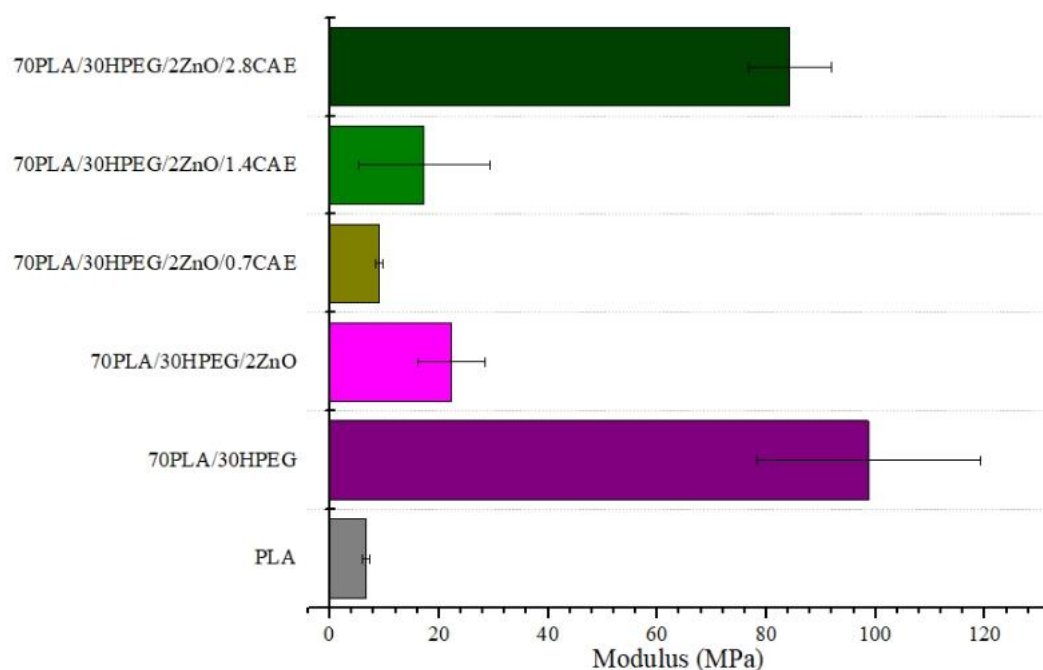


Figure 54. Comparison of modulus of PLA 70PLA/30HPEG/2ZnO and 70PLA/30HPEG/2ZnO loaded various CAE

Thus, the modulus increased by adding CAE at 2.8% wt in 70PLA/30HPEG/2ZnO which is the best condition.

4.3.6 Anti-bacterial activity of 70PLA/30HPEG/2ZnO

One of the main challenges in chronic wounds is an infection, which occurs with bacterial growth in the damaged skin of a wound, resulting in notable patient morbidity and mortality. Thus, infection prevention is necessary for wound healing. ZnO NPs affected antibacterial activities against many pathogenic microbes by a broad spectrum. They participate in the formation of reactive oxygen species (ROS), which penetrate the bacterial cell membrane producing oxidant injury and exhibiting

antibacterial activity. Additionally, zinc is an essential cofactor for many metalloenzymes required for cell proliferation and reepithelialization of skin wounds.

Table 15. Relative reduction percentage of 70PLA/30HPEG/2ZnO

| Bacterial name | %Reduction |
|-------------------------------|-------------------|
| <i>Pseudomonas aeruginosa</i> | 95 |
| <i>Staphylococcus aureus</i> | 100 |

In this study, the antibacterial activity of 70PLA/30HPEG/2ZnO electrospun fibers was calculated using a percentage reduction in bacterial count in the sample. PLA nanofibers loaded with ZnO nanoparticles 2 wt.% showed 95 and 100 % reductions in CFU/ml against *Pseudomonas aeruginosa* and *Staphylococcus aureus*, respectively as presented in Table 15. The results approve that 70PLA/30PLA/2ZnO electrospun nanofibers exhibited strong antibacterial activity against both *Pseudomonas aeruginosa* as gram-negative and *Staphylococcus aureus* as gram-positive bacteria. Comparing both types of bacteria, *P. aeruginosa* have low sensitivity to the electrospun membrane containing 2% ZnO nanoparticles.

4.3.7 Degradation of 70PLA/30HPEG loaded ZnO and CAE around 5 weeks

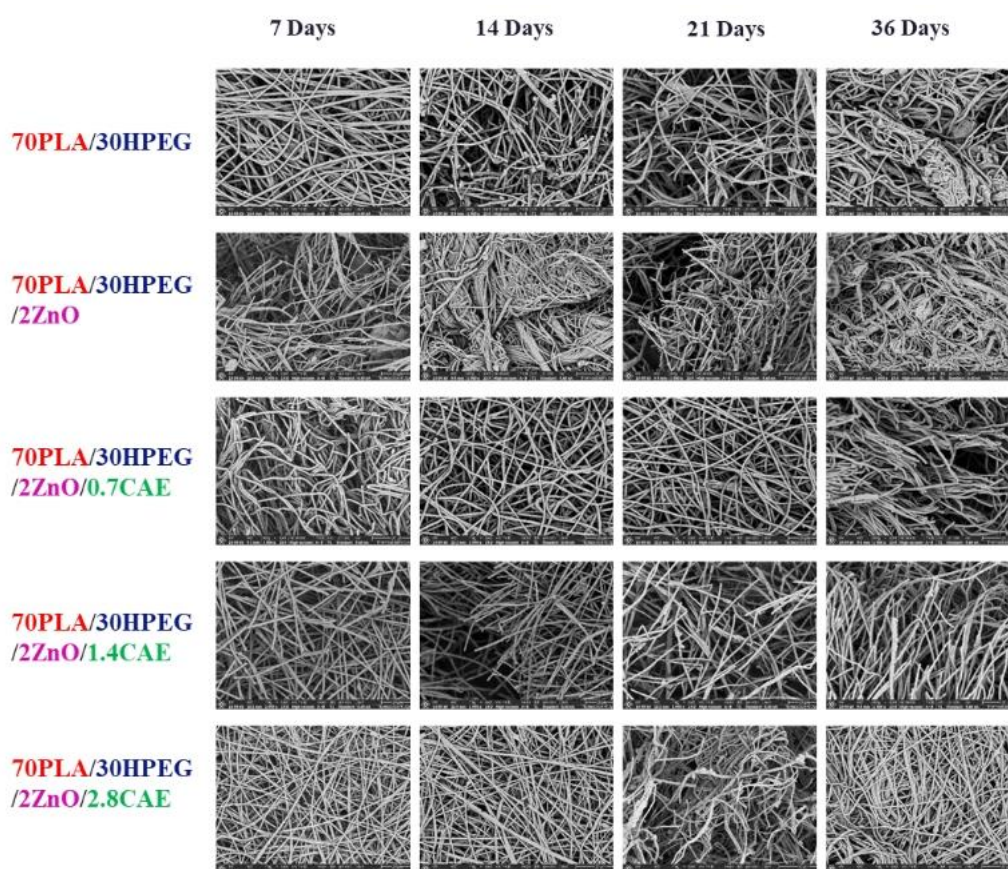


Figure 55. SEM illustrations of degradation of 70PLA/30HPEG and 70PLA/30HPEG loaded 2%ZnO NPs and various contents of CAE for 36 days

In Figure 55., SEM illustrations display degradation of 70PLA/30HPEG, 70PLA/30HPEG/2ZnO, and 70PLA/30HPEG2/ZnO loaded CAE electrospun fibers membrane from 7 days to 36 days. In this study, it was found that the ZnO and CAE reduced the degradation of 70PLA/30HPEG electrospun fiber which is related to the swelling and gel-fraction, thermal properties, and mechanical properties in the previous section. Thus, it could affect to the drug release profile of 70PLA/30HPEG2/ZnO loaded CAE. Additions of 0.7% CAE and 2.8 % CAE give low release whereas adding 1.4 % CAE shows higher degradation for 14 days to 21 days as depicted in Figure 56.

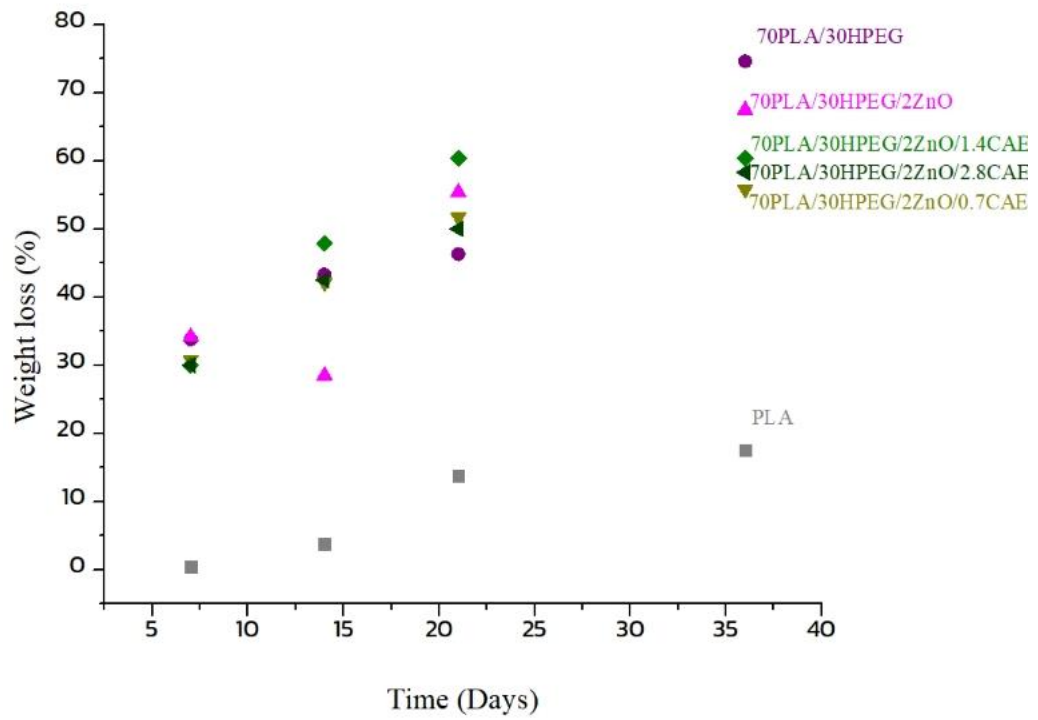
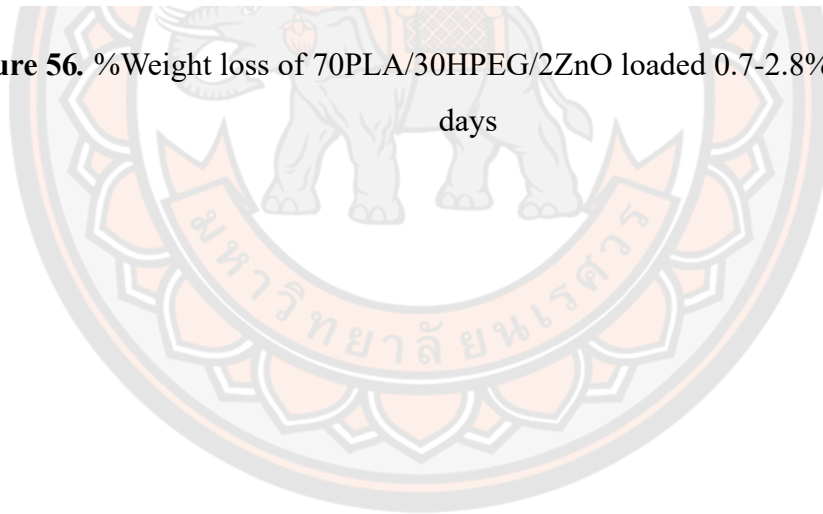


Figure 56. %Weight loss of 70PLA/30HPEG/2ZnO loaded 0.7-2.8% CAE for 36 days



4.3.8 Drug-control release profile of 70PLA/30HPEG/2ZnO loaded CAE

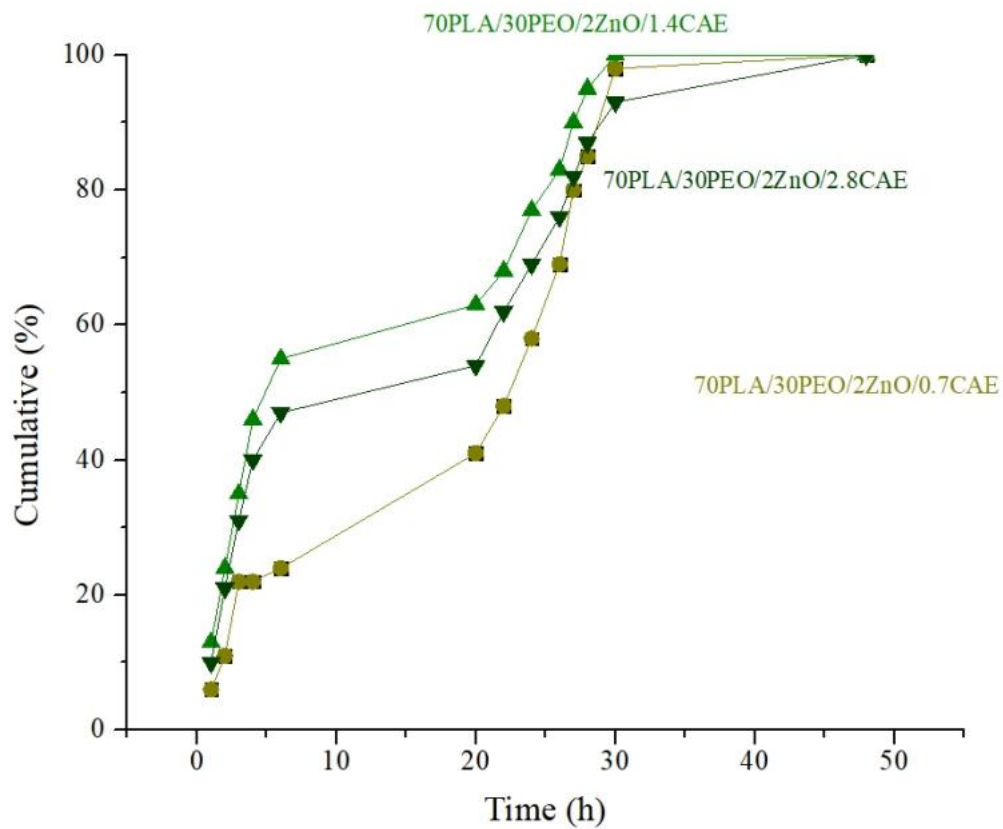


Figure 57. Shows cumulative percentage of 70PLA/30HPEG/2ZnO loaded 0.7%CAE, 1.4%CAE, and 2.8%CAE

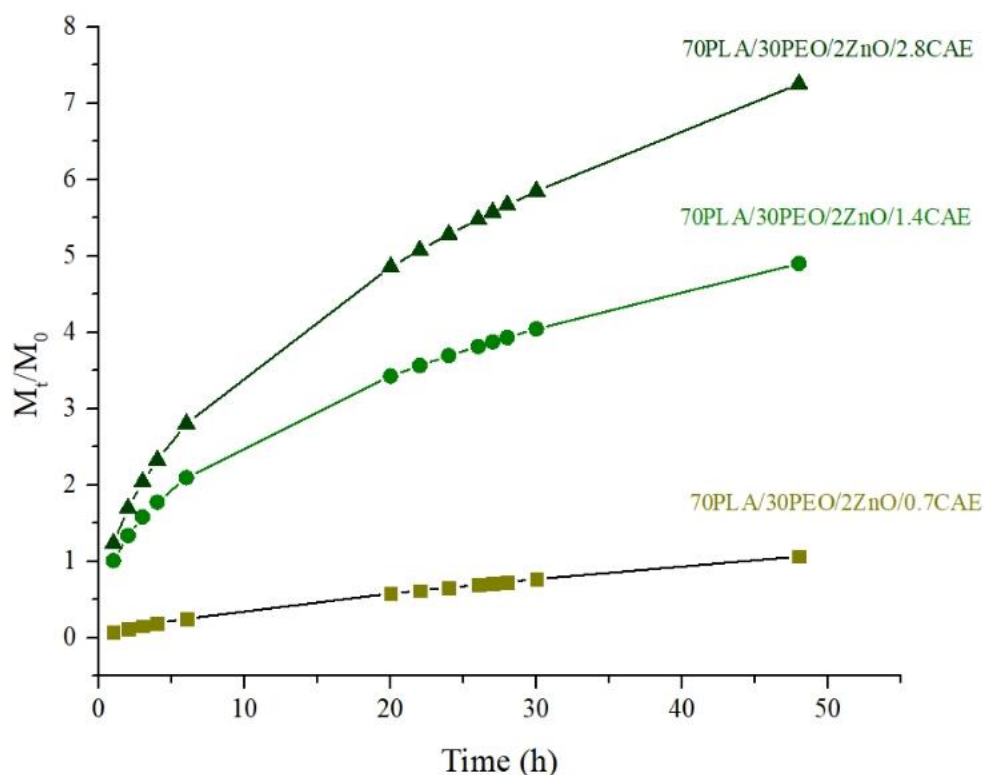


Figure 58. The Korsmeyer-Peppas graph of 70PLA/30HPEG/2ZnO loaded 0.7%CAE, 1.4%CAE, and 2.8%CAE

The drug release of 70PLA/30LPEG was degraded gradually in the process of degradation as the main material for the wound dressing. Meanwhile, the drug of CAE, which was carried by the 70PLA/30LPEG, was released from the carrier. The accumulated rate of drug release was applied to evaluate the drug-release behavior of drug-loaded PLA by being soaked in PBS instead of Blood and incubated at 37 °C for 48 h, as shown in Figure 57. It can be observed clearly the drug-release rate of all samples was very fast at the initial stage of degradation for 0.5 h, and then after 4 h, the drug-release rate of all samples slowed down. In this case, CAE release of 0.7% is like a stable constant line, with 1.4% as a linear line, and 2.8% logarithm because the 70PLA/30LPEG contained a lot of CAE in the early stage of release in Figure 57. As a result, the drug-release rate of 70PLA/30LPEG/2ZnO/CAE was very fast in the early stage. In the later stage (48h), with the slow degradation of 70PLA/30LPEG/2ZnO carrier, the drug was released slowly from the drug-carrier of 70PLA/30LPEG/2ZnO. Therefore, the degradation rate and the drug-release rate are

reduced. Different drug-release models were used to characterize the release mechanism of drugs. The drug-release behavior was fitted by several classical drug-release models, such as the Korsmeyer-Peppas model of $M_t/M = Kt^n$, as shown in Figure 58. and Table 16.

Table 16. Fitting parameters of drug release of blended 70PLA/30HPEG NFs loaded 2%ZnO and 0.7-2.8%CAE by Korsmeyer-Peppas model

| Korsmeyer-Peppas Equation ($M_t/M = Kt^n$) | 70PLA/30HPEG/ 2ZnO/0.7CAE | 70PLA/30HPEG/ 2ZnO/1.4CAE | 70PLA/30HPEG/ 2ZnO/2.8CAE |
|---|------------------------------|------------------------------|------------------------------|
| K | 0.07 | 1.01 | 1.23 |
| n | 0.70 | 0.41 | 0.46 |
| R ² | 0.95 | 0.96 | 0.96 |

The mechanism of drug release was drug diffusion when $n \leq 0.45$ and $0.45 < n < 0.89$, the drug diffusion and the dissolution of the drug carrier have a synergistic effect on the release rate of the drug. The drug release mechanisms of 0.7, 1.4, and 2.8% CAE with Korsmeyer-Peppas $n=0.7$, 0.4, and 0.46, respectively, are anomalous diffusion, Fickian diffusion, and anomalous diffusion, respectively.

4.3.9 Cytotoxicity

The cytotoxicity of the pure PLA, 70PLA/30HPEG, 70PLA/30HPEG/2ZnO, and 70PLA/30HPEG/2ZnO loaded 0.7-2.8% CAE was investigated via quantitative analysis using the MTT assay. Cell viability of the samples after exposure to the extraction medium including 100% and 50% compared with 100% control. It showed that the metabolic activity of human skin fibroblast cells was not inhibited by the sample medium as represented in Figure 59.

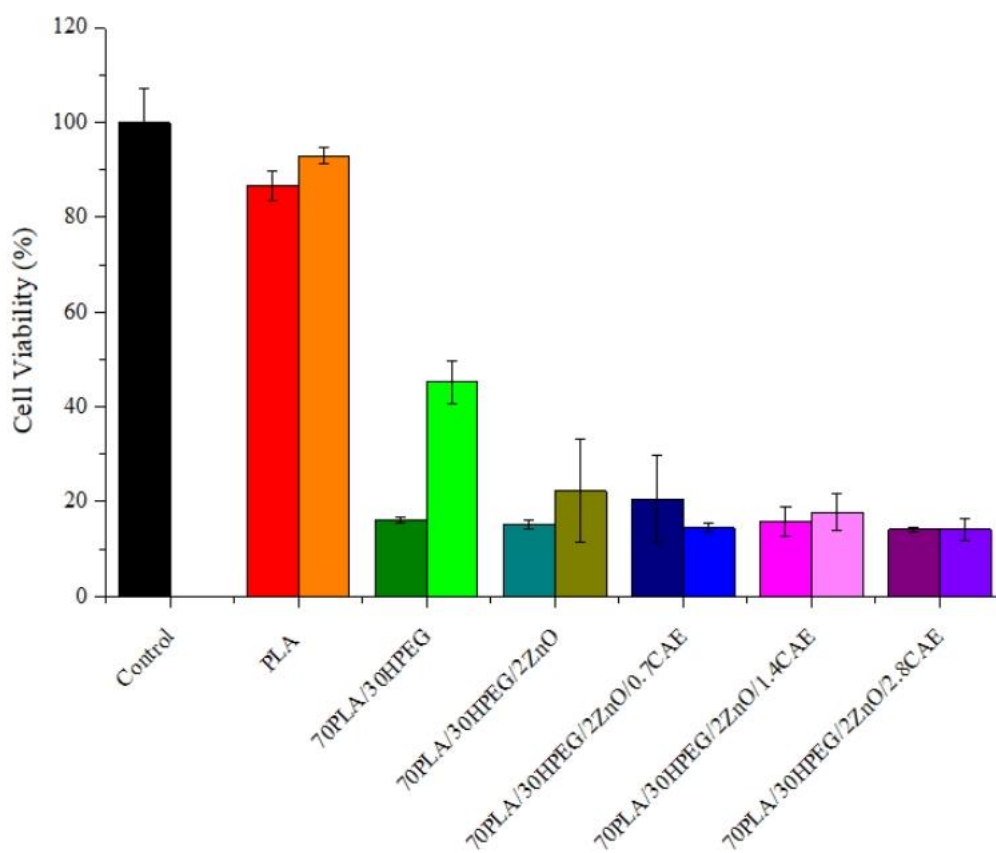


Figure 59. Cell viability of pure PLA, 70PLA/30HPEG, 70PLA/30HPEG/2ZnO and 70PLA/30HPEG/2ZnO loaded 0.7-2.8% CAE

The results indicated that pure PLA nanofibers displayed non-toxicity that is 86% whereas adding HPEG, ZnO, and 0.7-2.8%CAE showed cytotoxicity on human dermal skin fibroblast (HDFB) with 16.1, 15.3, 20.5, 15.8 and 14.1% loss of cell viability, respectively when incubated for 24 h. The *in vitro* cytotoxicity MTT assay of 70PLA/30HPEG/2ZnO loaded 0.7-2.8% CAE was evaluated as an effective therapeutic agent for chronic wound healing. The biosafety of polylactic acid has been approved by the FDA for use in the human body and has previously been studied by *in vivo* tests (6). The results indicated that 70PLA/30HPEG nanofibers loaded with ZnO-NP and CAE have a toxic effect on human skin fibroblasts. This phenomenon is still in doubt and needs further study to find out the reason and mechanisms of this toxicity.

CHAPTER 5

CONCLUSION

5.1 Conclusion

The fabrication of blended poly (lactic acid) (PLA) electrospun nanofibers was separated to be studied into 3 parts. The first part is PLA and blended PLA with Poly(ethylene glycol) (LPEG4000) and chitosan (CS) as bio-based polymers (PLA/LPEG/CS NFs) loaded with *Centella Asiatica* extracts (CAE) using the mixture solvents including Formic acid/chloroform/acetone and adding ethanol, were successfully prepared by electrospinning technique. It gave low solubility properties of PLA/LPEG/CS and PLA/LPEG/CS/CAE which are a separated layer of chitosan on the top of the solution after 2 hours because of the effect from LPEG gel and the physical and chemical properties were analyzed by SEM, Contact angle, FT-IR, DSC, and Tensile testing. The morphology of blended PLA nanofibers is continuous fiber characteristics when adding LPEG and CS. All samples showed hydrophobicity. PLA/LPEG/CS did not show the interaction between -OH and NH₂ and found another peak of LPEG, CS, and CAE in PLA/LPEG/CS/CAE nanofibers. T_g of PLA significantly decreased after the addition of 10 wt% of LPEG4000 to T_g of pure PLA nanofiber was ~63 °C when adding LPEG and CS was ~ 55 °C. The degree of crystallization decreased and PLA/LPEG/3.4CS loaded CAE had X_c higher than adding LPEG or CS in PLA 45-49% thus high tensile stress and Young's Modulus were higher than pure PLA nanofibers. Thus, we would like to develop the ratio of PLA and LPEG or HPEG in the new mixture solvent and change the antibacterial agent to ZnO nanoparticles instead of CS.

The second part is the development of blended poly (lactic acid) (PLA) electrospun nanofibers with LPEG and HPEG by various ratios of PLA and LPEG or HPEG as 90:10, 70:30, and 50:50 respectively using chloroform and acetonitrile by the ratio of 60:40 that are successfully fabricated via electrospinning. It was analyzed by SEM, water-contact angle, FTIR, swelling, gel-fraction, degradation, DSC, and tensile. Adding LPEG increased in PLA, the morphology was affected by the amount of LPEG which displayed a smaller diameter size than pure PLA NFs. However, adding HPEG increases diameter sizes higher than PLA and PLA/LPEG electrospun nanofibers. In the wettability study, adding LPEG in the PLA nanofibers cannot

enhance hydrophilicity, and the ratio of 90:10 of PLA/HPEG and 70PLA/30HPEG and 50PLA/50HPEG are hydrophilicity which FTIR shows characteristic of the sharp peak of HPEG at 2881 cm^{-1} is related to C-H stretching, and the smooth peak at 3464 cm^{-1} shows the presence of the OH group. Additionally, increased amounts of LPEG and HPEG provide higher swelling than pure PLA nanofiber. DSC thermogram shows low crystallinity when adding LPEG and HPEG but 90PLA/10LPEG and 70PLA/30HPEG are high compared to PLA and decreased T_g and T_m but 50PLA/50HPEG is high T_g as $64\text{ }^\circ\text{C}$ because of self-interaction. Adding LPEG and HPEG increased the tensile strength, elongation, and modulus. Adding HPEG increased % degradation when the increased amount of HPEG is high. Thus, we selected 70PLA/30HPEG for development with added ZnO and CAE because it is hydrophilic, and good mechanical properties, and has high elongation.

The final part is the fabrication of 70PLA/30HPEG electrospun fiber loaded 2% ZnO and 0.7-2.8% CAE that are characterized by the morphology by SEM, FTIR, DSC, tensile, anti-bacterial activity, swelling, and gel-fraction, degradation assay, release profile, and cytotoxicity (cell viability). The 70PLA/30HPEG electrospun fiber was compared with 70PLA/30HPEG/2ZnO and 70PLA/30HPEG/2ZnO/CAE and confirmed ZnO in fiber by EDS so were found the Zn spectrum. The average diameter size increased by adding ZnO and decreased by adding CAE. FTIR shows characteristic peaks in the regions of 1462 cm^{-1} , that represent bonds of CH_2 in scissoring, the sharp peak at 2881 cm^{-1} is related to C-H stretching, and the smooth peak at 3464 cm^{-1} shows the presence of the -OH group. Adding ZnO and CAE-affected thermal properties shows that the low crystallinity and increased T_g and T_m . The tensile strength, elongation, and modulus decreased when increased ZnO and CAE compared to 70PLA/30HPEG. 2% ZnO can be an anti-bacterial of *P. aeruginosa* and *S. aureus*. Adding ZnO and CAE decreased %swelling and gel fraction and adding CAE decreased degradation compared to 70PLA/30LPEG/2ZnO. Increasing CAE in the controlled release, 0.7%CAE provides a low amount of CAE but 1.4 and 2.8%CAE are higher than. The drug release mechanism of 0.7, 1.4, and 2.8% CAE with Korsmeyer-Peppas $n=0.7, 0.4, \text{ and } 0.46$, respectively is anomalous diffusion, Fickian diffusion, and anomalous diffusion, respectively. The cell viability

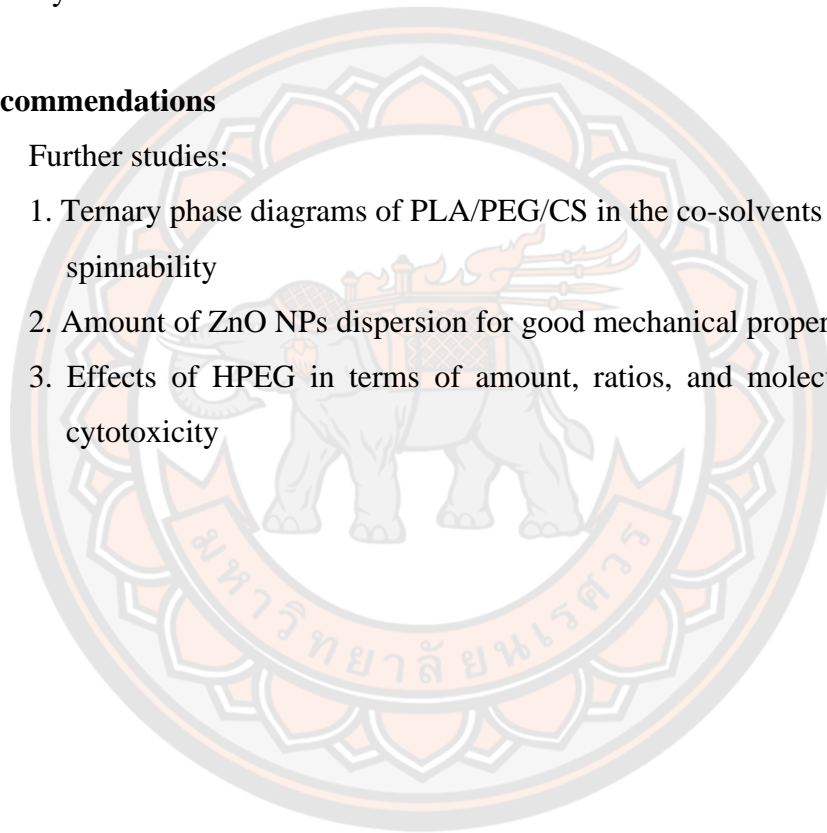
provides non-toxic pure PLA electrospun nanofiber because of 80% viability but adding HPEG, ZnO, and CAE is toxic that low cell viability around 14-20%.

In conclusion, adding HPEG to the PLA electrospun nanofiber has improved the wettability and good mechanical properties compared to the pure PLA nanofiber which is one of the requests of wound dressing. However, adding HPEG shows toxicity so it should be more studied, and developed the condition of the amount and types of molecular weight effects for the mechanism of electrospinning for cytotoxicity.

5.2 Recommendations

Further studies:

1. Ternary phase diagrams of PLA/PEG/CS in the co-solvents for the suitable spinnability
2. Amount of ZnO NPs dispersion for good mechanical properties
3. Effects of HPEG in terms of amount, ratios, and molecular weight on cytotoxicity



REFERENCES



REFERENCE

- [1] Smith and Nephew (2022). ACTICOAT is a Unique Antimicrobial Barrier Dressing. January 14th, 2022. Source: <https://www.smith-nephew.com/professional/products/advanced-wound-management/acticoat/>
- [2] Walker M, Parsons D. (2010), Hydrofiber Technology: its role in exudate management. *Wounds UK*. 6(2). 31-38.
- [3] Patrícia Coimbra; João P.Freitas; Teresa Gonçalves; Maria H.Gil, Margarida Figueiredo (2019), Preparation of gentamicin sulfate eluting fiber mats by emulsion and by suspension electrospinning. *Materials Science and Engineering: C*. 94. 86-93.
- [4] Radka Hobzova, Zuzana Hampejsova, Tereza Cerna, Jan Hrabeta, Kristyna Venclikova, Jarmila Jedelska, Udo Bakowsky, Zuzana Bosakova, Miloslav Lhotka, Simon Vaculin, Miloslav Franek, Milos Steinhart, Jana Kovarova, Jiri Michalek, Jakub Sirc (2019), Poly(D,L-lactide)/Poly(ethylene glycol) micro/nanofiber mats as paclitaxel-eluting carriers: preparation and characterization of fibers, in vitro drug release, antiangiogenic activity and tumor recurrence prevention, *Materials Science and Engineering: C*. 98. 982-993.
- [5] Leila Moradkhannejhad, Majid Abdouss, Nasser Nikfarjam, Mehrnoosh Hasan Shahriari, Vahid Heidary (2020), The effect of molecular weight and content of LPEG on in vitro drug release of electrospun curcumin loaded PLA/LPEG nanofibers, *Journal of Drug Delivery Science and Technology*. 56.A. 101554.
- [6] Samira Molapour Rashedi, Ramin khajavi, Abosaeed Rashidi, Mohammad Karim Rahimi, Abbas Bahador (2021), Novel PLA/ZnO Nanofibrous Nanocomposite Loaded with Tranexamic Acid as an Effective Wound Dressing: In Vitro and In Vivo Assessment, *Iran. J. Biotechnol.*. 19(3). e2737
- [7] Ingunn A. Hoell, Gustav Vaaje-Kolstad and Vincent G.H. Eijsink (2010), Structure and function of enzymes acting on chitin and chitosan, *Biotechnology and Genetic Engineering Reviews*. 27.1. 331-366.

- [8] N Gokarneshan (2017), Review article- Role of Chitosan in Wound Healing - a Review of the Recent Advances. 4(3). 555636.
- [9] Moore, K.; McCallion, R.; Searle, R. J.; Stacey, M. C.; Harding, K. G. (2006), Prediction and Monitoring the Therapeutic Response of Chronic Dermal Wounds. *Int. Wound. J.* 3 (2). 89-98.
- [10] Wiegand, C.; Winter, D.; Hipler, U. C., (2010), Molecular-Weight-Dependent Toxic Effects of Chitosans on the Human Keratinocyte Cell Line HaCaT. *Skin Pharmacology and Physiology.* 23 (3). 164-170.
- [11] Boniakowski, A.E.; Kimball, A.S.; Jacobs, B.N.; Kunkel, S.L.; Gallagher, K.A. (2017), Macrophage-mediated inflammation in normal and diabetic wound healing. *J. Immunol.* 199. 17–24.
- [12] Campbell, E.L.; Bruyninckx, W.J.; Kelly, C.J.; Glover, L.E.; McNamee, E.N.; Bowers, B.E.; Bayless, A.J.; Scully, M.; Saeedi, B.J.; Golden-Mason, L.; et al. (2014), Transmigrating neutrophils shape the mucosal microenvironment through localized oxygen depletion to influence resolution of inflammation. *Immunity.* 40. 66–77.
- [13] Tosello-Trampont, A.; Surette, F.A.; Ewald, S.E.; Hahn, Y.S. (2017), Immunoregulatory role of NK cells in tissue inflammation and regeneration. *Front. Immunol.* 8. 301.
- [14] Leal, E.C.; Carvalho, E.; Tellechea, A.; Kafanas, A.; Tecilazich, F.; Kearney, C.; Veves, A.; Kuchibhotla, S.; Auster, M.E.; Kokkotou, E.; et al. (2015), Substance P promotes wound healing in diabetes by modulating inflammation and macrophage phenotype. *Am. J. Pathol.* 185. 1638–1648.
- [15] Nagarajan, Vidhya; Mohanty, Amar K.; Misra, Manjusri (2016), Perspective on Polylactic Acid (PLA) based Sustainable Materials for Durable Applications: Focus on Toughness and Heat Resistance. *ACS Sustainable Chemistry & Engineering.* 4 (6). 2899–2916.
- [16] Monica Puri Sikka and Vinay Kumar Midha (2019), The role of biopolymers and biodegradable polymeric dressings in managing chronic wounds. *Advanced Textiles for Wound Care.* 463-488.
- [17]. Merin Sara Thomas, Prasanth K. S. Pillai, Marisa Faria, Nereida Cordeiro, Hernane Barud, Sabu Thomas¹, Laly A. Pothen (2018), Electrospun

- polylactic acid-chitosan composite: a bio-based alternative for inorganic composites for advanced application. *Journal of Materials Science: Materials in Medicine*. 29.137.
- [18] J. Wang, M. Windbergs (2017), Functional electrospun fibers for the treatment of human skin wounds, *European Journal of Pharmaceutics and Biopharmaceutics*. 119. 283–299.
- [19] R. Saraf (2013), Cost effective and Monodispersed Zinc Oxide Nanoparticles Synthesis and their Characterization. *Int. J. Adv. Appl. Sci.* 2. 85–88.
- [20] Q. Liu, M. Zhang, Z.x. Fang, X.h. Rong (2014), Effects of ZnO nanoparticles and microwave heating on the sterilization and product quality of vacuum packaged Caixin. *J. Sci. Food Agric.* 94 2547–2554.
- [21] Pijus Kanti Samanta (2017), Review on Wet Chemical Growth and Anti-bacterial Activity of Zinc Oxide Nanostructures. *Tissue Science & Engineering*. 8:1
- [22] Shamsuzzaman S, Ali A, Asif M, Mashrai A, Khanam H, et al. (2014), Green synthesis of ZnO nanoparticles using *Bacillus subtilis* and their catalytic performance in the one-pot synthesis of steroidal thiophenes. *Eur Chem Bull* 3: 939-945.
- [23] Samanta PK, Chaudhuri PR (2011), Growth and optical properties of chemically grown ZnO nanobelts. *Sci Adv Mater* 3: 112-117.
- [24] A. Azam, A.S. Ahmed, M. Oves, M.S. Khan, S.S. Habib, A. Memic (2011), Antimicrobial activity of metal oxide nanoparticles against Gram-positive and Gram-negative bacteria: a comparative study, *Int. J. Nanomedicine* 7. 6003–6009.
- [25] Y. Xie, Y. He, P.L. Irwin, T. Jin, X. Shi (2011), Antibacterial activity and mechanism of action of zinc oxide nanoparticles against *Campylobacter jejuni*, *Appl. Environ. Microbiol.* 77 2325–2331.
- [26] N. Padmavathy, R. Vijayaraghavan (2008), Enhanced bioactivity of ZnO nanoparticles—an antimicrobial study, *Sci. Technol. Adv. Mater.* 9. 1–7.
- [27] Solmaz Maleki Dizaj, Farzaneh Lotfipour, Mohammad Barzegar-Jalali, Mohammad Hossein Zarrintan, Khosro Adibkia (2014), Antimicrobial activity of the metals and metal oxide nanoparticles. *Materials Science and Engineering C*. 44. 278-284.

- [28] L. Zhang, Y. Ding, M. Povey (2008), D. York, ZnO nanofluids—A potential antibacterial agent. *Prog. Nat. Sci.* 18. 939–944.
- [29] P. Hosseinkhani, A. Zand, S. Imani, M. Rezayi, S. Rezaei Zarchi (2011), Determining the antibacterial effect of ZnO nanoparticle against the pathogenic bacterium, *Shigella dysenteriae* (type 1). *Int. J. Nano Dimens.* 1 279–285.
- [30] Z. Emami-Karvani, P. Chehrazi (2011), Antibacterial activity of ZnO nanoparticle on Gram positive and gram-negative bacteria. *Afr. J. Microbiol. Res.* 5. 1368–1373.
- [31] Paocharoen, V. (2010), The efficacy and side effects of oral *Centella asiatica* extract for wound healing promotion in diabetic wound patients. *J Med Assoc Thai.* 93(Suppl 7): p. S166-170.
- [32] Puttarak, P.; Brantner, A.; Panichayupakaranant, P (2016), Biological Activities and Stability of a Standardized Pentacyclic Triterpene Enriched *Centella asiatica* Extract. *Nat Prod Sci.* 22 (1). 20-24.
- [33] Saeidinia, A., et al (2017), Partial-thickness burn wounds healing by topical treatment: A randomized controlled comparison between silver sulfadiazine and centiderm. *Medicine (Baltimore)*,. 96(9): p. e6168.
- [34] Weerasing Muangman. (1984), The use of herbs in urinary tract diseases. *Euro Journal.* Vol. 8: pp. 7-12.
- [35] A.J. Meinel, O. Germershaus, T. Luhmann, H.P. Merkle, L. Meinel (2012), Electrospun matrices for localized drug delivery: current technologies and selected biomedical applications, *European Journal of Pharmaceutics and Biopharmaceutics.* 81. 1-13.
- [36] Bhardwaj, N., and S. C. Kundu. (2010), Electrospinning: A fascinating fiber fabrication technique. *Biotechnology Advances* 28. 325–347.
- [37] Andri Hardiansyah, Hartanto Tanadi, Ming-Chien Yang, and Ting-Yu Liu (2015), Electrospinning and antibacterial activity of chitosan-blended poly(lactic acid) nanofibers. *J Polym Res.* 22-59.
- [38] K. T. Shalumon, D. Sathish, S. V. Nair, K. P. Chennazhi, H. Tamura, and R. Jayakumar (2017), Fabrication of Aligned Poly(Lactic Acid)-Chitosan

- Nanofibers by Novel Parallel Blade Collector Method for Skin Tissue Engineering. *Journal of Biomedical Nanotechnology* Vol. 8. 405–416.
- [39] S.-F. Chou, D. Carson, K.A. Woodrow (2015). Current strategies for sustaining drug release from electrospun nanofibers. *Journal of Controlled Release*. 220 584-59.
- [40] J. Wang, M. Windbergs (2017), Functional electrospun fibers for the treatment of human skin wounds. *European Journal of Pharmaceutics and Biopharmaceutics*. 12557.
- [41] Yulianti, L.; Bramono, K.; Mardiyati, E.; Freisleben, H.-J (2016)., Effects of *Centella asiatica* Ethanolic Extract Encapsulated in Chitosan Nanoparticles on Proliferation Activity of Skin Fibroblasts and Keratinocytes, Type I and III Collagen Synthesis and Aquaporin 3 Expression In vitro. 6 (5).
- [42] Mustafa Abu Ghalia, Yaser Dahman (2017), Fabrication and enhanced mechanical properties of porous PLA/PEG copolymer reinforced with bacterial cellulose nanofibers for soft tissue engineering applications, *Polymer Testing*. 61. 114-131.
- [43] Nusavadee Pojanaukija and Somjai Kajorncheappunngam (2010), Comparison of antimicrobial activity of Mangosteen crude, Turmeric and Gotu Kola extract, *Naresuan University Journal*; 18(1)
- [44] Moore, K.; McCallion, R.; Searle, R. J.; Stacey, M. C.; Harding, K. G (2006), Prediction and Monitoring the Therapeutic Response of Chronic Dermal Wounds. *Int. Wound. J.* 3 (2). 89-98.
- [45] K. Gupta, R. Singh, A. Pandey, A. Pandey (2013), Photocatalytic antibacterial performance of TiO₂ and Ag-doped TiO₂ against *S. aureus*, *P. aeruginosa* and *E. coli*, *Beilstein J. Nanotechnol.* 4. 345–351.
- [46] J.W. Rasmussen, E. Martinez, P. Louka, D.G. Wingett (2010), Zinc oxide nanoparticles for selective destruction of tumor cells and potential for drug delivery applications, *Expert Opin. Drug Deliv.* 7. 1063–1077.
- [47] G. Han, R. Ceilley (2017), Chronic wound healing: a review of current management and treatments. *Adv. Ther.* 34 (3). 599–610.

- [48] Caitlin Berry-Kilgour, Jaydee Cabral, and Lyn Wise (2021). Advancements in the Delivery of Growth Factors and Cytokines for the Treatment of Cutaneous Wound Indications. *Advances in Wound Care*. Nov. 596-622.
- [49] Sen, C. K.; Gordillo, G. M.; Roy, S.; Kirsner, R.; Lambert, L.; Hunt, T. K.; Gottrup, F.; Gurtner, G. C.; Longaker, M. T. (2009), Human Skin Wounds: A Major and Snowballing Threat to Public Health and the Economy. *Wound Repair. Regen.*, 17 (6). 763-771.
- [50] Memic, A.; Abudula, T.; Mohammed, H. S.; Joshi Navare, K.; Colombani, T.; Bencherif, S. A. (2019), Latest Progress in Electrospun Nanofibers for Wound Healing Applications. *ACS Applied Bio Materials*, 2 (3). 952-969.
- [51] Das, S.; Baker, A. B. (2016), Biomaterials and Nanotherapeutics for Enhancing Skin Wound Healing. *Frontiers in Bioengineering and Biotechnology*. 4 (82).
- [52] Murphy, P. S.; Evans, G. R. (2012), Advances in Wound Healing: A Review of Current Wound Healing Products. *Plast. Surg. Int.* 2012, 190436.
- [53] Miguel, S.P., et al. (2018), Electrospun polymeric nanofibres as wound dressings: A review. *Colloids Surf B Biointerfaces*. 169: p. 60-71.
- [54] N Gokarneshan (2017), Review article- Role of Chitosan in Wound Healing - a Review of the Recent Advances. 4(3): 555636.
- [55] Howling, G. I.; Dettmar, P. W.; Goddard, P. A.; Hampson, F. C.; Dornish, M.; Wood, E. J. (2001), The effect of chitin and chitosan on the proliferation of human skin fibroblasts and keratinocytes in vitro. *Biomaterials*. 22 (22). 2959-2966.
- [56] Kong, M.; Chen, X. G.; Xing, K.; Park, H. J (2010.). Antimicrobial properties of chitosan and mode of action: A state of the art review. *International Journal of Food Microbiology*. 144 (1). 51-63.
- [57] Inamdar, P.K., Yeole, R.D., Srivastava, M.M., and de Souza, N.J (1996). Stability Study of Active Contitutents in the Centella Asiatica Exteact Formulations. *Drug Development and Industrial Pharmacy*. 22(3). 211-216.
- [58] Puttarak, P.; Charoonratana, T.; Panichayupakaranant, P. (2010), Antimicrobial Activity and Stability of Rhinacanthins-rich Rhinacanthus nasutus extract. *Phytomedicine*. 17. 323-327.

- [59] Azis, H. A.; Taher, M.; Ahmed, A. S.; Sulaiman, W. M. A. W.; Susanti, D.; Chowdhury, S. R.; Zakaria, Z. A (2017). In vitro and In vivo wound healing studies of methanolic fraction of *Centella asiatica* extract. *South African Journal of Botany*. 108. 163-174.
- [60] Wiegand, C.; Winter, D.; Hipler, U. C. (2010). Molecular-Weight-Dependent Toxic Effects of Chitosans on the Human Keratinocyte Cell Line HaCaT. *Skin Pharmacology and Physiology*. 23 (3). 164-170.
- [61] Howling, G. I.; Dettmar, P. W.; Goddard, P. A.; Hampson, F. C.; Dornish, M.; Wood, E. J (2001). The effect of chitin and chitosan on the proliferation of human skin fibroblasts and keratinocytes in vitro. *Biomaterials*. 22 (22). 2959-2966.
- [62] Zhu, L., et al (2016). Preparation of asiaticoside-loaded coaxially electrospinning nanofibers and their effect on deep partial-thickness burn injury. *Biomed Pharmacother*. 83: p. 33-40.
- [63] Manotham, S., K. Pengpat, S. Eitssayeam, et al (2015)., Fabrication of Polycaprolactone/ *Centella asiatica* Extract Biopolymer Nanofiber by Electrospinning. *Applied Mechanics and Materials*,. 804: p. 151-154.
- [64] Yao, C.H., et al. (2017), Wound-healing effect of electrospun gelatin nanofibres containing *Centella asiatica* extract in a rat model. *J Tissue Eng Regen Med*.. 11(3): p. 905-915.
- [65] L.H. Li, M.Y. Yen, C.C. Ho, P. Wu, C.C. Wang, P.K. Maurya, P.S. Chen, W. Chen, W.Y. Hsieh (2013), H.W. Chen, Non-Cytotoxic Nanomaterials Enhance Antimicrobial Activities of Cefmetazole against Multidrug-Resistant *Neisseria gonorrhoeae*, *PLoS ONE* .8. e64794.
- [66] A. Zaleska (2008), Doped-TiO₂: a review. *Recent Pat. Eng*. 2 157–164.
- [67] T. Sun, H. Hao, W.T. Hao, S.M. Yi, X.P. Li, J.R. Li (2014), Preparation and antibacterial properties of titanium-doped ZnO from different zinc salts, *Nanoscale Res. Lett*. 9. 98.